Gait Event Recognition for Triggering Functional Electrical Stimulation during Robotic Gait Training

Dissertation

zur Erlangung des akademischen Grades

Doktoringenieur

(Dr.-Ing.)

von Dipl.-Ing. Andreas Schicketmüller

geb. am 07.07.1991 in Steyr (Österreich)

genehmigt durch die Fakultät für Elektrotechnik und Informationstechnik der Otto-von-Guericke-Universität Magdeburg

Gutachter:

Prof. Dr. rer. nat. Georg Rose

Prof. Dr.-Ing. Thomas Seel

Promotionskolloquium am 14.07.2022

Zusammenfassung

Der Rehabilitationsprozess von Patienten, die aufgrund von neurologischen Defiziten, wie sie zum Beispiel nach einem Schlaganfall auftreten, an Gangstörungen leiden, umfasst ein breites Spektrum an Behandlungsmethoden.
Nicht-pharmakologische Rehabilitationstechniken wie robotergestütztes Gangtraining oder funktionelle Elektrostimulation können dabei die Rehabilitation dieser Patienten unterstützen. In der klinischen Routine werden beide Technologien meist getrennt voneinander eingesetzt. Durch die Kombination dieser Techniken können jedoch potenzielle Nachteile wie eine inkorrekte Muskelaktivierung aufgrund passiv induzierter Bewegung kompensiert werden, was zu einer Verbesserung des Therapieeffektes und zu besseren Rehabilitationsergebnissen führen kann.
Für eine prospektive Kombination dieser Technologien wurde ein Algorithmus entwickelt, der Gangereignisse während des robotergestützten Gangtrainings unter Verwendung von linearer-Beschleunigungs- und Winkelgeschwindigkeitsdaten aus Inertialsensoren extrahiert. Diese Gangereignisse können perspektivisch zur Auslösung einer funktionellen elektrischen Stimulation während der robotergestützten Gangrehabilitation verwendet werden. Da dieser neuartige Ansatz unabhängig von den roboterspezifischen Schnittstellen und den vom Roboter bereitgestellten Daten ist, kann der Aufbau autonom betrieben werden, was die Möglichkeit bietet, eine große Bandbreite an Gangtrainern mit dieser Technologie auszustatten. In dieser Arbeit wurden Machbarkeit, Anwendbarkeit, Robustheit und Leistungsfähigkeit des neu entwickelten Konzepts evaluiert.
Zunächst werden die Entwicklung des Detektionsalgorithmus im Detail beschrieben und die Methoden zur Erkennung von Gangereignissen und zur Fehlerbehandlung erläutert. Des Weiteren wurde ein Algorithmus für eine willkürliche Sensorausrichtung entwickelt. Dieser wird im Detail beschrieben und evaluiert.
Als nächster Schritt wird die Machbarkeit des Systems bestehend aus Inertialsensoren für die Erfassung von Gangereignissen beim robotergestützten Gangtraining evaluiert. Für diese Auswertung führte ein gesunder Proband insgesamt sechs Trainingseinheiten mit zwei unterschiedlichen Gangtrainern durch (exoskelettales System und endeffektor-basiertes System). Die Daten wurden mit dem entwickelten Algorithmus analysiert, und es wurde eine Gesamterkennungsrate von ca. 99% für das exoskelettale System und ca. 96% für das endeffektor-basierte System erreicht. Zusätzlich wurden die Falsch-Positiven, welche falsch erkannte Schritte darstellen, berechnet. Der Gesamtwert der Falsch-Positiven betrug ca. 1% für beide Systeme.

In einem dritten Schritt werden die Anwendbarkeit und Robustheit des Systems in der klinischen Routine berücksichtigt. Dazu wurde eine Gesamtzahl von n=10 Probanden mit Schlaganfall für die Teilnahme an einer klinischen Studie rekrutiert.
Die Patienten wurden entsprechend ihrem Leistungsniveau in zwei Gruppen aufgeteilt und den robotergestützten Gangtrainern (exoskelettales System und endeffektor-basiertes System) zugewiesen. Mit den entsprechenden Gangtrainern führten sie ihre normale Rehabilitationsroutine durch, die Erhebung der Bewegungsdaten erfolgte mittels Inertialsensoren. Der entwickelte Algorithmus wurde mit den Daten der klinischen Studie getestet. Die Erkennungsrate über alle Patienten betrug ca. 96% für das endeffektor-basierende System, die Analyse des exoskelettalen Systems zeigte einen Erkennungsrate von ca. 99%. Zusätzlich wurden die Falsch-Positiven berechnet; der Wert über alle Patienten betrug ca. 1% sowohl für das endeffektor-basierte System als auch das exoskelettale System.
In einem letzten Schritt wurde die Leistungsfähigkeit des Algorithmus und die Möglichkeit zur Auslösung einer funktionellen elektrischen Stimulation auf Grundlage der extrahierten Gangereignisse untersucht. Die Leistung des Algorithmus basiert dabei auf der induzierten Verzögerung der Mess- und Ausführungskette des Konzepts. Insgesamt induziert der Algorithmus (bei einem Sensor) eine mittlere Latenzzeit von ca. 282µs. Die mittlere Latenzzeit einer seriellen Übertragung zum Senden des Stimulationsbefehls der funktionellen elektrischen Stimulation betrug ca. 2µs. Darüber hinaus wurden die Bluetooth-induzierte Latenz und die Latenz aufgrund physiologischer Prozesse wie der elektromechanischen Verzögerung theoretisch untersucht. Das Resultat war eine Gesamtverzögerung von ca. 148ms, die eine realisierbare Grundlage für eine zukünftige funktionelle elektrische Stimulation während der Behandlung mit Gangtrainern darstellt.
Im Ergebnis liefert das Konzept in Abhängigkeit der Schrittdauer des Gangtrainers und der induzierten Verzögerung durch die Mess- und Ausführungskette sowie der Verzögerung durch physiologische Prozesse vielversprechende Ergebnisse für die zukünftige Forschung – und eine Technik, die den Rehabilitationsprozess von Menschen mit Gangstörungen durch die Kombination von roboterunterstütztem Gangtraining mit funktioneller elektrischer Stimulation verbessern kann. Die in dieser Arbeit vorgestellten Ergebnisse zeigen den ersten wissenschaftlich fundierten Ansatz der Verwendung von Inertialsensoren zur Gangereigniserkennung beim robotischen Gangtraining mit der Perspektive, die Therapie mit funktioneller elektrischer Stimulation zu unterstützen.

Abstract

The rehabilitation process of patients who suffer from gait disorders caused by neurological defects such as stroke involves a broad variety of treatment methods. Non-pharmacological rehabilitation approaches such as robotic gait training or functional electrical stimulation have shown to support the rehabilitation of these patients. In clinical rehabilitation routine, both technologies are mainly used separately from each other. By combining these techniques, potential disadvantage such as improper muscle activation due to passively induced movement can be compensated and can lead to an improvement of therapy effects and better rehabilitation results.

For a prospective combination of the mentioned technologies, an easy and lightweight algorithm was designed. The goal of the algorithm is to detect certain gait events during clinical robotic gait therapy. The detection is based on sensor data such as linear acceleration and angular velocity. Recognized phases perspectively can be utilised to activate functional electrical stimulation during the rehabilitation with robotic gait trainers. As this novel setup is independent from robot-specific interfaces, it can be operated autonomously, which offers the possibility to equip a wide variety of robotic gait trainers with this technology. In this work the feasibility, applicability, robustness and performance of the newly developed concept was evaluated.

First, the development of the algorithm is described in detail and the gait event detection and error handling methods are elaborated. Furthermore, an arbitrary sensor alignment algorithm is introduced and explained.

Second, the feasibility of a concept with inertial sensors for the acquisition of gait events during robotic gait therapy is evaluated. For this evaluation, a healthy subject performed six recording sessions with two different robotic gait trainers (one exoskeletal robotic system and one end-effector based system). The data was analysed with the generated algorithm and detection rates were calculated. A value of approx. 99% for the exoskeletal system and a value of approx. 96% for the end-effector based system were achieved. Additionally, false-positives representing incorrect detected steps were calculated. The value for both systems was approx. 1%.

As a third step, the applicability and robustness of the proposed system during clinical routine was taken into consideration. Therefore, a number of n=10 stroke patients was recruited to participate in a clinical study. Before the recordings, as a part of the normal rehabilitation routine, specially trained therapists screened the participants and decided whether the subject should perform the therapy in the exoskeletal robotic system or in the

end-effector based system. The specially designed algorithm was tested using the collected data from the clinical trial. As a result, an approximate value of 96% over all patients for the detection rate in end-effector based system was achieved. The detection rate of the exoskeletal system over all patients had a value of approx. 99%. Furthermore, false-positives were calculated. The value of false-positives over all patients was approx. 1% for both systems.

As a last step, the performance of the algorithm and possibility to trigger functional electrical stimulation based on the extracted gait events was investigated. The performance of the algorithm is focussed on the induced delay of the measurement and execution chain of the proposed concept. Overall, the algorithm for one sensor induces a mean latency of approx. 282µs. The mean latency of a serial transmission to send the stimulation command for the trigger of functional electrical stimulation was approx. 2µs. Furthermore, the Bluetooth-induced latency and the latency due to physiological processes such as the electromechanical delay were investigated theoretically and resulted in an approximate overall delay of the proposed concept of approx. 148ms, which provides a feasible basis for a future functional electrical stimulation during the robotic treatment.

As a result, depending on the step duration of the robotic system, the induced delay due to the measurement/execution chain and the delay due to physiological processes, the proposed concept delivers encouraging findings for future research and provides a method that can improve the recovery of people with walking disturbances by actively activating the muscles with electrical stimulation during the robotic gait therapy. The results presented in this thesis show the first scientifically based approach of using inertial measurement units for the gait recognition during robotic gait training with the perspective of triggering functional electrical stimulation during the therapy.

Declaration of Honour

„I hereby declare that I produced this thesis without prohibited external assistance and that none other than the listed references and tools have been used. I did not make use of any commercial consultant concerning graduation. A third party did not receive any nonmonetary perquisites neither directly nor indirectly for activities which are connected with the contents of the presented thesis.
All sources of information are clearly marked, including my own publications.
In particular I have not consciously:

- Fabricated data or rejected undesired results
- Misused statistical methods with the aim of drawing other conclusions than those warranted by the available data
- Plagiarized data or publications
- Presented the results of other researchers in a distorted way

I do know that violations of copyright may lead to injunction and damage claims of the author and also to prosecution by the law enforcement authorities. I hereby agree that the thesis may need to be reviewed with an electronic data processing for plagiarism.
This work has not yet been submitted as a doctoral thesis in the same or a similar form in Germany or in any other country. It has not yet been published as a whole."

Berlin, 02.08.2022
Andreas Schicketmüller

Funding
This research received funding from the European Union's Horizon 2020 research and innovation programme under the Marie Skłodowska-Curie grant agreement No 721577.

Table of Contents

1 Introduction ... 1

1.1 Goals and Non-Goals ... 4

2 Theoretical Background ... 5

2.1 Nervous System ... 5
2.1.1 Brain ... 6
2.1.2 Spinal Cord ... 6
2.1.3 Neurons ... 8
2.1.4 Chemical Synapse ... 9
2.1.5 Defects of the Nervous System ... 10
2.1.6 Neuroplasticity ... 11
2.2 Human Gait Cycle ... 13
2.2.1 Muscle Activation during Gait ... 14
2.3 Electrical Stimulation ... 17
2.3.1 Functional Electrical Stimulation ... 17
2.4 Robotic Gait Training ... 20
2.5 Inertial Measurement Units ... 25

3 State-of-the-Art ... 27

3.1 Gait Recognition Methods with Wearable Sensors ... 27
3.1.1 Inertial Measurement Units ... 27
3.1.2 Electromyography Sensors ... 27
3.1.3 Force Sensors ... 28
3.2 Detection Methods ... 29
3.3 Comparison ... 29
3.4 Hybrid Robotic Rehabilitation Systems ... 32
3.4.1 Lokomat ... 32
3.4.2 Gangtrainer GT II ... 34
3.4.3 WalkTrainer ... 34
3.4.4 MotionMaker ... 35
3.4.5 G-EO ... 36
3.4.6 RT 600 ... 36

4 Materials and Methods ... 38

4.1 Robotic Systems ... 38
4.1.1 Lokomat ... 38
4.1.2 Lyra ... 39
4.2 MotionSensor ... 40
4.3 Electrical Stimulator ... 41

5 Results ... 43

5.1 Development and Training—Algorithms ... 44
5.1.1 Arbitrary Sensor Alignment Algorithm ... 46

5.1.2 Gait Event Recognition Algorithm 51
5.1.3 Initial Contact 52
5.1.4 Full Contact 53
5.1.5 Heel Off 54
5.1.6 Toe Off 54
5.2 Techniques to enhance Confidence of the Algorithm 56
5.2.1 Dynamic Threshold—Initial Contact 56
5.2.2 Sequence Detection 56
5.2.3 Temporal Dependencies 57
5.2.4 Dynamic Threshold—Toe Off 58
5.2.5 Adaptions—Robot-specific 58
5.2.6 Adaptions—Stroke Patients 59
5.3 Testing—Arbitrary Sensor Alignment Algorithm 62
5.3.1 Testing 62
5.3.2 Evaluation 66
5.4 Testing—Gait Event Detection Algorithm 71
5.4.1 Healthy Adult 71
5.4.2 Stroke Patients 76
5.4.3 Performance 79
5.5 Analysis—Gait Event Detection Algorithm 81
5.5.1 Healthy Adult 81
5.5.2 Stroke Patients 85
5.5.3 Performance 89
5.6 Application—Functional Electrical Stimulation 90
5.6.1 Testing and Application—Trial 1 90
5.6.2 Testing and Application—Trial 2 100
5.6.3 Testing and Application—Trial 3 108
5.6.4 Performance 112
6 Discussion and Conclusion 115
6.1 Gait Event Detection—Healthy Adult 115
6.1.1 Discussion 115
6.1.2 Conclusion 116
6.2 Gait Event Detection — Stroke Patients 119
6.2.1 Discussion 119
6.2.2 Conclusion 120
6.3 Performance and Applicability of the Concept 124
6.3.1 Discussion 124
6.3.2 Conclusion 126
7 Outlook and Future Works 129
8 Appendix 134
8.1 Measurement Protocols—Healthy Adult 134

8.2 Measurement Protocols—Stroke Patients 135
8.3 Ethical Approval 137
8.4 Own Publications incorporated within this Work 139
9 List of Figures 140
10 List of Tables 143
11 References 145

1 Introduction

Human walking requires a close collaboration of the motor and sensory system of human beings. Besides, it is a vital activity of daily living and a key factor for well-being and health. Diseases of the nervous or the cardiovascular system such as stroke, multiple sclerosis and parkinsonism as well as trauma such as spinal cord injury, can disturb the precision and the coordination of the collaborating systems and can lead to gait disorders or walking impediments. Particularly the performance of activities of daily living such as functional mobility is highly restricted for people with walking dysfunctions. Moreover, they can lead to falls and can decrease the overall quality of life. As reported by Global Health Estimates of the World Health Organization, cerebrovascular diseases like strokes are the second most frequent causes of death and the third most frequent reasons for disability worldwide [1]. Furthermore, for stroke survivors, gait disorders and walking impediment are main problems in their daily life [2,3]. As a result, for stroke survivors, the restauration of gait and independent walking is seen to be a major goal of rehabilitation [4]. For the treatment of gait disorders in the clinical routine, various rehabilitation techniques such as physiotherapy and occupational therapy are used. In addition to the conventional therapy, modern techniques like robot-assisted gait training (also called electromechanical gait training, robotic gait training or robotic gait therapy) are more frequently used to support the treatment of the patients. The technical setup of robotic gait trainers incorporates a body strap attached to a supporting system, which is needed as a support for the paretic lower limbs and which can act as a compensation for insufficient balance reactions. In addition, it provides physical relief for the therapists as the body weight of the patient is carried by the robot. The gait is thereby induced by a robot-specific pattern and defines the cyclic movement of the gait. Robotic gait trainers can be classified as exoskeletal types that move the joints such as ankle or knee of a patient during the training, and end-effector based systems that move only the feet of a patient [5]. Thus, gait robots can be categorized based on their principal of motion. Two successive systematic reviews dedicated to robot-assisted gait training for walking after stroke conclude that the combination of robotic gait training and conventional physiotherapy is more effective in achieving independent walking in stroke survivors with gait disorders compared to patients who did not receive robotic gait training [6,7]. Nonetheless, negative aspects of robotic gait training are described in the literature as well. For example, the harness which supports the body weight of the patient can lead to the inhibition of muscle activity [8].

Additionally, depending on the robot-specific movement strategy, the movement of pelvis and legs are constrained to a certain degree, which can influence the natural occurring muscle activation pattern [9]. In order to tackle these drawbacks, some manufacturers of robotic gait trainers developed techniques which aim to allow the subject to influence the induced movement pattern actively to enhance the rehabilitation output. An example for that is a biofeedback mode which allows the robotic device to measure the patients' remaining walking activity and adapts the induced gait pattern. Another example would be the change of the guidance force of the exoskeleton which can be altered towards the abilities of the patient.

Another commonly used technique in rehabilitation to promote lower and upper extremity function is functional electrical stimulation [10–17]. The rehabilitation approach of functional electrical stimulation (FES) describes the usage of external artificial electrical impulses to stimulate muscles with disrupted nervous control. The aim of the stimulation is to provide a muscular contraction and to produce a functional useful movement [18]. For stroke survivors, FES has shown to be beneficial in improving aspects of everyday activity performance [19]. Additionally, for patients with multiples sclerosis, FES can provide a positive orthotic effect [20]. Nevertheless, innovations and advances in clinical approaches for the FES therapy are needed to increase medical efficacy and usability of this treatment method [20]. Compared to conventional neuromuscular electrical stimulation which does not elicit a distinct movement of the muscles, FES treatment for gait training of stroke survivors can be considered superior as it improves mobility and balance, reduced spasticity in the muscles and can improve the overall gait performance [21]. Furthermore, for spinal cord injury patients, medical benefits such as the incremental change in the activity of the nervous system following FES treatment contribute significantly to the improvement in quality of life [22].

The combination of a guided movement like cycling and FES has shown to provide positive effects on parameters like speed of walking and walking ability [23]. Furthermore, the combination of FES and the aforementioned robotic gait training seems to be a promising technique for stroke rehabilitation. The combination of FES and robot-assisted gait training can be termed "hybrid robotic rehabilitation system". This combination of rehabilitation techniques has demonstrated a higher medical efficacy in comparison to robotic gait training alone [24]. The goal of hybrid robotic rehabilitation systems is to combine the positive aspects of both approaches and simultaneously counteracting potential drawbacks of the individual techniques. In particular, the advantages of robotic gait training such as high repetition, long durations and physical relief of the therapists can be maintained with simultaneous improvement of muscle activation through active electrical

stimulation of the muscles of the lower limbs. Approaches to combine commercially available gait trainers with electrical stimulation are promising.
So far, however, the approaches require information provided by the robot itself [25–32], focus on intramuscular electrodes [25,33], require human interaction using a finger switch [33], or provide only limited amounts of stimulated muscles such as stimulation for foot drop [26,27]. Furthermore, some commercially available systems do not publish their operating principle scientifically or do not have open hard/software interfaces to allow a connection with external systems, limiting the possibility for peer reviewing and research.
An approach to overcome the above-mentioned limitation (that information provided by the robotic system itself is needed for the setup) is to use sensors like inertial measurement units (IMU) to record the movement of the subject or the robot during therapy. Based on the recorded movement, events during the gait cycle can be detected and further be processed with the aim to use them as a trigger instant for FES during the gait training. Additionally, due to the independent data collection, the scope of potential robotic gait trainers is large. Furthermore, the number of stimulated muscles can be improved by the explicit knowledge of the individual gait events.
Gait event detection is a well-researched area and commercially available analysis systems as described in [34–37] provide valid and reliable spatial-temporal gait parameters. Yet, the main focus of these systems is to analyse human walking rather than recording and analysing robotic gait trainers with their system-dependent characteristics of movement. Furthermore, most of them do not aim to use gait events as a trigger instant for FES.
Therefore, within this work we propose a novel technique which records the movement of robotic gait trainers and provides a real-time gait event detection algorithm including an unsupervised adaptability to the robotic gait pattern with the future aim to use the detected gait events as a trigger instant for FES to support future rehabilitation.

1.1 Goals and Non-Goals

Goals

One goal of this thesis is to develop an algorithm for gait recognition during robotic training. The algorithm should be able to process data which is gathered by IMUs. The raw data consists of linear acceleration (m/s^2) and angular velocity (°/s). Based on the raw data, the developed algorithm should extract four main gait events from the gait cycle in real time. The feasibility of the algorithm should be tested. Furthermore, the suitability for the usage in a clinical setting should be evaluated. The algorithm should be developed in MATLAB in such a way that it can be extracted as C-Code using the MATLAB Coder in order to provide the basis for a potential implementation in external processing units. The developed algorithm should be adaptable to provide the possibility for the usage of various robot-assisted gait trainers. Additionally, the usage for a broad range of training velocities should be possible. The algorithm should support an arbitrary sensor alignment to ensure an easy set-up of the IMUs. The developed concept should be able to provide a trigger instant for FES during robotic gait training based on the detected gait cycle. The concept should take the meaningfulness and applicability of the electrode positioning during clinical routine into account. Thus, a reasonable number of muscles on the lower extremity must be identified. Furthermore, the detected gait events must be mapped to the muscle activity during walking in order to define the stimulation patterns. The concept must provide the possibility to freely choose the stimulation patterns and the parameters for the electrical stimulation. Bench testing of the proposed concept should be executed.

Non-Goals:

The developed algorithm does not have to be validated against gold standards for gait event detection such as optical marker systems or pressure sensitive walkways.

The medical efficacy of the developed system with functional electric stimulation does not have to be shown. Furthermore, the usage of the concept together with patients in a clinic does not have to be evaluated.

2 Theoretical Background

The following chapters provide a theoretical background on the topics addressed within this thesis. It is split into the following parts: 2.1 Nervous System, 2.2 Human Gait Cycle, 2.3 Electrical Stimulation, 2.4 Robotic Gait Training and 2.5 Inertial Measurement Units. Depending on their importance in the context of the thesis, the respective chapters vary in detail of their explanation.

2.1 Nervous System

The nervous system can be separated according to its localisation (central – peripheral) and functionality (somatic – autonomic). The brain and the spinal cord form the central nervous system. The peripheral nervous system is formed by the somatic and the autonomic nervous system. Additionally, the autonomic nervous system can be further divided into sympathetic nervous system and parasympathetic nervous system. The separation of the various parts is visualised in Figure 1.

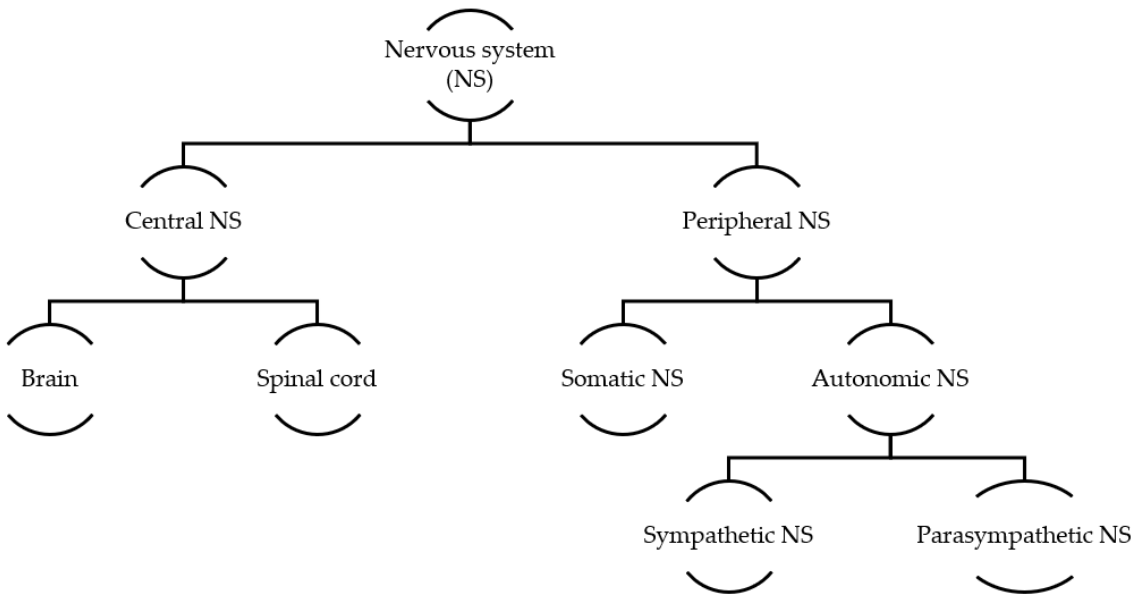

Figure 1: Structure of the nervous system

2.1.1 Brain

To simplify the segmentation of the brain, it can be separated into three domains: cerebrum, cerebellum and brain stem (Figure 2).

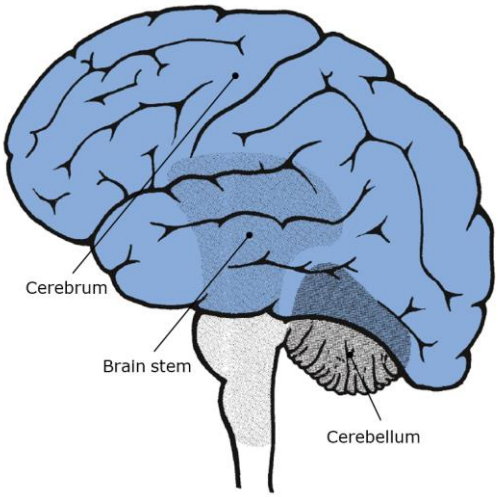

Figure 2: Brain—simplified segmentation [38]

The brainstem is connected to the spinal cord and comprises important centres for breathing and the circulatory system. The pons which is located in the brain stem works as a connection between the cerebrum and the cerebellum. Other important parts of the brain stem are the mid brain, the formation reticularis, the nucleus ruber and the substantia nigra (affected region of Parkinson's disease, chapter 2.1.5) which work as motoric centres. The remaining parts of the brain stem are called striatum, thalamus and palladium. The cerebrum can be separated in frontal, parietal, occipital and temporal lobe. Arbitrary movements are represented in the motoric cortex which is located in the frontal lobe. The cerebellum takes part in the regulation and correction of the motoric system and therefore is part of the static of a human being [38].

2.1.2 Spinal Cord

Within the spinal cord there is a clear differentiation between grey and white matter. The grey matter in the centre of the spinal cord mainly consists of nerve cells. It is surrounded by the white matter which consists of axons. The grey matter can be separated into posterior horn and anterior horn (Figure 3). Sensory information collected by the spinal ganglion is forwarded via the posterior root and the posterior horn to the brain (ascending pathways). Motoric information coming from the brain use the pyramidal pathways

(descending pathways) which pass signals via the anterior horn and root to motor neurons and result in an innervation of a muscle.

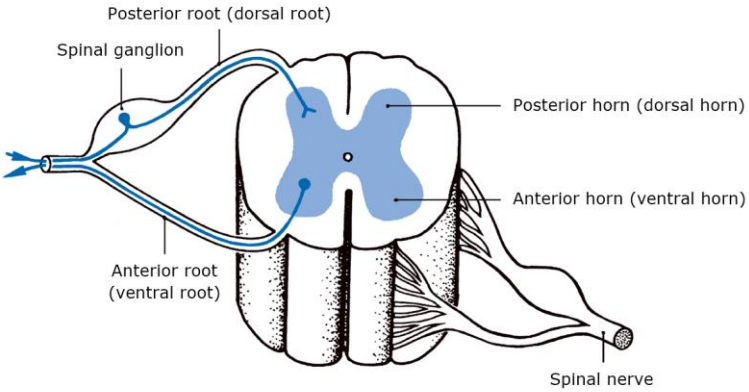

Figure 3: Cross-section of the spinal cord [38]

Spinal nerves consisting of posterior and anterior horn are specifically designated to a segment of the spinal cord. The segments are called cervical (C 1-8), thoracic (Th 1-12), lumbar (L 1-5) and sacral (S 1-5). The segments are represented in the periphery as dermatomes on the skin (Figure 4). Dermatomes are important indicators for the severity of paralysis as a lack of sensation in a specific dermatome can be exactly assigned to a specific spinal cord segment and its nerve.

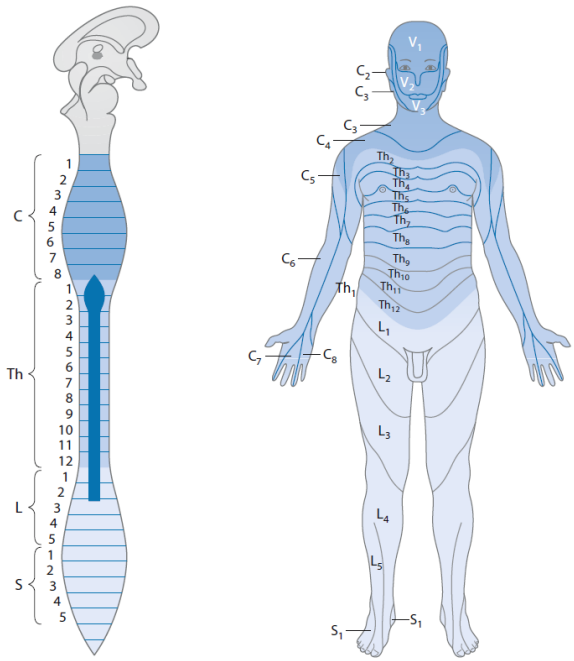

Figure 4: Spinal cord segments (left) and corresponding dermatomes (right) [39]

2.1.3 Neurons

Functionality

Neurons, also called nerve cells, can be divided into three main groups. Motoric neurons (efferent) sensory neurons (afferent) and interneurons. Motoric neurons are coupled with muscles or glands; their task is to pass information from the spinal cord to the distinctive muscle or gland, therefore they are called efferent neurons which means "away from the brain". In contrast to that, afferent neurons pass sensory information from the periphery of various receptors to the brain. Inter neurons are neither specifically afferent nor efferent and can operate between motoric and sensory neurons.

A neuron can be divided into four main functional units (Figure 5). Signals which are gathered by the dendrites are integrated by the soma and passed to the axon hillock. The axon hillock summarises this information and an action potential is created. The information of the summarized signals is encoded in the frequency of the action potential [40]. The propagation of the action potential is done by an axon. At its end, the axon is either connected to an electrical synapse (gap junction) or to a chemical synapse. In case of a motoric neuron, the synapse is called neuromuscular junction which is a chemical synapse and triggers a muscle fibre [40]. Details for chemical synapses are elaborated in section 2.1.4.

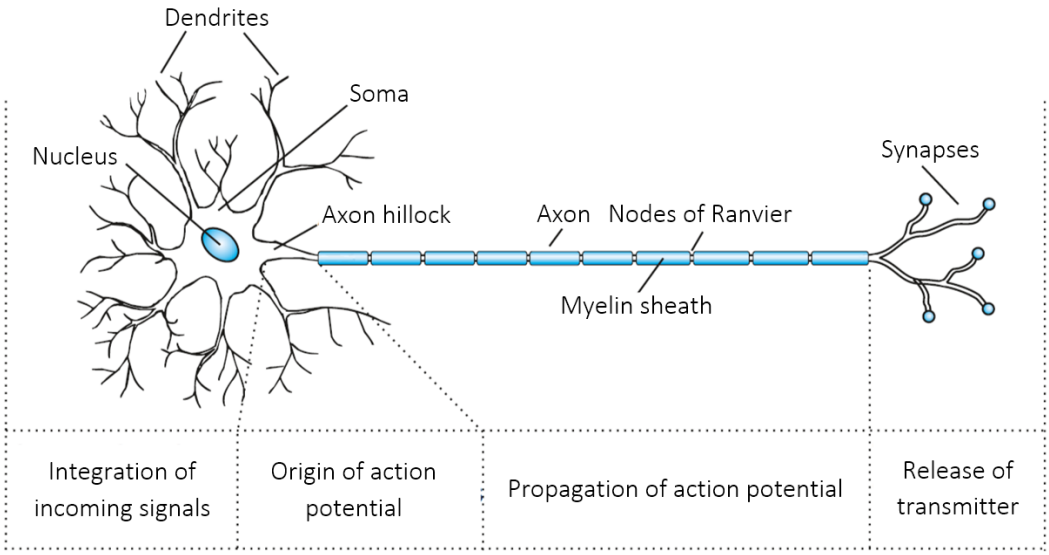

Figure 5: Structure and function of a neuron [40]

Action Potential (AP)

The nerve impulse is initiated if a neuron is excited, and the balance of its charges is altered. This alteration of charges occurs due to chemical disturbances at a synapse or receptor or due to disturbances such as an external electrical impulse [41]. The AP is initiated by a depolarisation which starts slowly from the resting potential of about -70mV. When a certain threshold is reached, the depolarisation briefly speeds up to a maximum value of about 30mV (all-or-nothing principle). This is followed by a repolarisation and a hyperpolarisation which restores the resting potential. Figure 6 shows a sample AP, V_{RP} indicates the rest potential, V_T the threshold potential and V_H the potential reached during hyperpolarisation.

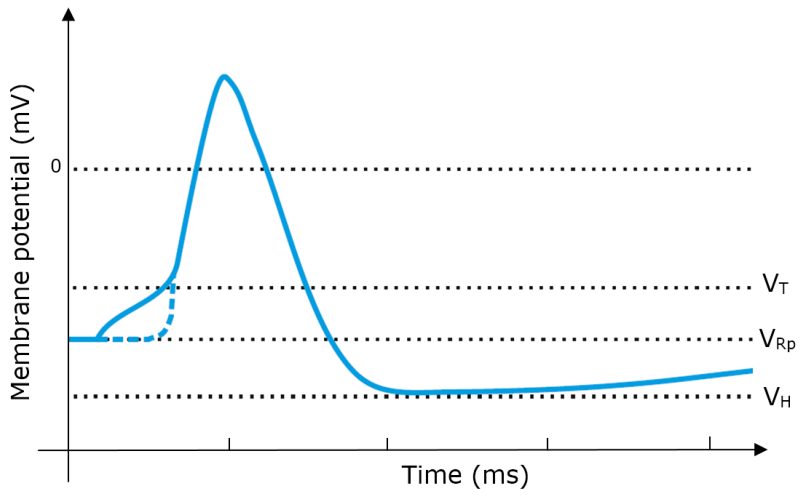

Figure 6: Schematical representation of an action potential [40]

The creation of action potential of all excitable cells (nerve cells, skeletal muscle cells, heart muscle cells) work in the same way but they differ in shape and curve [40].

2.1.4 Chemical Synapse

A chemical synapse or neuromuscular junction (Figure 7) is needed for the propagation of a signal between a neuron and other cells. The AP of an axon leads the synapse to release neurotransmitters. The neurotransmitter diffuses through the presynaptic membrane into the synaptic gap. The transmitter diffuses through the synaptic gap to the postsynaptic membrane. In the membrane the transmitter can bind to the corresponding receptors. This binding leads to a depolarisation of the postsynaptic membrane which excites the

propagation of the signal (excitatory synapse) or to a hyperpolarisation which inhibits the propagation (inhibitory synapse) [42].

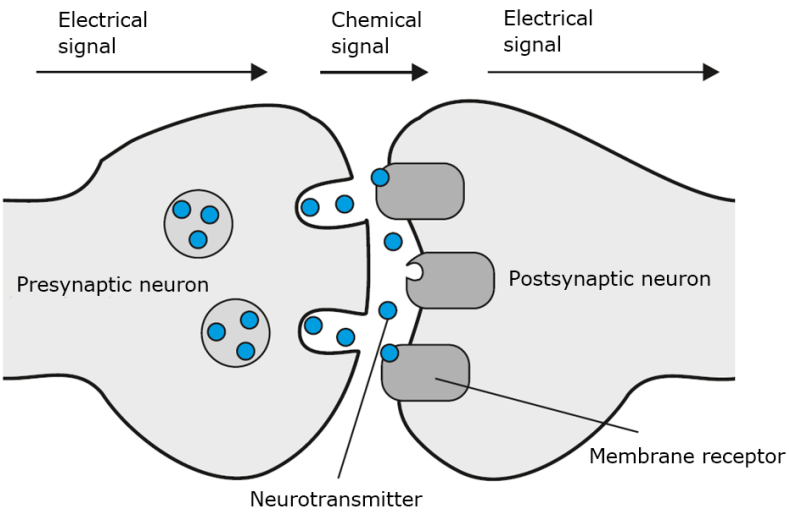

Figure 7: Chemical synapse [40]

With this process, an electrical signal is converted to a chemical signal. This chemical signal is translated via neurotransmitters and specific membrane receptors back into an electrical signal. Action potentials in motoneurons result in the release of acetylcholine. Acetylcholine triggers the depolarization of the muscle fibre membrane resulting in a wave of depolarisation along the muscle fibre membrane causing the whole muscle fibre to contract and trigger a movement [40].

2.1.5 Defects of the Nervous System

Stroke: A stroke is a medical condition mostly caused by insufficient blood circulation in the brain leading to cellular death of the affected area. The two major types of stroke are the ischemic stroke caused by clot narrowing or blocking of blood vessels (ICD–10–GM–I63) and the haemorrhagic stroke caused by blood from a damaged blood vessel in the brain or in the subarachnoid space (ICD–10–GM–I61) [43]. Early symptoms of a stroke include face dropping or numbness, arm weakness and slurred speech. Common long-term effects include muscles weakness, spasticity and drop foot.

Spinal cord injury (SCI): Spinal cord injury (ICD–10–GM–S14, S24, S34) describes damages of the spinal cord with temporary or permanent changes in its function. SCI can be divided into traumatic and non-traumatic causes [44]. Traumatic SCI refers to damages

of the spinal cord, which are caused by external impacts such as car accidents, falls or violence. In contrast to that, non-traumatic SCI are caused by disc diseases (acute, chronic, degenerative) or infection [45]. Depending on the localisation of the lesion (cervical, thoracic, lumbar, sacral; see Figure 4) different segments and dermatomes of the body are affected. Symptoms include impairment of sensory and motor function and are graded according to the ASIA Impairment Scale [46].

Parkinson's disease: Parkinson's disease (ICD–10–GM–G20) refers to a neurodegenerative disorder caused by the death of dopamine-producing neurons located in the substantia nigra. Symptoms include motoric symptoms (e.g.: bradykinesia, tremors, etc.) and non-motoric symptoms (e.g.: depression, insomnia, etc.) [47].

Multiple's sclerosis: Multiple sclerosis (ICD–10–GM–G35) is a disease which destroys the myelin sheath of nerve cells in the brain and the spinal cord. This disease is also referred to as encephalitis disseminate, which indicates the occurring centres of inflammation that are scattered throughout the central nervous system. Despite increasing understanding of the disease mechanisms and the increase of therapeutic options, the exact cause of multiple sclerosis is unknown, yet a combination of genetic and environmental factors act to confer susceptibility to the disease [48]. Symptoms may include unsafe movement (ataxia), loss of muscle mass, spasticity and sensitive disorders.

Treatment: The above-mentioned defects of the nervous symptoms and their symptoms such as spasticity, drop foot, and other impairments, are treated using pharmacological and non-pharmacological methods. Non-pharmacological treatments such as functional electrical stimulation (section 2.3.1) and robot-assisted gait training (section 2.4) are therapies recommended by the guidelines of the German Association of Neurology [49,50].

2.1.6 Neuroplasticity

Neuroplasticity is the neurobiological basis of functional restitution of the nervous system. Neuroplasticity can be seen as the ability to make adaptive changes related to the structure and function of the nervous system [51]. The two types which are mainly described in this context are the structural neuroplasticity which refers to changes in the structure, such as change in strength between neurons, whereas functional neuroplasticity refers mainly to the learning process and memory [52]. Thus, neuroplasticity is a summation of various biological adjustment procedures which can an occur during rehabilitation with

techniques such as robotic gait training and functional electrical stimulation. The underlying mechanisms can be described as follows [53]:

Vicariation: Vicariation describes the function that a destroyed area of the brain is adopted by an intact but not related area of the brain. An example is that the visual cortex of blind people can be adopted and is activated when learning braille. Nevertheless, vicariation is a hypothetical concept and is replaced by a more plausible concept called unmasking/redundancy recovery [54].

Plasticity of cortical representations (unmasking/redundancy recovery): This concept describes the ability of the brain to use connections which are normally not used but already available. This means redundant (latent) connections are activated if the initial connections are destroyed. This redundant connectivity is already existent but stays inactive until activated.

Sprouting of nerve endings: As the name indicates, sprouting refers to the recovery of injured or cut nerve endings. In the peripheral nervous system, this process leads to new functional neural connections. This process is less relevant in the central nervous system as the basic conditions for sprouting such as the existence of swan cells is not given there.

Collateral axon sprouting: This mechanism refers to denervated neurons which can receive signals from other synapses. Collateral axon sprouting lead to untwined functionality as nerve cells in the CNS are highly specific regarding their tasks. Intact areas may create a plasticity. Intact areas form axon collaterals act as a plastic response to a distant lesion, which sprout as denervated areas and form synapses.

Diaschisis: The concept describes that a lesion in the brain can affect other, more distant areas of the brain. This affects the functionality and has no structural changes. The functional changes are reversible as soon as the impact of the lesion fades.

Synaptic plasticity: Synaptic plasticity describes the process where synchronous activation patterns of synapses change their synaptic strength ("Cells that fire together, wire together" [55]). This process is thought to contribute to memory and learning.

Enriched environment: The environment of the patient influences the neurorehabilitation. A high motivation with better goals and a good quality of social contacts leads to better results of plasticity. As it is quite difficult and ethically problematical to control the environment of a human being, this concept is hard to evaluate.

Neurogenesis: Neurogenesis is the process of creating nervous system cells out of neural stem cells.

Neuronal stem cells: Neuronal stem cells are immature cells of the central nervous system. They have the ability to divide and renew themselves and produce mature neurons.

2.2 Human Gait Cycle

The human gait is one of the most essential activity of daily living. It is executed by a repetitive movement of the extremities propelled by the muscles. Corresponding to Figure 8, the functional basis for walking can be described in seven steps. The gait is initiated by the CNS which registrates the gait command and activates the motor neurons (1). As a next step, the signals are transmitted via the peripheral nervous system (2). The muscles are activated and muscle tension is developed (3). Forces and moments are generated using the synovial joints (4). The skeletal muscles support the regulation of joint forces and moments (5). This interplay leads to a displacement of the limbs, causes a gait movement (6) and thus, ground reaction forces are generated (7) [56].

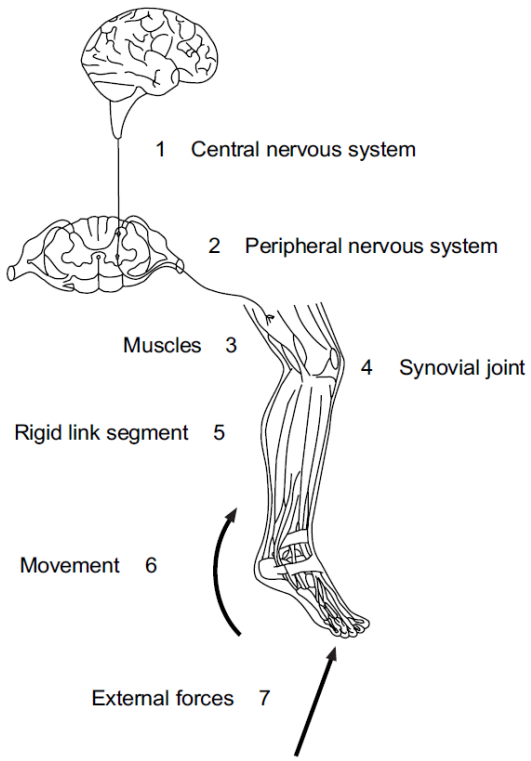

Figure 8: Seven components that form the functional basis for walking [56].

The generated gait cycle is defined by two phases and eight gait events as depicted in Figure 9. The start is indicated by the initial contact (IC) which corresponds to the first contact of the foot with the ground. This event is followed by the load response (LR) when the contralateral foot lifts off. The LR incorporates the full contact (FC). Heel off (HO) corresponds to the heel lifting off the ground. Opposite initial contact corresponds to the first contact of the heel from the opposite limb with the ground. During a normal gait cycle,

this happens at 50% of gait cycle. Toe off (TO) is indicated by the lifting of the forefoot from the ground. Feet adjacent (FA) refers to when the swing leg passes stance leg. Tibia vertical (TV) corresponds to the vertical oriented tibia of the swing leg. The end of the movement sequence is again indicated by an IC. Thus, the IC starts and ends a gait cycle.

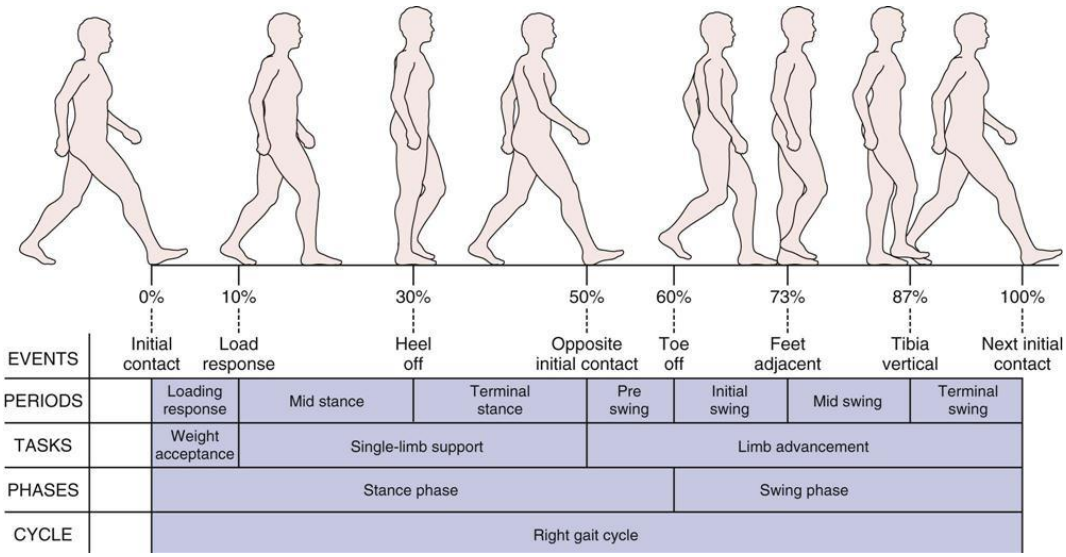

Figure 9: Human gait cycle [57]

2.2.1 Muscle Activation during Gait

The proportion of the muscle activity during gait is not permanent; many factors such as age, walking speed, personal fitness, injuries and anthropometric data influence the muscle contribution during gait. Nevertheless, the activation of muscles during gait can be defined as a function of the movement pattern. The muscle activation can be divided into the muscle sequence of the stance phase and the sequence of the swing phase. Additionally, the muscle activation needed for controlling the foot joint can be taken into consideration. During stance phase, three main activities are performed by the muscles: 1.) swing to stance transition at the terminal swing phase, 2.) weight acceptance during initial contact and loading response, and 3.) progression over the supporting foot during mid stance, terminal stance, and start of pre swing [58]. The corresponding muscle activation sequences of the upper leg can be seen in Table 1:

Muscle	On (% of gait cycle)	Peak (% of gait cycle)	Off (% of gait cycle)
Anterior tibialis	56	0	13
Semimembranosus	81	88	15
Biceps femoris long head	82	93	5
Semitendinosus	88	98	17
Vastus medialis oblique	89	6	14
Vastus lateralis	90	8	16
Vastus medialis longus	91	4	16
Vastus intermedius	95	8	20
Adductor magnus	92	1	7
Gluteus maximus, lower	95	3	10
Gluteus maximus, upper	95	3	24
Gluteus medius	96	7	29
Posterior tibialis	0	44	50
Soleus	7	43	52
Gastrocnemius	9	40	50
Flexor digitorum longus	1	47	54
Peroneus longus	15	41	51
Peroneus brevis	20	46	55
Flexor hallucis longus	31	49	54

Table 1: Muscle activation sequence during stance, adapted from [58]

The swing phase is initiated by the pre swing and limb advancement is accomplished during this phase. The muscle activation patterns with regards to the gait cycle, in particular the swing phase, can be seen in Table 2.

Muscle	On (% of gait cycle)	Peak (% of gait cycle)	Off (% of gait cycle)
Adductor longus	46	50	77
Gracilis	50	69	4
Rectus femoris	57	59	65
Sartorius	60	65	71
Iliacus	63	69	74
Biceps femoris short head	65	71	82
Anterior tibialis	56	0	13
Extensor digitorum longus	57	70	12
Extensor hallucis longus	58	74	9

Table 2: Muscle activation sequence during swing, adapted from [58]

Throughout the stance phase, the foot joints must be stabilised and are supported by the muscles of the lower leg. Furthermore, the swing and stance phase requires the foot to fulfil movements such as plantar and dorsiflexion, inversion and eversion. The according muscles and their activation sequence can be seen in Table 3.

Muscle	On (% of gait cycle)	Peak (% of gait cycle)	Off (% of gait cycle)
Anterior tibialis	56	0	13
Extensor digitorum longus	57	70	12
Extensor hallucis longus	58	74	9
Posterior tibialis	0	44	50
Soleus	7	43	52
Gastrocnemius	9	40	50
Flexor digitorum longus	13	47	54
Peroneus longus	15	41	51
Peroneus brevis	20	46	55
Flexor hallucis longus	31	49	54

Table 3: Muscle activation sequence of the foot joints, adapted from [58]

2.3 Electrical Stimulation

For the treatment of patients with neurological disorders, various types of electrical stimulation can be used. The most common terms for electrical stimulation are: electrical muscle stimulation (EMS), neuromuscular electrical stimulation (NMES), motor electrical stimulation (MES), functional electrical stimulation (FES), and transcutaneous electrical nerve stimulation (TENS). The terms EMS and NMES are similar as both describe the creation of isolated muscle contraction using electrical impulses. In TENS, electric current is mainly used to stimulate the nerves for therapeutic purposes such as the reduction of pain [41]. The term MES refers to the production of a muscle contraction by the use of electrical stimulation [41]. Furthermore, MES can be differentiated into two subsections whereas one section refers to electrical stimulation which is applied to the nerve (electrical stimulation of innervated muscles) and the other section refers to electrical stimulation which is applied directly to the muscles (electrical stimulation of denervated muscle). In FES, the main goal of the applied electrical impulses is the production of a functional movement such as walking or grasping. However, all abbreviations mentioned above refer to the same basic principle—the application of electrical impulses to increase or decrease the muscular activity or the activity in the CNS. The differentiation between the terms is not unified in the literature and mainly depends on the intended use of the stimulation. A detailed elaboration of the inconsistencies of the terminology and its application can be found in [59].

2.3.1 Functional Electrical Stimulation

After a damage of the CNS (brain or spinal cord, section 2.1), the transmission of motor commands to the muscles in the periphery can be interrupted. In case the innervating nerves of the muscle are intact, a localized external electrical field can be applied to replace the missing physiological signal. The method of applying an external electrical impulse to generate muscle contraction of paralyzed muscles with the aim to mimic a functional movement such as walking or grasping is termed functional electrical stimulation (FES). Referring to the terms introduced in section 2.3, FES can also be described as organised and patterned NMES with the aim to create a coordinated movement [60]. Furthermore, the application of FES can refer to the restoration of functions of the human sensory system such as auditory or visual neuroprostheses. In order to replace the interrupted pathway between the CNS and the peripheral muscles, the applied electric field generates an artificial action potential. This AP depolarises the neuromuscular junction which

ultimately leads to a functional muscular contraction. The device creating the artificial AP is placed on the motor neuron (lower motor neuron) of the affected muscle and the energy is transmitted via stimulation electrodes (Figure 10).

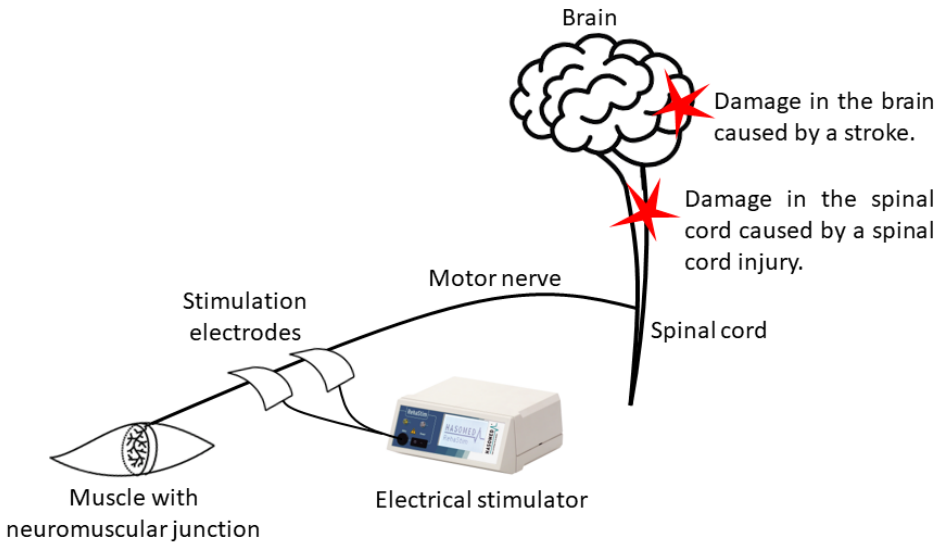

Figure 10: Schematic representation of a surface FES system

FES applications for motor functions generally activates rather nerve (electrical stimulation of innervated muscles) than muscle fibres (electrical stimulation of denervated muscle) [61]. A reason for that is that the threshold for producing AP in neurons is lower compared to muscle fibres (Figure 11). Furthermore, FES usually only benefits patients with an intact lower motor neuron (spastic paraplegia). Patients who suffer from a flaccid paralysis often have a very low response to electrical stimulation and thus FES does not support their treatment [62].

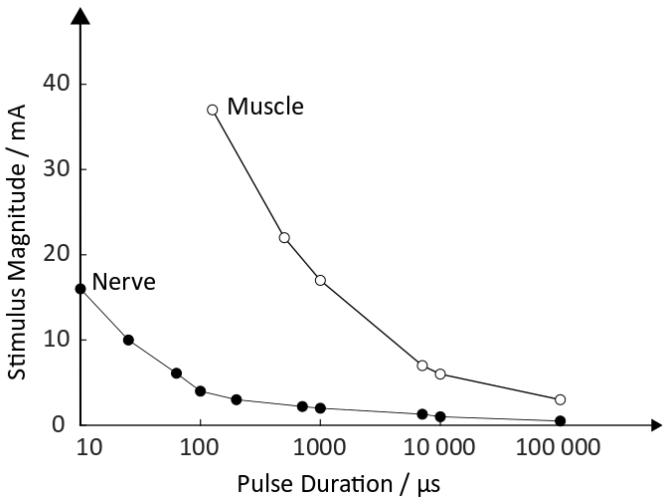

Figure 11: Strength-duration curve of a denervated cat tibialis anterior muscle [61]

The clinical use of FES is broad and depending on the field of application, the efficacy of the treatment can be determined. Especially the use of FES combined with other technologies such as robot-assisted gait training or cycling seem to be a promising rehabilitation modality for the future rehabilitation.

2.4 Robotic Gait Training

Since high repetition in the movement pattern tends to play a significant role in the recovery of walking function [63], rehabilitation approaches such as body-weight-supported treadmill training (BWSTT) which provide a highly repetitive movement seem to be a promising training method. In BWSTT (Figure 12), the bodyweight of the subject is supported by a harness and a control unit while the lower limbs are moved and guided by therapists.

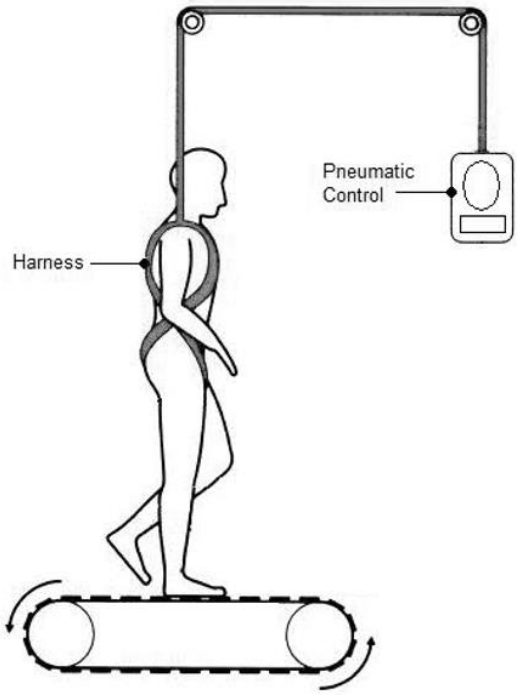

Figure 12: Body-weight-supported treadmill training (BWSTT), adapted from [64]

BWSTT can improve walking function for patients after stroke or SCI [65,66]. Moreover, the LEAPS study which included more than 400 stroke patients showed the superiority of BWSTT followed by overground training compared to conventional care with regard to the walking ability of the patients [12]. Despite the positive aspects of BWSTT, the therapy setting is labour-intensive as it mostly requires two therapists (one therapist per lower extremity). Additionally, the non-ergonomic working posture of the therapists and the high physical effort needed to move the lower extremities of the patient may limit the duration of the training due to exhaustion of the therapist.

Rehabilitation technologies such as robot-assisted gait training (RAGT) also termed robotic gait training can compensate the aforementioned drawbacks of BWSTT by guiding the gait cycle of the patient with a robot-specific movement strategy. This may lead to longer training time as the physical exhaustion of the therapist is minimized. Longer training

durations have shown to provide positive effects on the activities of daily living (ADLs) [66,67]. Additionally, the therapist can focus on other aspects of the rehabilitation such as correct breathing or the posture of the patient and robot-assisted gait trainer may offer the possibility to use technologies like virtual reality to enhance the participation of the patients during therapy [68]. Furthermore, robots can provide objective data using embedded sensors of the individual device which may be used to overcome some limitations of traditional clinical assessments [69]. Two successive systematic reviews dedicated to RAGT for walking after stroke conclude that the combination of RAGT and conventional physiotherapy is more effective in achieving independent walking in stroke survivors with gait disorders compared to patients who did not receive robotic gait training [6,7]. Additionally, neural plasticity as mentioned in section 2.1.6 can be enhanced as robotic gait training allows high-dosage and high-intensity training [70]. The movement principle of the robotic devices categorises the specific robots; so far there are two main groups: exoskeletal robotic systems and end-effector-based systems [5].

Exoskeletal robotic systems: In an exoskeletal robotic system, the joints of the patients (knee and ankle) are moved to produce the gait pattern. They are designed in a way that the mechanical structure of the device is similar to the human anatomy of lower limbs and the corresponding joints [71]. Most of the segments of the exoskeleton can be adjusted to the individual subject. This individual adjustment offers a high flexibility but also increases setup time. A crucial point concerning the setup is the alignment as the segments of the exoskeleton have to be carefully aligned with the joints of the subject in order to generate a physiological walking movement. Typical examples for exoskeletal robotic systems are depicted in Figure 13.

Figure 13: Left: Lokomat (Hocoma, Volketswil, Switzerland)
Right: ReoAmbulator (Motorika, Mount Laurel, USA)

End-effector-based systems: In end-effector-based systems, also termed controllers of endpoint trajectories, solely the feet of the subject are moved by the robot, the knee joint is not connected to a mechanical structure of the robot [5]. The subject's leg is usually fixed to footplates the trajectories of which simulate the movement. On the one hand, these systems are easy to adjust to different subjects and reduce donning time compared to exoskeletal systems; on the other hand, subjects may lack in movement guidance as the hip and knee joints are not guided by the robot. Typical examples for these systems are depicted in Figure 14 and Figure 15.

Figure 14: Left: Lyra (Thera Trainer, Hochdorf, Germany)
Right: G-EO (Reha Technology AG, Olten, Switzerland)

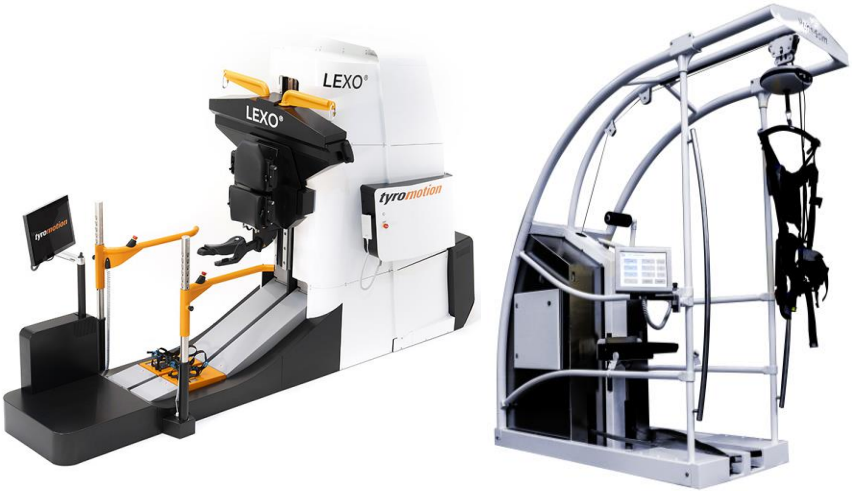

Figure 15: Left: LEXO® (Tyromotion, Graz, Austria)
Right: Gangtrainer GTII (Reha-Stim Medtec, Schlieren, Switzerland)

Despite the positive aspects of RAGT, drawbacks must be mentioned as well. Compared to manually assisted therapy, the guided movement of RAGT may decrease metabolic costs of the subject during training. However, these differences can be minimised when the patients are asked to maximise their effort during robotic therapy [72]. Thus, it could be possible that the guided training promotes slacking which would decrease the effect of recovery [71]. Furthermore, RAGT could cause alterations in the naturally occurring muscle activation patterns [8]. Additionally, the robot-induced movement and the weight support system can partially impede muscle activity [9]. Some of these drawbacks have already been tackled by introducing new developments for the individual robots. Examples in this regard are change of the guidance force and FreeD mode of Lokomat, the biofeedback mode of Lyra, the support of active walking of LEXO and the active-assistive/active mode of G-EO. These control strategies are aiming on supporting the patients' efforts and encouraging the self-initiation of movements. As a result, all strategies aim to prevent the "learned non-use phenomenon" (Figure 16) of the affected side.

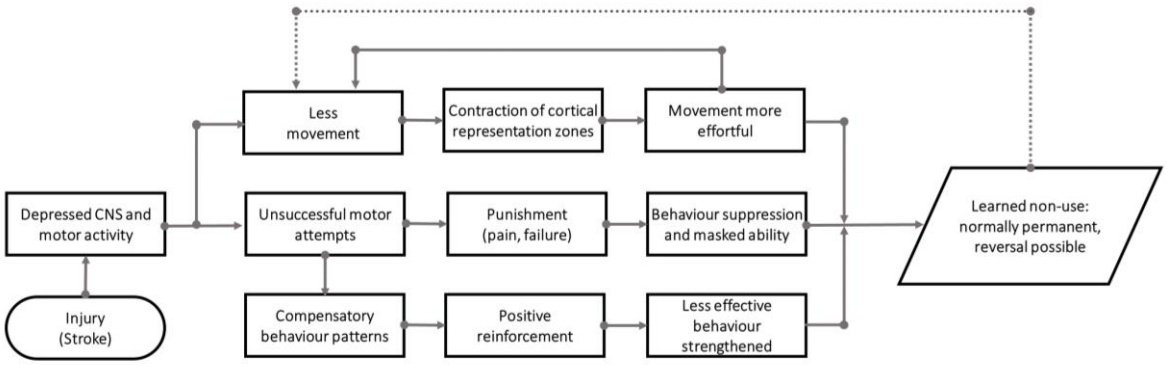

Figure 16: Development of learned non-use phenomenon [73]

Overground gait training: The mentioned robotic systems specify the trajectory of the feet and lower limbs and guide the movement of the subject. As there is no clear evidence that a fixed gait pattern is the best approach to maximise brain plasticity, studies which investigated a more functional training approach including overground walking were performed [74,75]. Based on the results of the performed investigations, overground gait training seems to be another valuable technique for gait rehabilitation. Depending on the degree of disability and the stage of rehabilitation, devices such as Andago or FLOAT (Figure 17) enable the subject to move more freely compared to the gait robots mentioned so far. These systems include a body strap attached to a supporting system which catches the patient in case of falling.

Figure 17: Left: FLOAT (Reha-Stim Medtec, Schlieren, Switzerland)
Right: Andago (Hocoma, Volketswil, Switzerland)

Furthermore, ambulatory exoskeletons such as EksoGT and ReWalk (Figure 18) which both provide overground walking must be mentioned. Another positive aspect for ambulatory exoskeletons is that they could provide more physiological movement and allow patients to move around in an environment that is similar to their home environment [5].

Figure 18: Left: EksoNR™ (Ekso Bionics, Richmond, USA)
Right: ReWalk (ReWalk Robotics, Yokneam, Israel)

Most of the devices require a specific training for safe and effective usage and all have their specific field of application in the context of rehabilitation. Their usage must be carefully adjusted to the patients' needs and to the specific goal of the rehabilitation.

2.5 Inertial Measurement Units

Inertial measurement units (IMU) are physical sensors which typically contain three orthogonal accelerometers and three orthogonal gyroscopes, enabling the sensors to measure linear acceleration and angular velocity. Additionally, some IMUs provide magnetometers offering the possibility to measure the local gravitational field. IMUs collect the raw data in their local coordination system (Figure 19).

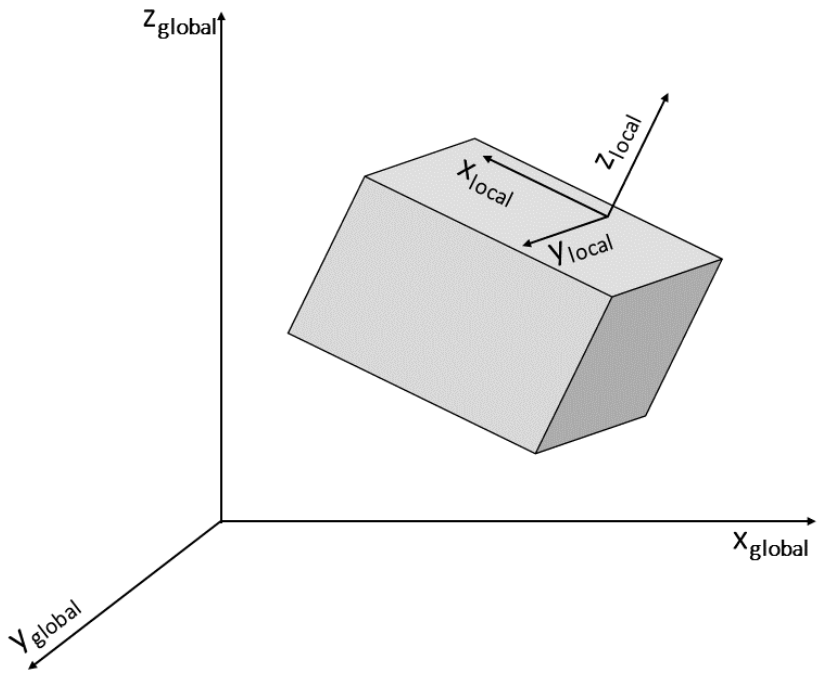

Figure 19: Global and local coordinate system

The local coordinate system of most sensors is a cartesian coordinate system (right hand rule [76]) by default, the global coordinate system can be defined as a cartesian coordinate system as well and represents the earth-fixed coordinate system.

A sensor rigidly attached to a body is commonly termed strapdown system. For strapdown systems, it is necessary to define the coordinate system of the body. Depending on the application and the targeted body, the body coordinate system should be chosen reasonably so that it can reflect the movement of the object. A schematic representation of a strapdown system can be seen in Figure 20.

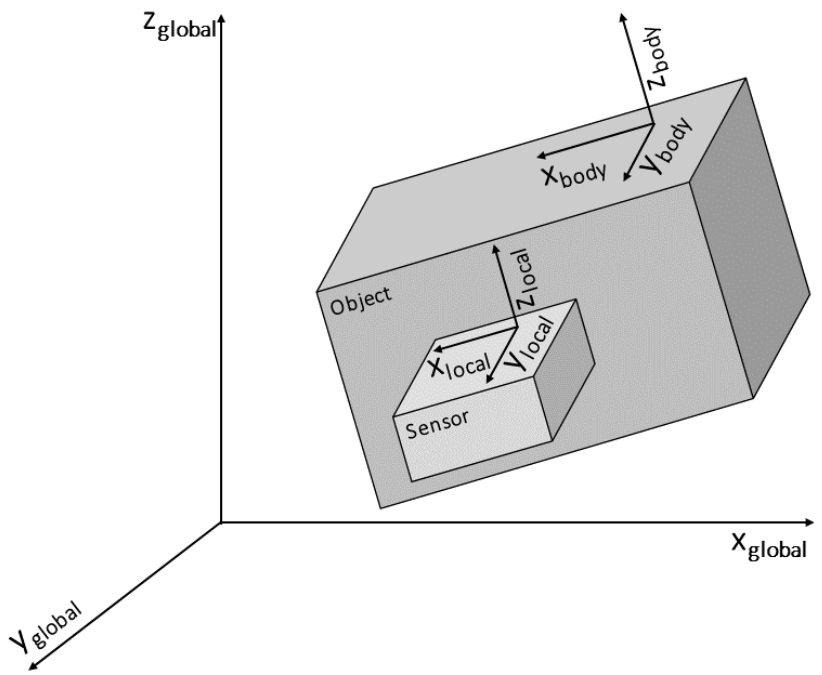

Figure 20: Strapdown system

For most applications with a moving body, it is necessary to align the local coordinate system of the sensor with the body coordinate system of the moving object to guarantee that the gathered data reflects the targeted movement. For that purpose, two approaches can be used.

1. The sensor can be tightly attached to the object and the coordinate system can be aligned manually.
2. The current alignment of the sensor in respect to the object can be determined and the coordinate systems can be aligned mathematically using a rotation matrix.

Both approaches aim to align the coordinate systems to enable a recording of data in the body coordinate system, yet the latter option is desirable under real conditions as it allows flexibility in the attachment. Furthermore, it offers the possibility to repeat the process throughout the measurements allowing the alignment of the coordinate systems to be adjusted frequently. Thus, slight movements of the sensor attachment are less likely to cause errors in the recording sessions. The used mathematical approach within this work is presented in section 5.

3 State-of-the-Art

The state-of-the-art section aims to address the current research in the related topics gait event detection methods with wearable sensors and hybrid robotic rehabilitation systems whereas both topics will be addressed individually. Section 3.1 and 3.2 will introduce current methods used for gait event detection in various applications, section 3.3 will provide a comparison of the relevant algorithm approaches. The last section will provide an overview of hybrid robotic rehabilitation systems available on the market.

3.1 Gait Recognition Methods with Wearable Sensors

Wearable sensors such as IMUs, force sensors and EMG sensors can be used as a clinical tool for rehabilitation approaches, for sports activities to optimise movement patterns, in movement sciences to assess movement disorders and various other fields. The following paragraphs reviews state-of-the-art approaches of wearable sensors for the use in gait event detection / gait recognition.

3.1.1 Inertial Measurement Units

IMUs as described in section 2.5 are small and rugged devices which can be easily attached to an object in order to measure the object's movement. Despite the possibility to gather three different kinds of data (liner acceleration, angular velocity and magnetic field), a lot of gait phase classification methods solely use acceleration data [77–82] or gyroscope data alone [83–92]. However, the combined use of angular velocity and linear acceleration data, with the aim to enhance the robustness of the algorithms, has increased over the last years [93–97]. Additionally, the sensor positions such as pelvis, feet, shank can influence the chosen algorithm approach [78].

3.1.2 Electromyography Sensors

Electromyography (EMG) sensors assess the activity of the muscle by recording the electrical impulses of the muscles and the corresponding nerves. Approaches for gait event detection mostly use surface electrodes as intramuscular electrodes would interfere with

the movement and cause pain. Due to difficulties in data acquisition such as electrode positioning, displacement of electrodes during movement and muscle variations, EMG sensors are less commonly used for gait event detection. However, some approaches provide promising results for the implementation of EMG sensors in gait recognition algorithms [98–102].

3.1.3 Force Sensors

Force sensors are often placed inside the shoe or under the foot of a subject and assess the contact between the sensor and the ground. These can be binary switches, single Force Sensing Resistors (FSR) or full pressure insoles which can be adjusted to the subject's shoe size. Force sensors have been used within several approaches for gait event detection [94,103–109]. Despite their high accuracy, approaches for applications in everyday life are not yet considered suitable due to their limited lifetime. Additionally, when using pressure insoles, a large variety of different insoles must be available in order to cover different shoe sizes. However, due to their high accuracy, force sensors are often used as reference systems for validation studies [83,93,94].

3.2 Detection Methods

Threshold methods and machine learning methods are two main categories for gait event detection methods. Threshold methods use the identification of peak values and other characteristics to classify the gait events according to certain thresholds. Machine learning approaches use models such as Hidden Markov Models (HMM) and Neural Networks (NN) for gait event detection. Threshold methods are mostly easy and lightweight, machine learning approaches are more elaborate, need more data and require more computational power. Threshold approaches can be categorised in two main groups such as computation threshold methods where different kinds of thresholds are used to detect certain characteristics of the gait phases [77,83,93,97,110–113] and time-frequency analysis based on thresholds [94,114–117]. Machine learning approaches such as HMM and neural networks are amongst the most popular used for the recognition of gait events. Approaches using HMM for gait recognition are described in [84–87,103,104,118,119]. Approaches with artificial neural networks for gait event detection can be found in [85,98,120,121].

3.3 Comparison

When comparing different approaches, it is of importance, whether the gait event detection algorithm is used offline or online. Online algorithms provide the possibility to detect the gait events in real time whereas offline algorithms at first gather the data and have a downstream recognition of gait events. Table 4 provides a comparison of online and offline algorithms (using signals from IMUs) in terms of the methods used, the gait events detected and the amount and location of the used sensor technology.

Publication	Method	Detected events	Amount / Location of IMUs	Detection
[85]	FNN/HMM	IC, FC, HO, TO, MS	Seven / Feet, shanks, thighs, pelvis	Online
[86]	HMM	IC, FC, HO, TO	Four / Foot, shank, thigh, waist	Online
[93]	Threshold	IC, TO, HO	One / Shank	Online
[115]	Heuristic approach, Frequency analysis	IC, TO	One / Shank	Online
[117]	Threshold, LDA, QDA	IC, TO	One / Shank	Online
[122]	Threshold	IC, FC, HO, TO	One / Foot	Online
[123]	Threshold	IC, TO, MS	Two / Feet	Online
[124]	Threshold	IC, TO	One / Foot	Online
[77]	Thresholds	LR, MSt, PS, SW	One / Foot	Offline
[79]	NN	ST, SW	Three / Foot, calf, shank	Offline
[87]	HMM	IC, LR, MS, TS, PS, SW	Two / Foot, Shank	Offline
[94]	Time-Frequency analysis	IC, TO	One / Foot	Offline
[118]	HMM, Threshold	IC, FC, HO, SW	One / Foot	Offline
[119]	HMM	IC, FC, HO, TO	One / Foot	Offline
[125]	NN	Left and Right: initial-SW, middle-SW, terminal-SW, double-ST,	Four angular sensors/ knees, hips	Offline
[126]	Heuristic based	IC, TO, MSt, MS	One / Foot	Offline
[127]	NN, HMM	IC, FC, MSt, HO, TO, SW	Two / Feet	Offline
[128]	NN	IC, LR, FC, HO, initial SW	Three / Foot, Calf, Thigh	Offline

Table 4: Online and offline algorithms for gait event detection.
IC: Initial contact, FC: Full contact, HO: Heel off, TO: Toe off, MS: Mid swing, TS: Terminal swing, PS: Pre swing, SW: Swing phase/swing, MSt: Midstance, ST: Stance phase/period

All online approaches in Table 4 aim to detect human walking including overground walking, walking on a treadmill and walking detection of subjects with particular gait impairments such as an amputated leg. The reported metrics are heterogenic. In [85] the sensitivity (true positive rate: 88.49%) and the specificity (true negative rate: 97.12%) compared to an optical marker system were reported. The approach described in [86] was analysed towards the detection latency (45ms early detection and 35ms late detection) of gait events compared to an optical marker system. The combination of detection rate (100%) and detection latency (±50ms) compared to a pressure insole were reported in [93]. The F1 score, a metric derived from a relation between true-positives, true-negatives and false-positives, was analysed in [115] (F1 scores of 0.95-0.98). In [117] the early and late detection compared to force plates as metrics of frequency error (8.2%) and temporal error

(0.2%) were reported. Latency measures in terms of mean recognition delays (0.1-0.05s) compared to an optical marker system were reported in [122]. Similar to [115] in [123] F1 scores (0.998-0.944) compared to a pressure walkway were reported, additionally the analysis included mean detection delays below 31ms. The approach in [124] was validated against foot switches and the analysed metrices were latency measures which detected early (-8ms) and late contact (13ms).

Despite the wide usage of IMUs for gait recognition, the majority is focussed on detecting gait during walking of healthy people or aim to detect particular movements of patients who have gait deficits. To date, there are no algorithms designed to detect a robot-specific movement pattern using IMU data. As a result, the approaches are not directly comparable to the approach within this work. Thus, a detailed comparison of the different existing methods was not performed. Yet, in order to compare the outcome metrics, the detection rate including true-positives and false-positives measures as used in a majority of the approaches were chosen for the analysis of the recorded data within this work.

3.4 Hybrid Robotic Rehabilitation Systems

As mentioned in 2.4, robot-assisted gait trainers are classified regarding their principle of motion. Combinations of RAGT and FES are conventionally termed hybrid robotic rehabilitation systems. Hybrid robotic rehabilitation systems can be further differentiated in how they transmit energy to the patient. In this chapter, only hybrid systems where the electrical stimulation and the robot are both torque-generating devices are taken into account. In addition, all mentioned approaches are partially or fully available in the market. Systems where electrical stimulation is the main source of torque generation while the robotic system only acts as a passive device are excluded as they are not comparable to the developed concept within this work.

3.4.1 Lokomat

Several different approaches combining the Lokomat (Figure 13) with FES have been investigated so far (Table 5).

The first approach used a finger switch controlled by the patient or the therapist for synchronising the Lokomat and the stimulator [33]. Eight muscles (eight channels) were stimulated using intramuscular electrodes (IM) and the stimulator was worn on a belt. The patient or the therapist activated the finger switch at every heel-strike in order to provide FES therapy during training. Despite proven feasible, the approach still was subject to human error. Thus, the approach was further developed and an automatic synchronisation was introduced [25]. The onset of the stimulation was triggered by a pulse created by the robot itself at each right initial contact. This information was sent to an external device which initiated the stimulation. According to [25] in order generate a feasible stimulation, the latency of the stimulation must be short enough to ensure that the stance muscles are activated prior to loading more than 50% of body weight onto the stance limb. Otherwise, the control of the stance phase in the knee could not be performed during the loading of the limb. For healthy adults, the acceptance of 50% of the weight is reached after 5% of the gait cycle [129]. The mean latency between the recognition of the initial contact and the actual electrical impulse was 69.05ms ± 12ms. The time for one gait cycle of the Lokomat was 2.6s. As a result, the latency was only 2.5% of the gait cycle. Thus, this approach was considered feasible; additionally, it was more accurate and repeatable compared to the manually triggered stimulation. Yet the electromechanical delay of the muscles was not considered within this work. A further approach was developed in order to correct foot drop during Lokomat training [26]. In contrast to the approach mentioned before, surface

electrodes on the peroneal nerve on the hemiparetic leg were used (one channel). Similar to the approach mentioned before, synchronisation of the FES was realised using the output signals (rectangular pulse) of the Lokomat. The ascending of edge of the pulse of the output signal indicating the beginning of the stance phase triggered the onset of the stimulation of the contralateral leg allowing the peroneal nerve to be stimulated. The stimulation was stopped when the ascending pulse of the ipsilateral leg was triggered. As a result, during the swing phase a dorsiflexion of the foot was achieved. This approach is considered feasible and was tested in clinical practice [27].

Publication	**Synchronisation approach**	**Number of stimulated muscles/nerves**	**Feasibility and clinical application**	**Commercial availability with FES**
[33]	Finger switch operated by patient or therapist	Eight (IM): tibialis anterior, peroneus longus, lateral head of the gastrocnemius, short head of the biceps femoris, semitendinosus, semimembranosus, vastus lateralis, gluteus medius	Feasibility study with six subjects (stroke) Clinical application: Yes	No
[25]	Synchronised using information provided by robot—gait event control.	Eight (IM): tibialis anterior, peroneus longus, lateral head of the gastrocnemius, short head of the biceps femoris, semitendinosus, semimembranosus, vastus lateralis, gluteus medius	Feasibility, reliability and consistency was valuated. Bench testing only. No subject involved. Clinical application: No	No
[26], [27]	Synchronised using information provided by robot—gait event control.	One (SE): Peroneal nerve at the hemiparetic leg	[26]: Feasibility study with three subjects (one stroke patient, two healthy subjects). [27]: Feasibility study with five patients (acquired brain injury) Clinical application: Yes	No

Table 5: Lokomat: Hybrid robotic rehabilitation system

3.4.2 Gangtrainer GT II

Approaches to combine the end-effector based gait rehabilitation system Gangtrainer GTII (Figure 15) with FES are similar to the approaches of Lokomat (Table 6). The FES is gait-phase controlled using information provided by the robot. The gait trainer was linked with two wires to the FES stimulators. This connection was used to guarantee synchronisation between the gait phases and the stimulation [28]. During the stance phase, the stimulation was used to activate the quadriceps femoris. The common peroneal nerve received electrical stimulation during the swing phase. This approach was evaluated in a randomised clinical controlled trial with 54 subjects who suffered from stroke and the concept was considered feasible.

Publication	Synchronisation approach	Number of stimulated muscles/nerves	Feasibility and clinical application	Commercial availability with FES
[28],[130]	Synchronised using information provided by robot—gait event control.	Two (SE): quadriceps femoris, nervus peroneus	[28]: Case report with two subjects (stroke) [130]: randomised clinically controlled trial with 54 subjects (stroke)	Yes

Table 6: Gangtrainer GT II: Hybrid robotic rehabilitation system

3.4.3 WalkTrainer

The WalkTrainer (Figure 21) is a commercially available gait trainer with an integrated electrical stimulator for additional FES treatment (Table 7). In contrast to the aforementioned stationary devices, the WalkTrainer is used for overground ambulation [29]. The stimulation was triggered by a feedback controller. An update of the muscle stimulation was done at every step to minimise the users-applied force between the user and the orthosis [30].

Publication	Synchronisation approach	Number of stimulated muscles/nerves	Feasibility and clinical application	Commercial availability with FES
[29], [30], [31]	Feedback controller to minimise interaction forces.	Seven (SE): Gluteus maximus, rectus femoris, castus medialis, vastus lateralis, hamstrings, tibialis anterior, gastrocnemius	[31]: Clinical trial with 6 subjects (paraplegic)	Yes

Table 7: WalkTrainer: Hybrid robotic rehabilitation system

3.4.4 MotionMaker

MotionMaker (Figure 21) is a stationary robotic system for active mobilisation of the lower limbs and incorporates interactive and variable FES (Table 8). Synchronisation is realised using position and force sensors mounted on the orthosis of the system. This concept was tested with 5 patients (press-leg exercises) [32], yet it does not provide upright walking.

Figure 21: Left: MotionMaker (Swortec, Monthey, Switzerland)
Right: WalkTrainer (Swortec, Monthey, Switzerland)

Publication	Synchronisation approach	Number of stimulated muscles/nerves	Feasibility and clinical application	Commercial availability with FES
[32]	Feed-forward controller using position and force sensors.	Five (SE): gluteus maximus, quadriceps, gastrocnemius, hamstrings, tibialis anterior	Clinical trial with 5 subjects (4 incomplete and 1 with complete spinal cord lesion)	Yes

Table 8: MotionMaker: Hybrid robotic rehabilitation system

3.4.5 G-EO

The G-EO (Figure 14) is an end-effector based system with optional functional electrical stimulation (Table 9).

Publication	Synchronisation approach	Number of stimulated muscles/nerves	Feasibility and clinical application	Commercial availability with FES
Information gathered from the website and product catalogue	Synchronised using information provided by robot—gait event control.	8 (SE)	-	Yes

Table 9: G-EO: Hybrid robotic rehabilitation system

3.4.6 RT 600

The RT600 (

Figure 22) is an upright therapy system which fully incorporates an FES therapy system (Table 10).

Figure 22: RT 600 (Restorative Therapies, Baltimore, USA)

Publication	**Synchronisation approach**	**Number of stimulated muscles/nerves**	**Feasibility and clinical application**	**Commercial availability with FES**
Information gathered from the website and product catalogue	Synchronised using information provided by the robot—gait event control.	Up to 12 (SE): Quadriceps, hamstrings, gluteals, gastrocnemius, anterior tibialis, abdominals and back muscle groups for core strength, stability, and postural correction	-	Yes

Table 10: RT 600: Hybrid robotic rehabilitation system

4 Materials and Methods

In this chapter, the robotic systems and the measurement devices used throughout this work are described in sections 4.1, 4.2 and 4.3. The developed algorithm including the arbitrary sensor alignment, dynamic adaptions and methods to enhance the confidence of the algorithm are elaborated in section 5.

4.1 Robotic Systems

Within this work, an algorithm for gait recognition during robotic gait training is developed. For developing and testing the algorithm and for conducting experiments and a clinical trial, two robotic systems—one exoskeletal-based system and one end-effector-based system—were considered. These robotic systems are described in detail in sections 4.1.1 and 4.1.2. The information within the following sections is mainly based on information provided by the user manuals of the individual gait trainers or on information provided by specially trained therapists of MEDIAN rehabilitation clinic in Magdeburg.

4.1.1 Lokomat

The Lokomat is an exoskeletal robotic gait trainer (section 2.4). It is comprised of a body strap, robotic orthosis for the guidance of the lower limbs and an electric treadmill. The system is considered to be is a state-of-the-art gait robot [6] which offers effective gait training [131]. The cyclic gait pattern is induced by programmable actuators located in the mechanical structure of the robot. The Lokomat is a medical device used in clinic and rehabilitation centres. According to the manufacturer, it provides a highly intensive physiological gait rehabilitation for severely impaired neurological patients. The orthosis is adjusted by specifically trained therapists and each patient has their own settings. All settings can be stored within the terminal of the Lokomat. During therapy, further parameters such as the speed and the guidance force can be adjusted throughout rehabilitation.

Speed: The speed defines the speed of the treadmill in kph and thus can be considered as the walking speed of the patient during training. The default value for this gait trainer is 1.5 kph. When using orthosis, the walking speed can be changed from 0.5 to 3.2kph. Based on to the speed of the treadmill, the orthosis speed can be adapted. The adaption of the

speed of the orthosis allows to individualise the patient cadence and is utilized for the synchronisation of orthosis and treadmill. This setting is adjusted through the graphical user interface (GUI) of the Lokomat with a digital slider.

Guidance force: The guidance force determines the percentage of guidance with which the robotic orthosis guides the motion of the patient's leg during therapy. A guidance force of 100% means that the forces are acting in such a way that the patient cannot deviate from the induced trajectory. A low guidance force requires more active involvement of the patient to follow the walking pattern.

Types of the device: Two types of the Lokomat are existing on the market—LokomatNanos and LokomatPro. Within this work, LokomatPro was used. LokomatPro includes the aforementioned FreeD module which allows the patient a lateral translation and transverse rotation of the pelvis. Depending on the patient, the FreeD module can be activated or deactivated. Within this work, the activation/deactivation of this module was not further investigated.

4.1.2 Lyra

The Lyra is an end-effector based robotic gait trainer (section 2.4). It consists of a harness and adjustable foot plates. Compared to conventional gait training, robotic gait training with end-effector systems have shown to have a superior effect with regard to ADLs and gait parameters [132]. Similar to Lokomat, Lyra is a medical device used in clinics and rehabilitation centres. According to the manufacturer, it provides a physiological pattern and is the gait trainer with the highest net therapy time as the ground-level access allows a very easy and short transfer. The foot plates and the according foot bindings are adjusted by specifically trained therapists. The bindings are fixed with adjustable straps to ensure firm support. During therapy, the speed of the footplates can be adjusted.

Speed: The speed defines the speed in kph at which the patient walks during the training. Furthermore, it can be changed to steps/min. Within this work, the kph setting was used. The speed is adjusted with a digital slider and the maximum speed is 4kph or 100steps/min.

Biofeedback module: The biofeedback module recognises the training intensity and analyses the individual activity level of the patient. The patient can therefore influence the training intensity by increasing, holding or reducing their own activity. Depending on the patient, the biofeedback module can be activated or deactivated. Within this work, the activation/deactivation of this module was not further investigated.

4.2 MotionSensor

For data recording, two IMUs (MotionSensor, HASOMED GmbH, Magdeburg, Germany) were used. Each sensor consisted of a three-axis accelerometer (± 8g) and a three-axis gyroscope (± 1000°/s) [35]. A sampling frequency of 500Hz was chosen for the recordings. For the synchronisation of the IMUs, an inbuilt Bluetooth clock form the device was used.

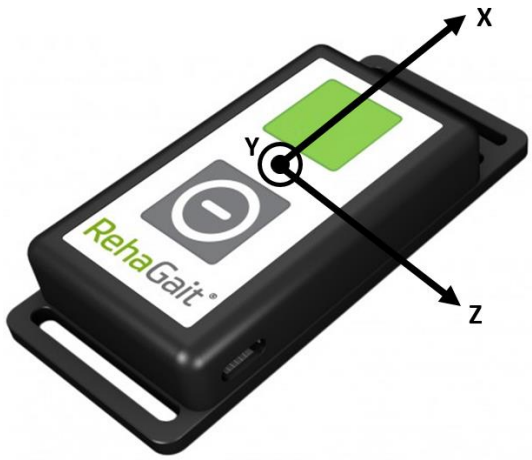

Figure 23: MotionSensor with its local coordinate system

The sensor and the commercially available software RehaGait Analyzer are medical devices according to the medical device directive (Council Directive 93/42/EEC of 14 June 1993 concerning medical devices). The accuracy of the device is clinically tested and has been published in several scientific studies [34,35]. For the fixation of the sensor, a custom-made fixation strap as seen in Figure 40 was used. The fixation strap is adaptable in its length which allows the application for a wide variety of shoe sizes. Within this work, the software of the RehaGait Analyzer was solely used for data recording.

4.3 Electrical Stimulator

RehaStim (HASOMED GmbH, Magdeburg, Germany) is a current-controlled stimulation device for functional electrical stimulation (Figure 24). The stimulator can be equipped with surface electrodes to stimulate paralysed muscles. The device has a certificate according to the EU guideline EN60601-2-10 for medical technical devices and systems. The stimulator can be used as a standalone device. Additionally, the stimulator can be controlled by external devices and has been used in current research [133]. The stimulator has two independent stimulation modules whereas each module has its own current source. The stimulation modules are named A (channel 1-4) and B (channel 5-8), and each module incorporates a microprocessor for the timing of the pulse. Thus, the pulse generations of modules A and B are independent from each other, and stimulation can be triggered simultaneously.

Figure 24: Electrical stimulator (RehaStim)

RehaStim provides stimulation impulses ranging up to 130mA. The step size of the adjustable current is 2mA. Stimulation frequencies range between 10Hz and 50Hz, the according step size is 5Hz. The pulse width (pulse duration) can be set from 20µs up to a maximum pulse width of 500µs. The step size of the pulse width is 1µs. The generated impulses of the simulator are biphasic and rectangular as visualised in Figure 25. This distinct shape is used to guarantee charge neutrality when applying the stimulation. A fixed pause of 100µs is pre-defined by the stimulator. Before a stimulation pulse is sent to the electrodes, a skin resistance check is performed for safety reasons of the user. In case the resistance check fails, no stimulation is generated. According to the manufacturer, the stimulator has a maximum internal latency of 2ms.

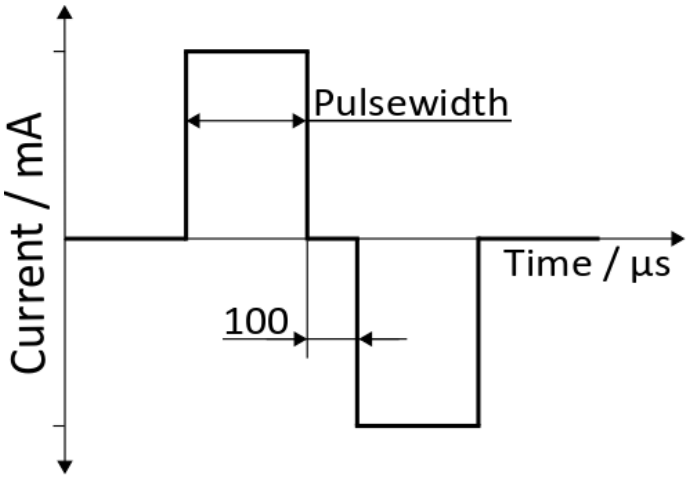

Figure 25: Biphasic rectangular pulse

Furthermore, the stimulator offers three pulse generation modes for altering the frequency. The different modes are described in more detail in section 5.6.1. Thus, a wide range of settings is given, which allows clinicians and researchers to customise the parameters based on their needs.

5 Results

The aim of the developed concept is to stimulate paralysed muscles of patients during robotic therapy by using extracted gait events as a trigger for FES. A schematical representation of the concept is visualised in Figure 26.

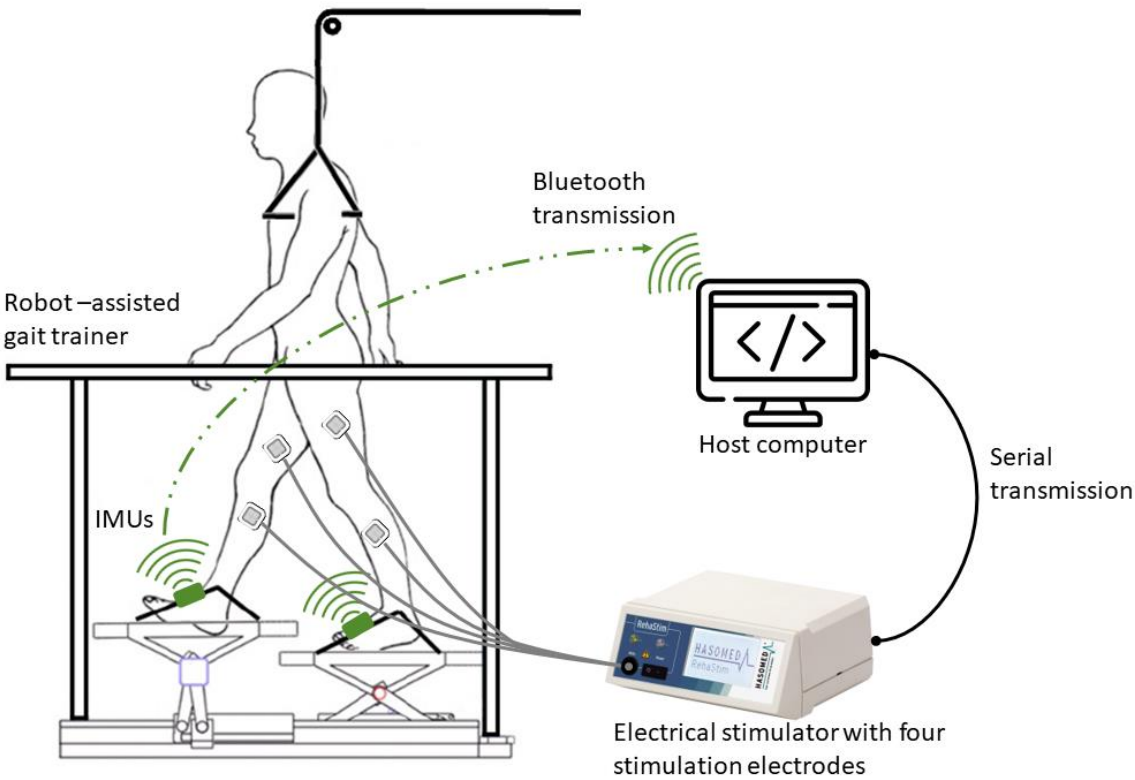

Figure 26: Concept: Robotic gait training with IMUs to trigger FES

The development of the concept can be divided into six parts with individual results as follows: The first part elaborates the development and training of the gait event detection algorithm and an arbitrary sensor alignment algorithm. The second part is focussed on describing the functionality of an unsupervised adaptability of the gait detection algorithm. The third part is dedicated to the testing and evaluation of the arbitrary sensor alignment algorithm. The fourth and the fifth part elaborate the testing, application and analysis of the developed algorithm with datasets from a healthy adult, and datasets from stroke patients. In the last part, bench testing trials with functional electrical stimulation including an analysis of the performance are described.

5.1 Development and Training—Algorithms

The developed algorithm for gait event recognition during robotic gait therapy with the capability of an unsupervised adaption to IMU data from healthy subjects and stroke patients consists of three main functionalities:

Firstly, the incoming data stream from a sensor is automatically aligned (rotated) to the desired coordinate system to ensure a consistent and recognisable data stream. Secondly, the aligned data can be recognised by the algorithm as gait events. Thirdly, the algorithm is capable to adapt automatically to the changes of the data while processing the incoming data stream. All three steps serve as a basis to provide the possibility of triggering an electrical stimulation during robotic gait training. The first two steps are described within this section. The methods to enhance the confidence of the algorithm including the techniques for the unsupervised adaptability of the algorithm are elaborated in section 5.2.

As mentioned in section 2.5, an alignment of the local coordinate system and the coordinate system of a rigid body enable an IMU to record data which reflects the movements of the desired object. During robotic gait training, the desired objects are mostly the lower limbs; in this work in particular the desired objects are the left and right foot of a human being. Depending on the robotic gait trainer used, the walking pattern is guided by a robot-specific motion. Depending on the gait trainer and its settings, the subject is able to influence the gait pattern. The gait cycle as described in section 2.2 (Figure 9) consists of eight events. As a matter of fact, when using only one sensor per foot, not all gait events and periods as described in Figure 9 are reliably recognisable. Therefore, the developed algorithm is focussed on detecting four main events (initial contact, full contact, heel off, and toe off) during robotic gait training. Furthermore, robotic gait training provides a physiological and reproducible gait pattern [134]. When the cyclic gait pattern is disturbed by a restraining force (applied by the subject or by the therapist) or a spasticity, a robot specific strategy can recognise this event and stops the therapy in order to reduce the risk of injury for the subject or therapist. Thus, switching between the phases caused by gait disorders or a sloppy gait can be excluded. In addition, the motion of most robotic gait trainers is largely constraint into the sagittal plane. Exploiting the features of the algorithm for the arbitrary sensor alignment and the boundary conditions for the robotic gait training, the gait cycle during robotic gait can be simplified and a flow chart of the algorithm including the bench testing with electrical stimulation as shown Figure 27 can be obtained.

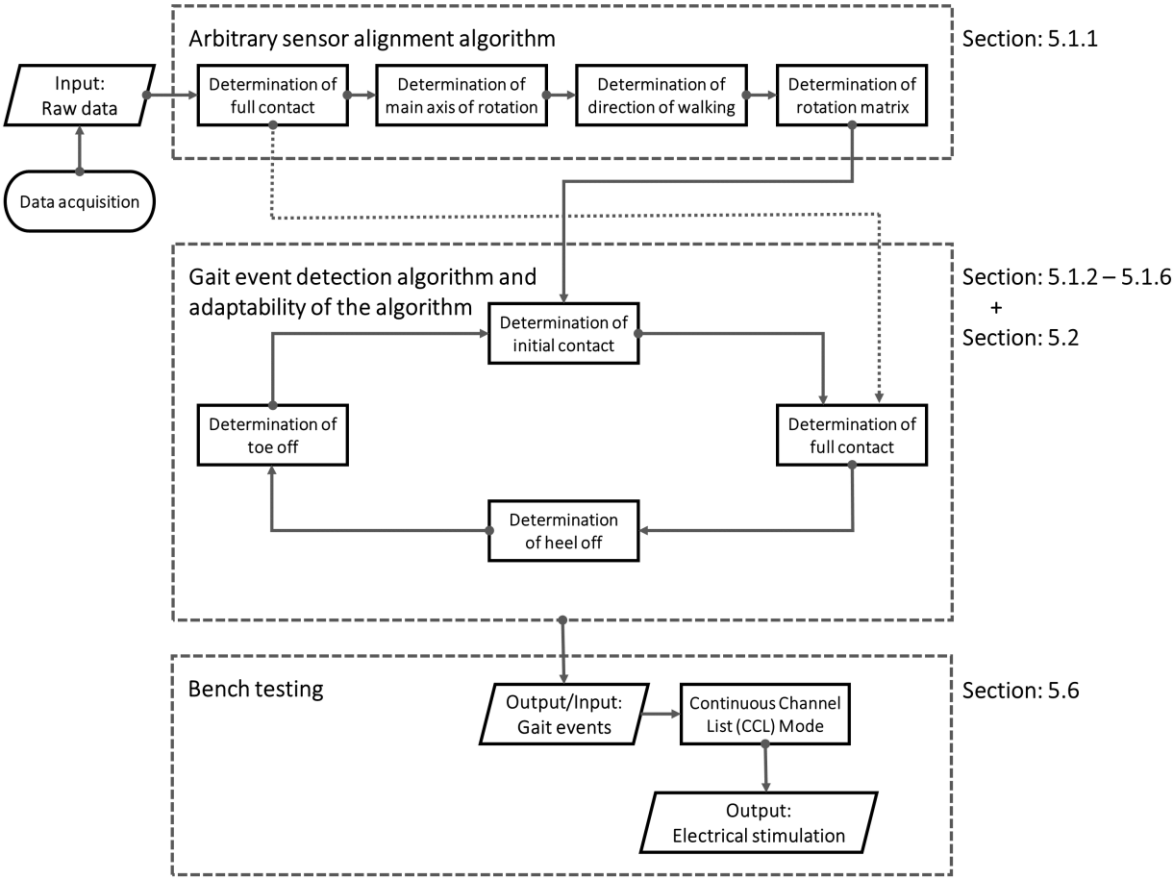

Figure 27: Flowchart of the algorithms

After data acquisition, the raw data (liner acceleration and angular velocity) of the IMU are used as input. The arbitrary sensor alignment algorithm (section 5.1.1) rotates and aligns the incoming data stream in order to supply the gait event detection algorithm with recognisable data. The gait events are detected within the algorithm (sections 5.1.2—5.1.6), the techniques to enhance the confidence of the algorithm (section 5.2) enable the algorithm to autonomously adjust the detection. As the determination of the full contact event is implemented in the process of the arbitrary sensor alignment, the algorithm for gait event detection can use this information, this is visualised within the flowchart with a dotted line. The output from the gait event detection algorithm serves as an input for the electrical stimulation. The testing application of the stimulation is described in detail in sections 5.6. The development and training of the arbitrary sensor alignment algorithm is based on a small set of training data (human walking) which was recorded during overground walking. For the training of the gait event detection algorithm, small datasets during robotic gait therapy from of healthy adults and people who suffered a stroke were used. Within the training, the functionalities for gait event detection and the methods to enhance the confidence of the algorithm were developed. All datasets used for training and

developing the algorithm were not considered for the evaluation of the algorithm in order to avoid skewing of the results. Thus, the results elaborated in section 5.5 show the capability of the algorithm to recognise gait events and show its autonomous adaptability to various datasets.

5.1.1 Arbitrary Sensor Alignment Algorithm

This algorithm is based on the assumption that the global coordinate system is the room a person is standing, respectively the room a robotic gait trainer is placed. Thus, an IMU attached to a foot can be schematically represented as seen in Figure 28, whereas the body coordinate system is defined in such a way that during standing the $\vec{x}_{axis}$, points ventral (towards walking direction), the $\vec{y}_{axis}$ points lateral (towards the side) and the $\vec{z}_{axis}$ points cranial (vertical axis).

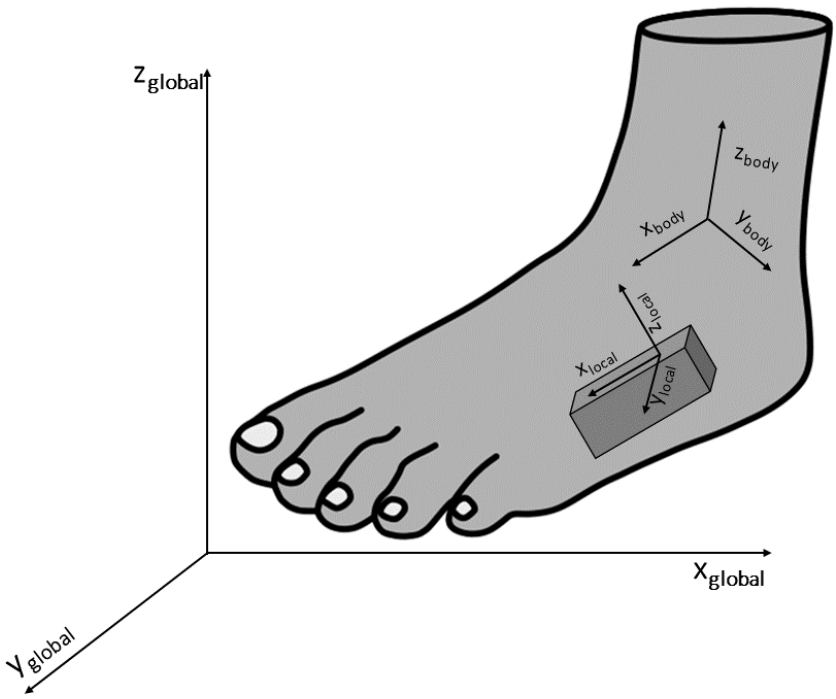

Figure 28: Schematic representation of an IMU attached to the left foot

For an arbitrary sensor alignment, the phases of gait and their particular movement behaviour can be exploited in order to generate boundary conditions for the alignment of the coordinates. For the alignment procedure, a rotation matrix is generated that represents the rotation from the local coordinate system of the sensor to the body coordinate system of the foot. The rotation matrix can be generated in four main steps and is defined as follows:

$$\text{RotationMatrix} = \begin{pmatrix} x_{\text{axis x}} & y_{\text{axis x}} & z_{\text{axis x}} \\ x_{\text{axis y}} & y_{\text{axis y}} & z_{\text{axis y}} \\ x_{\text{axis z}} & y_{\text{axis z}} & z_{\text{axis z}} \end{pmatrix} \tag{1}$$

Step 1: As a first step, the $\vec{z}_{\text{axis}}$ of the rotation matrix can be determined by exploiting the stance phase, in particular the mid stance period of the gait cycle. As soon as the forefoot hits the floor, the ankle becomes the pivot point for further progression and the foot itself is stationary [58]. In gait trainers, the robot-guided movement may result in the subject's foot never touching the ground. Nevertheless, the induced gait cycle mimics this movement pattern as it aims to replicate a physiological gait pattern, therefore the approach can be applied to the robotic movement. During this full contact event (section 5.1.4), the $\vec{z}_{\text{axis}}$ of the foot aligns with the $\vec{z}_{\text{axis}}$ of the defined global coordinate system. During that time, the foot as well as the attached IMU experience only the earth gravitational acceleration. An IMU which would already align with the body coordinate system would thus only experience an acceleration in the z-direction of its local coordinate system. As a result, the linear acceleration of the IMU can be used as the representation of the $\vec{z}_{\text{axis}}$ of the rotation matrix.

Taking real life conditions into account, slight movements and rotations of the foot and ankle or movements of the sensor attachment are always present. These disturbances lead to the fact that a perfectly resting foot with no other influences other than the earth gravitational acceleration is not plausible. As a result, the full contact must be determined within certain thresholds which allow the arbitrary sensor alignment algorithm to detect the event. Full contact can thus be determined as soon as the bias corrected angular velocity of the sensor $\vec{\omega}_{\text{FullContact}}$ is in a small range (Figure 33) for all directions of its coordinate system:

$$\begin{aligned} |\omega_{\text{FullContact x}}(i)| &< \omega_{\text{FullContact tresh}} \\ |\omega_{\text{FullContact y}}(i)| &< \omega_{\text{FullContact tresh}} \\ |\omega_{\text{FullContact z}}(i)| &< \omega_{\text{FullContact tresh}} \\ \forall\, i \in (n \ldots . k) \end{aligned} \tag{2}$$

The variable n denotes the current sample of the sensor and k denotes a reasonable number of samples passed through

As soon as the condition for the full contact event is fulfilled, the acceleration vector $\vec{a}_{FullContact}$ is in accordance with the $\vec{z}_{axis}$ of the rotation matrix. As a result, the $\vec{z}_{axis}$ shows the inclination of the IMU in its local coordinate system during full contact (Figure 29) and can be determined as follows:

$$\vec{z}_{axis} = \begin{pmatrix} a_{FullContact\,x} \\ a_{FullContact\,y} \\ a_{FullContact\,z} \end{pmatrix} \tag{3}$$

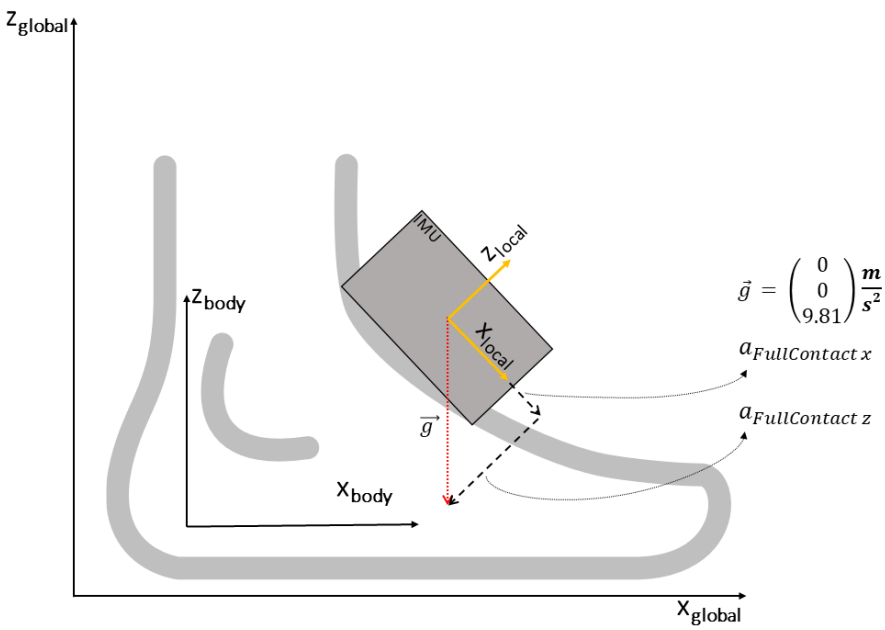

Figure 29: Visualisation of an IMU during full contact in the sagittal plane

Step 2: After the mid stance period has taken place, the main axis of rotation of the sensor and the $\vec{y}_{axis}$ of the rotation matrix can be determined. After the full contact event, the ankle experiences a flexion in dorsal direction [58], causing the heel to rise and inducing a rotational movement in the $\vec{y}_{axis}$ of the foot (Figure 30). The induced rotation affects the IMU as well and depending on the location of the sensor, one of its axes in the local coordinate system experiences a greater angular velocity during the rotation compared to the other axes.

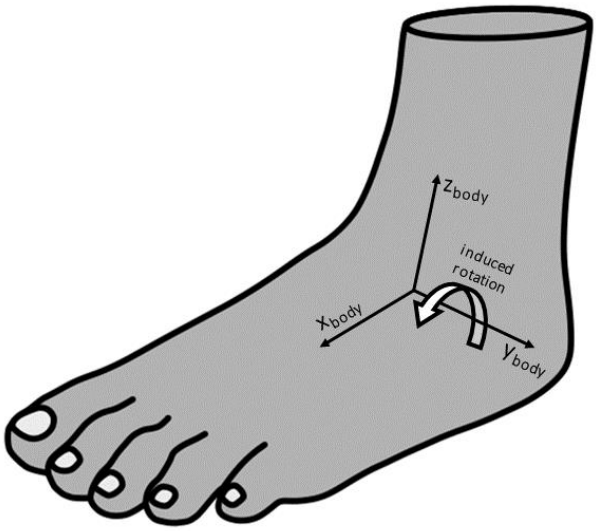

Figure 30: Rotation of the foot after the mid stance

The main rotational axis and the $\vec{y}_{axis}$ of the rotation matrix are found by adding up the data from the angular velocity of all individual axes of the local coordinate system during the rotation as shown in the following conditions:

$$y_{axis\,x} = \left|\sum_{i=n}^{k} \omega_{x(i)}\right| \qquad (4)$$
$$y_{axis\,y} = \left|\sum_{i=n}^{k} \omega_{y(i)}\right|$$
$$y_{axis\,z} = \left|\sum_{i=n}^{k} \omega_{z(i)}\right|$$

The calculation is initiated after mid stance has passed, starting with the first sample n and ending after a certain amount of data points k.

In Figure 31, the process of rotation and the according angular velocities are visualised. In this particular example, the y-direction experiences the largest change of angular velocity while the x- and z-direction are less effected by the heel lifting off the ground.

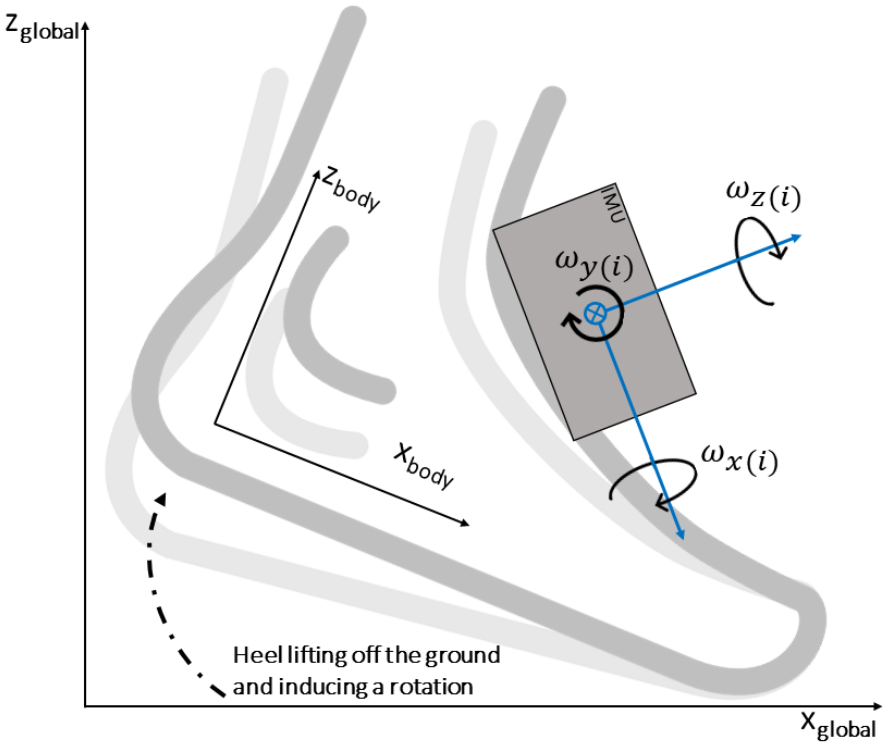

Figure 31: Angular velocities during heel off, whereas (i) denotes the current sample and refers to condition (4).

The absolute values of the summed up angular velocity data are then stored in a vector which defines the $\vec{y}_{axis}$ of the rotation matrix. Furthermore, the highest angular velocity within this axis defines main axis of rotation of the sensor. The goal of this approach is the detection of the main rotational axis, therefore a prior information of the sensor alignment with regard to the foot is not required [97] allowing an arbitrary positioning of the sensor.

Step 3: As a next step, the $\vec{x}_{axis}$ of the rotation matrix must be defined. The $\vec{x}_{axis}$ represents the direction of walking. As the $\vec{z}_{axis}$ is a vertical axis and the $\vec{y}_{axis}$ describes an axis perpendicular to a parasagittal plane, they can be used as linear independent vectors to compute the $\vec{x}_{axis}$ using the cross product:

$$\vec{x}_{axis} = \vec{y}_{axis} \times \vec{z}_{axis} \tag{5}$$

Step 4: As soon as all elements of the rotation matrix are filled with the corresponding data, the matrix has to be normalised in order to generate the final rotation matrix. The normalisation is necessary as the matrix will be used for rotating all incoming datapoints.

$$\text{RotationMatrix} = (\hat{x} \quad \hat{y} \quad \hat{z}) \tag{6}$$

Rotating the data: Once the rotation matrix is created, each incoming data point (angular velocity and linear acceleration) of the IMU can be rotated to reflect the movement of the body coordinate system.

$$\begin{aligned} \vec{\omega}_{\text{rotated}} &= \text{RotationMatrix} * \vec{\omega}^{\text{T}}_{\text{current}} \\ \vec{a}_{\text{rotated}} &= \text{RotationMatrix} * \vec{a}^{\text{T}}_{\text{current}} \end{aligned} \tag{7}$$

The process of creating the rotation matrix is repeated at each step. This is done to ensure that variations of individual movements do not distort the data. Furthermore, the frequent recalculation of the alignment process takes into account that a sensor attachment might shift during a recording session. If a shift of the sensor attachment occurs and the rotation matrix is not adjusted accordingly, the further processing of the data might lead to incorrect results.

5.1.2 Gait Event Recognition Algorithm

The detection of gait events starts with the initial contact and is followed by the full contact, heel off and toe off. This detection describes the process for one foot independently of the other foot. Therefore, gait events such as feet adjacent and opposite initial contact (as introduced in Figure 9) are not part of this sequence. Moreover, load response and tibia vertical are not part of this sequence as with one sensor they would not be reliably detectable. As a result, a simplified state diagram of the detection sequence of gait events as shown in Figure 32 can be deduced.

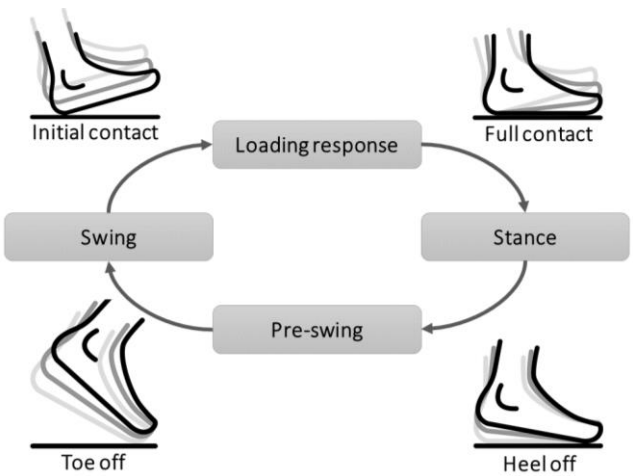

Figure 32: State diagram of gait events during robotic gait training, adapted from [122]

This distinct sequence must be present for the correct functioning of the presented algorithm. Additionally, it is important to mention that a correct functioning arbitrary sensor alignment algorithm is needed prior to the detection of gait events. In the following sections, the individual detection processes for the gait events will be described in detail.

5.1.3 Initial Contact

According to [58], the initial contact is the first event of the gait cycle; furthermore, it represents the first event of the detection algorithm. The tasks of the initial contact and the corresponding weight acceptance are shock absorption, limb stability and preservation of progression [58]. The duration of the initial contact is very short and starts with the first contact of the heel with the ground, respectively the corresponding motion of the gait trainer. During this event, the ankle moves from dorsiflexion to a neutral position and afterwards to a plantar flexion [135]. For the detection of this event with an IMU, the shock absorption and the resulting change in acceleration is of importance. At the moment when the first contact is made with the ground, a stabilisation and damping of the body is performed. This is done by an interplay of the muscles and the robotic orthosis. This event results in rapid change of linear acceleration. The impact and the resulting abrupt change in linear acceleration is reflected in a high peak of the jerk. Within this work, the jerk reflects the rate of acceleration change of the foot, respectively the sensor attached to it. Thus, to detect this specific behaviour which defines the initial contact, the corresponding jerk ($\overrightarrow{\mathrm{jerk}}_{\mathrm{InitialContact}}$) is of importance.

The incoming data stream of the recorded data consists of linear acceleration data and angular velocity data. By calculating the first derivation of the linear acceleration data, the jerk is computed. The jerk is calculated for all three axes and is summed up afterwards in order to reflect the full impact of the heel striking the floor. After the computation of the jerk, the initial contact can be detected using the following condition.

$$\mathrm{jerk}_{\mathrm{min}} < |\mathrm{jerk}_{\mathrm{initialContact\ z}}| < \mathrm{jerk}_{\mathrm{max}} \tag{8}$$

The variables $\mathrm{jerk}_{\mathrm{min}}$ and $\mathrm{jerk}_{\mathrm{max}}$ define the detection limits within which the current jerk must be located to enable the detection of the initial contact.

5.1.4 Full Contact

Shortly before the full contact event is present, the load of the body is accepted by the leg (loading response). During that time, the body absorbs the impact by rolling the foot into pronation [135], respectively the robotic device absorbs the impact by rotating the mechanical structure accordingly. For the detection of the full contact, it is of importance that the foot is at rest and does not experience any propelling forces. This is given as soon as the angular velocity of the sensor is in a small range for all directions of its coordinate system (Figure 33).

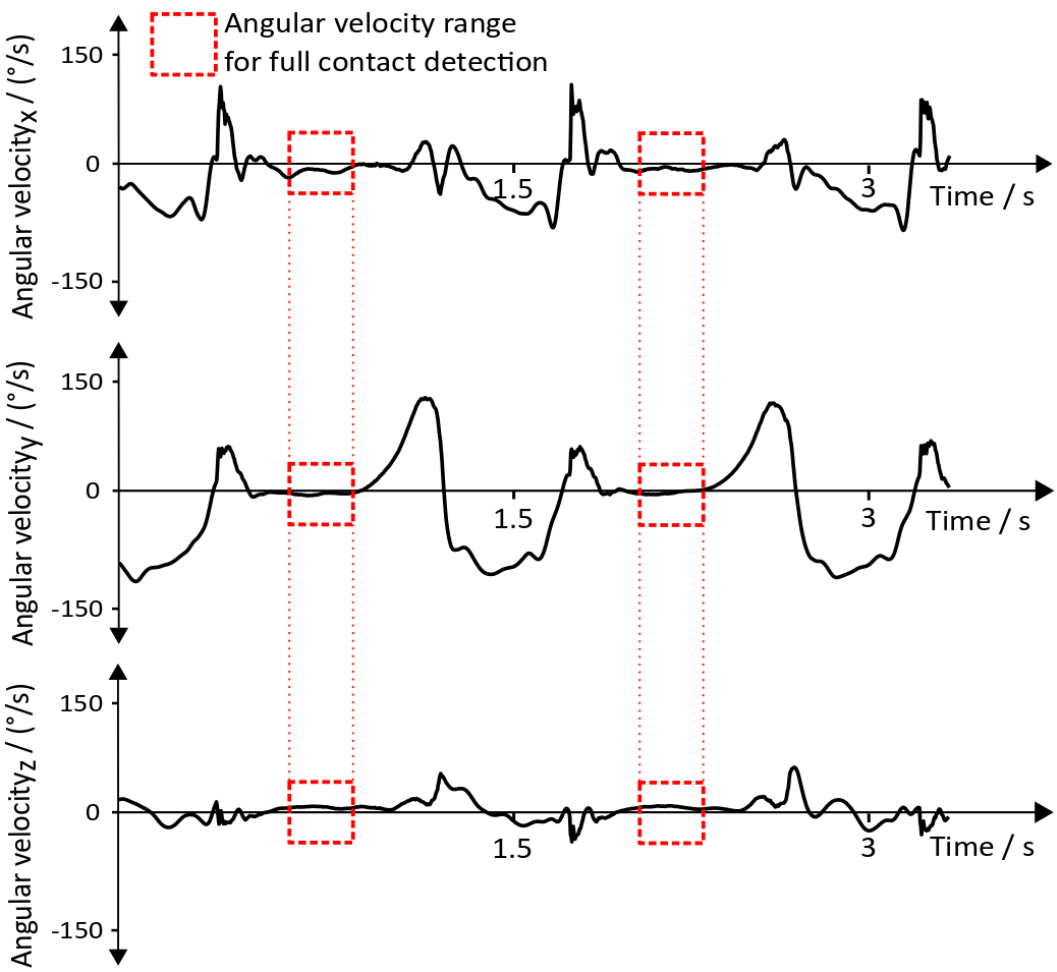

Figure 33: Angular velocity during the full contact event

The conditions to detect the full contact event are already elaborated in section 5.1.1 as they are necessary to enable the arbitrary sensor alignment algorithm.

5.1.5 Heel Off

The heel off comes subsequently to the full contact event. This event is indicated once the heel lifts off the ground. In robotic gait training this happens when induced gait pattern provides the corresponding robotic motion. The body is in single support and the swing leg progresses ahead the stance leg [135]. During the terminal stance phase, an extension of around 10 degrees in dorsal direction is reached [58]. Caused by that, the $\vec{y}_{axis}$ experiences a rotation and subsequently the heel rises. Furthermore, the ankle starts a forward movement. As a result, the angular velocity in the primary axis of rotation $(\omega_{HeelOff\,y})$ and the acceleration $(\vec{a}_{Heeloff})$ of the attached IMU starts to rise. Based on this information, and by exploiting the functionalities of the arbitrary sensor alignment algorithm the heel off event can be detected utilising the following conditions:

$$\begin{aligned} |\omega_{HeelOff\,y}| &< \omega_{HeelOff\,tresh\,y} \\ |a_{HeelOff\,x}| &< a_{HeelOff\,tresh\,x} \\ |a_{HeelOff\,y}| &< a_{HeelOff\,tresh\,y} \\ |a_{HeelOff\,z}| &< a_{HeelOff\,tresh\,z} \end{aligned} \tag{9}$$

The parameters $a_{HeelOff\,tresh\,x}$, $a_{HeelOff\,tresh\,y}$, $a_{HeelOff\,tresh\,z}$, and $\omega_{HeelOff\,tresh\,y}$ represent threshold values. The acceleration $\vec{a}_{HeelOff\,z}$ is adjusted to gravity by exploiting the boundary condition, that the robotic gait is performed on a horizontal surface. The heel off is detected if either the threshold value $\omega_{HeelOff\,tresh\,y}$ is reached or all acceleration thresholds are reached. For real life applications, the acceleration thresholds serve as a backup in case the heel of a subject is not lifted properly.

5.1.6 Toe Off

The end of the heel off initiates the pre swing phase. During that event, a plantar flexion of around 20 degrees is induced and the toe lifts off the ground [58,135]. After that, the initial swing phase causes a reduction of the flexion to approx. 5 degrees, followed by an extension into dorsal direction of the ankle in the middle swing [58]. The change in ankle flexion and the according rotation of the foot is described by a pronounced alteration of the angular velocity ($\omega_{ToeOff\,y}$) of the sensor as shown in Figure 34.

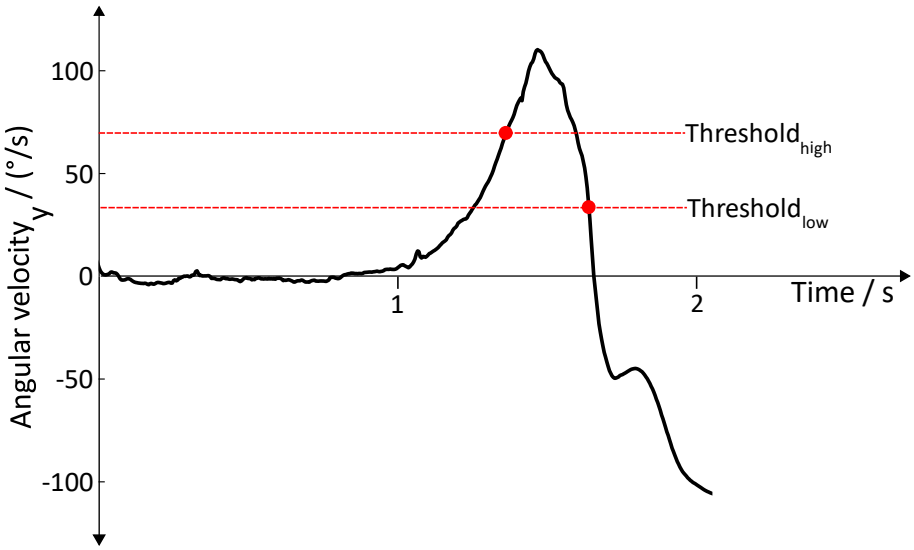

Figure 34: Angular velocity within the $\vec{y}_{axis}$ during the toe-off event

This motion sequence indicates the toe-off event. Based on this particular change of the angular velocity, three conditions can be used to detect the toe-off event:

$$\omega_{ToeOff\,y} > \omega_{Threshold_{high}} \tag{10}$$

$$\omega_{ToeOff\,y_{(i)}} < \omega_{y_{(i-1)}} \tag{11}$$

$$\forall\, i \in (n \ldots . k)$$

$$\omega_{ToeOff\,y} < \omega_{Threshold_{low}} \tag{12}$$

The variable n denotes the current sample of the sensor and k denotes a reasonable number of samples passed through

The parameters $\omega_{Threshold_{high}}$, $\omega_{Threshold_{low}}$ represent threshold values as shown in Figure 34. In order to detect the toe-off event, the conditions (10), (11) and (12) have to be satisfied sequentially. If the motion sequence and one of the corresponding conditions are not fulfilled or if the sequence of conditions is not satisfied, no toe-off event is detected.

5.2 Techniques to enhance Confidence of the Algorithm

Robotic gait training is a dynamic process resulting in a variability of measurable parameters. Therefore, the presented detection algorithm adapts itself autonomously to ensure proper functioning without human intervention. Furthermore, errors throughout the chain of measurement can occur. For example, defects in the Bluetooth connection can lead to improper communication and missing data, outliers caused by unwanted high peaks during the recording can mimic false gait events. Moreover, the robotic induced movement pattern can cause vibrations due to the mechanical structure. Problems with the calibration of the sensor can additionally lead to unwanted behaviour of the data. These potential events should be handled by certain methods to guarantee an exact recognition of gait events. To fulfil these requirements, techniques for an unsupervised adaption were developed and are presented in the following sections.

5.2.1 Dynamic Threshold—Initial Contact

The variables jerk_{min} and jerk_{max} (section 5.1.3) which define the detection bounds do not have fixed values; they rather describe a dynamic (floating) threshold with continuous adaptability. A floating threshold (Figure 36) was implemented as the jerk while training with a robotic gait training can vary in-between steps. Additionally, outliers such as a rapid drop of the subject's foot due to voluntary influence of the induced gait pattern may distort the jerk signal. This floating threshold is computed by adding a particular percentage of the actual jerk to the previous jerk in order to calculate detection bounds. Using this hysteresis, the threshold can adapt autonomously after every step and an exceeding of limits due to unwanted outliers can be diminished.

5.2.2 Sequence Detection

For the recognition of gait events, it is important that the detection sequence of events is defined. The state diagram in Figure 32 shows in which sequence the algorithm is detecting the events. A correctly recognised gait cycle is defined as follows:
The initial contact defines the start and the end of a gait cycle. Between these two events, the algorithm is enabled to detect full contact, heel off, and toe off sequentially. The time of detection is stored for further processing. Events that do not correspond to the defined

sequence are discarded and the detection of gait events continues. Thus, the approach rejects falsely recognised gait events. If the sequence of detection is not present, no successful step is present, and the recognised events are rejected. A correctly detected sequence over three gait cycles can be seen in Figure 35.

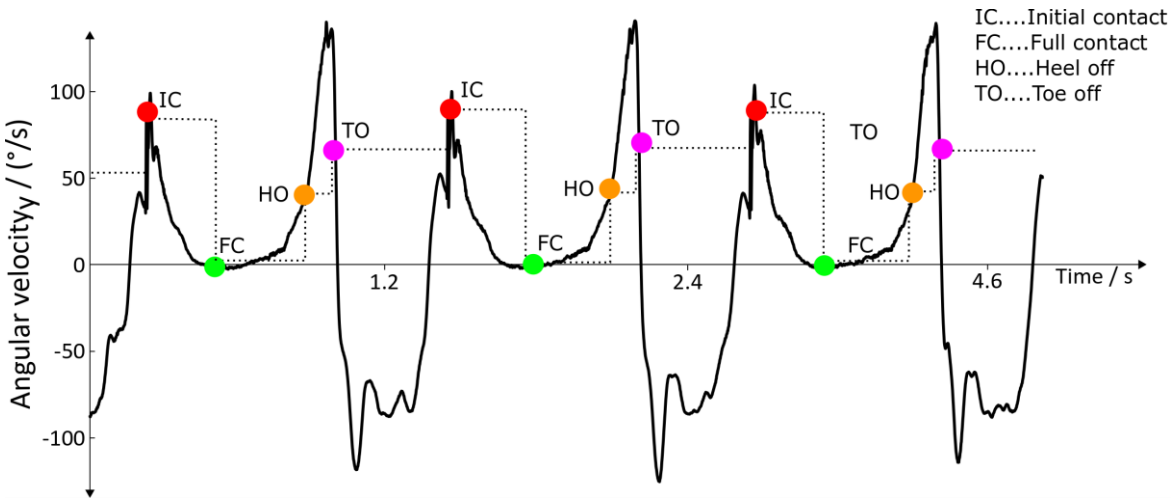

Figure 35: Detection sequence of the gait event detection algorithm

5.2.3 Temporal Dependencies

An additional approach addresses solely the detection of correct gait events rather than rejecting incorrectly recognized ones. For that approach, time dependent constraints between certain events can be used. After an initial contact, the loading response and full contact follows, and the foot touches the ground before the heel can rise again. This period is named roll time and indicates the duration between the initial contact and the heel off. This duration must have passed before the heel off can take place. Thus, a minimum roll time was introduced to ensure that a heel off can only be detected after the minimum roll time has elapsed. Following the toe-off event, the foot is in the swing phase. The time until a new initial contact takes place is called swing time. Thus, a minimum swing time was introduced to ensure this interaction. This temporal relation happens after the toe-off event. The next initial contact can only be recognised subsequently to this duration. This condition prevents the incorrect recognition of other peaks in the jerk which could appear during walking [97]. The start and the end of a gait cycle is determined by initial contacts; the duration between these events can be termed step time. To ensure that no initial contact is incorrectly detected, a minimum duration (minimum step time) in between the recognition of two initial contacts must elapse.

5.2.4 Dynamic Threshold—Toe Off

Different speeds of the robotic device (orthosis or treadmill) result in different behaviour of the angular velocity and require an adaption of the conditions. For that purpose, an angular velocity-dependent adaptation (unsupervised) for the toe-off event (section 5.1.6) is introduced. For the computation of this adaption, the highest angular velocity during the toe-off event is recognised and stored as a reference value. Depending on this maximum angular velocity, the threshold conditions $\omega_{\mathrm{Threshold_{high}}}$ and $\omega_{\mathrm{Threshold_{low}}}$ from section 5.1.6 are autonomously adapted to correspond the current state. Furthermore, the temporal relations mentioned in section 5.2.3 are adapted within this process (unsupervised adaption), since higher angular velocity values lead to shorter times in between the individual events.

5.2.5 Adaptions—Robot-specific

Robotic gait trainers like Lyra and Lokomat state that they provide a physiological walking pattern. Although this applies to optical observation, data collected with IMUs (angular velocity data and the linear acceleration) differs between the system when collected with a sensor on a distinct position on the foot (Figure 40). As a result, these differences have to be taken into account and robotic trainer specific optimisations were realised. The adaptions can be found in several events.

Initial contact: When comparing the jerk (m/s^3) of Lokomat and Lyra, the data of Lyra shows lower amplitudes during the initial contact. Thus, the algorithm needs to adapt for correct detection of the initial contact. As a result, when analysing signals recorded with Lyra, lower thresholds and different threshold adaptions were established.

Initial contact: A second adaption for the initial contact was realised as the behaviour of the data, especially of the jerk, differs between the systems. Figure 36 shows the angular velocity and the jerk during walking in a Lyra system. Before the actual jerk signal of the initial contact, a couple of peaks in the jerk signal are clearly visible. These peaks may happen after the duration of the minimum swing time. Furthermore, their amplitude can be large enough to pass the floating threshold. Therefore, these peaks could be wrongly detected as an initial contact and lead to an improper gait event detection. In order to avoid this failure of the algorithm, the angular velocity can be used by introducing an angular

velocity band. The velocity band as shown in Figure 36 ensures that the initial contact can only be recognised within this band and can discard the unwanted signals.

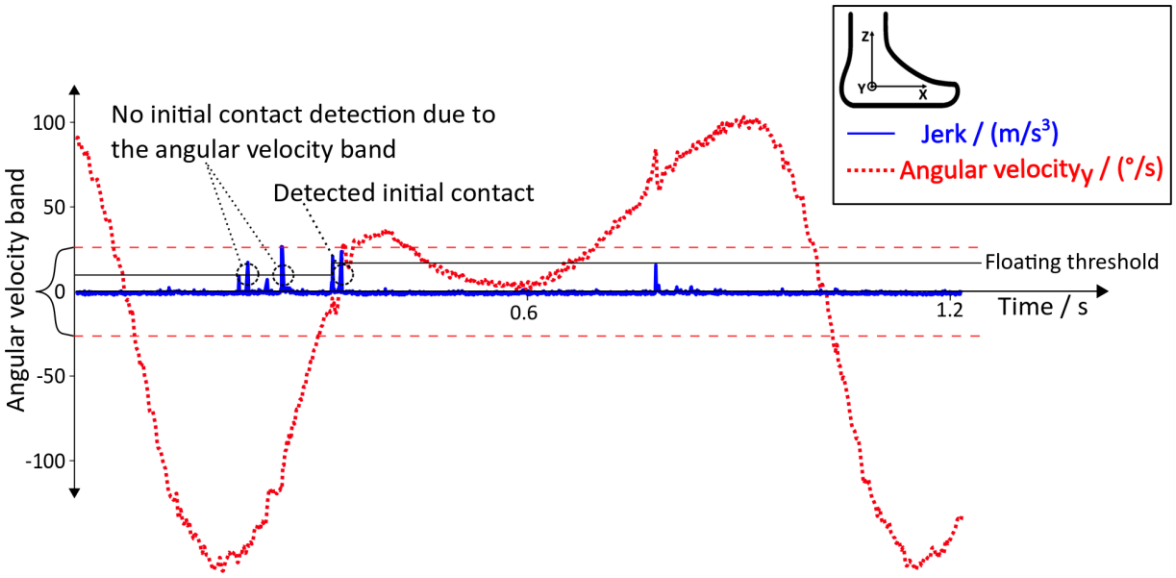

Figure 36: Detection of initial contact: Floating threshold and angular velocity band

Minimum roll time and minimum swing time: A further modification was realised for the time dependencies. The durations' minimum swing time and minimum roll time got modified to fulfil the requirements of the different robots.

5.2.6 Adaptions—Stroke Patients

As mentioned in section 5.1.3, the jerk can be used for the detection of the initial contact. Various techniques for an unsupervised adaption were created to ensure the proper detection of this event. The described approach delivered satisfying results for the robotic training of a healthy adult. Details of the recordings and the analysis of results are elaborated in sections 5.4.1 and 5.5.1. However, based on the training datasets, the typical behaviour of the jerk and the corresponding angular velocity during robotic gait training of a healthy subject and a stroke patient can vary as visualised in Figure 37. In the left image of Figure 37, the jerk signal clearly identifies the initial contact during robot-assisted gait training. There is another spike in the jerk signal before the actual initial contact; this spike might correspond to a rapid change in acceleration during the swing phase. The methods described in the previous sections can identify this behaviour and no initial contact is detected. However, when looking at the right image of Figure 37, the behaviour of the jerk is fuzzy and seems not to follow the expected pattern. As a result, the described approaches might not be able to detect the initial contact as patient-specific movements or

the lack of movement on an affected lower limb seems to influence the acceleration data. Thus, another technique for the unsupervised adaption of the algorithm was implemented.

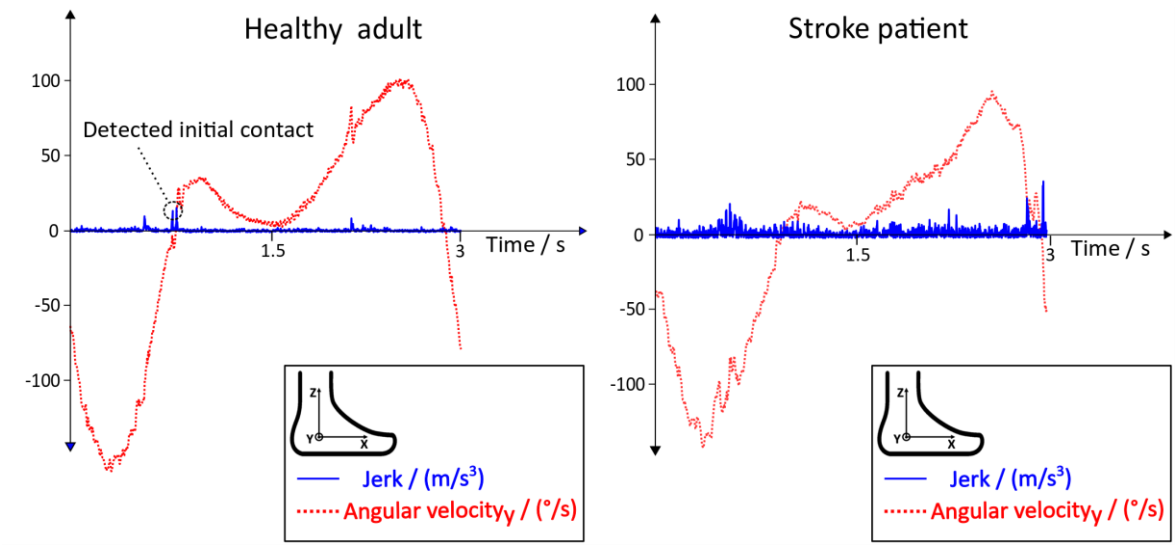

Figure 37: Angular velocity signal and jerk signal during robotic gait training (sagittal plane)

Based on observations of data from healthy adults, the interplay between jerk during initial contact and angular velocity was exploited. The initial contact takes place at a time when the angular velocity crosses the zero line. Moreover, the angular velocity comes from a negative value and after crossing the zero line, the value stays in a positive range. In Figure 38, the new detection method including the additionally developed conditions can be seen.

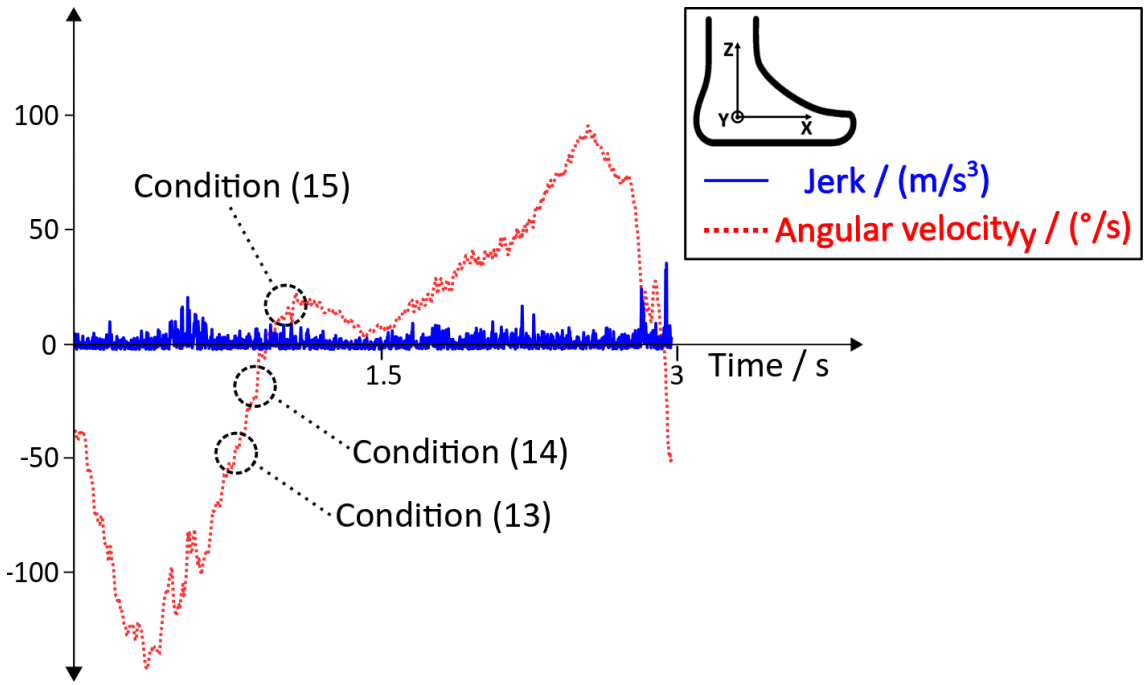

Figure 38: Angular velocity signal and jerk signal during robotic therapy (stroke patient)

The method aims to exploit the angular velocity data by using the following conditions: Condition (13) checks that the angular velocity is in the negative range prior to the recognition of an initial contact. Condition (13) has to be fulfilled prior to the algorithm checking for condition (14).

$$\omega_{\text{InitialContact}\,y_{(i)}} < 0 \qquad (13)$$
$$\forall\, i \in (n \ldots . k)$$

In condition (14), the positive gradient of the angular velocity is investigated. Once this can be is ensured, condition (14) is fulfilled. Subsequently, condition (15) can be evaluated.

$$\omega_{\text{InitialContact}\,y_{(i)}} > \omega_{\text{InitialContact}\,y_{(i-1)}} \qquad (14)$$
$$\forall\, i \in (n \ldots . k)$$

The final step in this sequence is condition (15). The condition verifies if the angular velocity has exceeded the zero line. Additionally, the condition checks if the data stays in a positive range for a specific amount of passed samples.

$$\omega_{\text{InitialContact}\,y_{(i)}} > 0 \qquad (15)$$
$$\forall\, i \in (n \ldots . k)$$

Throughout all conditions, the variable n refers to the present data sample of $\omega_{\text{InitialContact}\,y}$, and k describes a certain number of samples passed. As soon as the final condition of this sequence is satisfied, an initial contact can be recognised. Subsequently, the other gait events as described in Figure 32 can be detected. To pursue the goal of increasing robustness and a higher detection rate, the conditions were integrated into the proposed algorithm to enhance the detection efficiency.

5.3 Testing—Arbitrary Sensor Alignment Algorithm

The functionalities of the arbitrary sensor alignment algorithm such as the arbitrary mounting of the IMUs and the automatic adjustment in case of a shift of the attached sensor are essential for presented gait recognition algorithm. Therefore, a careful testing and evaluation of this process was carried out before the application, to ensure the correct functioning of the implemented methods.

5.3.1 Testing

The testing process is divided into the parts data recording, data processing and data visualisation, subsequently followed by the data evaluation including a discussion of the results in section 5.3.2.

Data recording: For the data recording, gait cycles with different sensor positions were carried out. The sampling frequency of the sensor was 500Hz, the measurement ranges for the linear acceleration and angular velocity were ±8g and ±1000°/s. Under the consideration of meaningfulness and the practical application of the sensors, two different sensor positions, position A and position B, as illustrated in Figure 39 were chosen for experimental evaluation.

Figure 39: Left: Position A—Inside of the foot
Right: Position B—Dorsum of the foot

Additionally, a reference sensor as shown in Figure 40 representing the body coordinate system was used. The reference sensor was firmly secured to the foot using a custom-made fixation strap from HASOMED GmbH. Anatomical landmarks (calcaneus and the cuboid bone) were used as reference to position the sensor. The fixation strap ensured that the reference sensor was not moving during data recording.

Figure 40: Reference position

Two sensors (position A and reference position or position B and reference position) were simultaneously attached to one foot. For synchronisation of the recordings, the commercially available software RehaGait Analyzer was used. The software started the recording of the sensors simultaneously which guaranteed the same time base of the raw data acquisition. The subject, a 29-year-old healthy adult performed overground walking on a self-chosen comfortable speed between 1m/s and 1.7m/s. A walking paradigm as shown in Figure 41 was chosen for the recording. A total amount of ten recordings was performed and analysed.

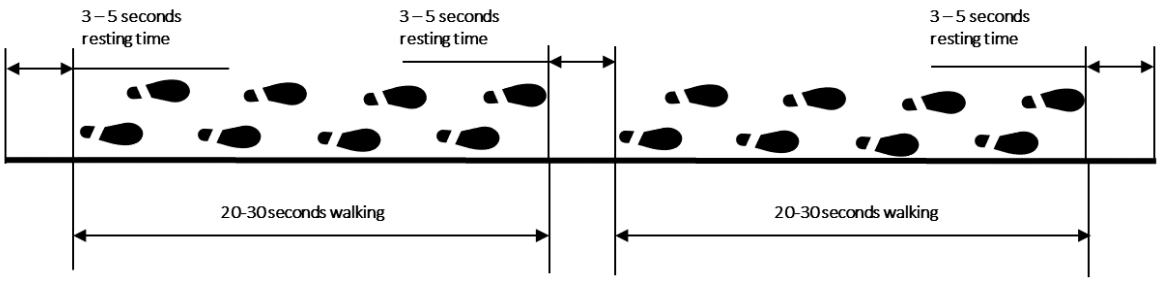

Figure 41: Walking paradigm for the evaluation of the arbitrary sensor alignment algorithm

Data processing: After the recordings, the data was stored on a host computer. The raw data was rotated using the introduced arbitrary sensor alignment algorithm from section 5.1.1. The algorithm was developed in MATLAB 2018b (MathWorks, Massachusetts, USA). Each sample of the data was sequentially forwarded to the algorithm in order to simulate a real-time data stream. An example of how data processing was realised is shown in Figure 42. The results of the data processing are visualised in following next section.

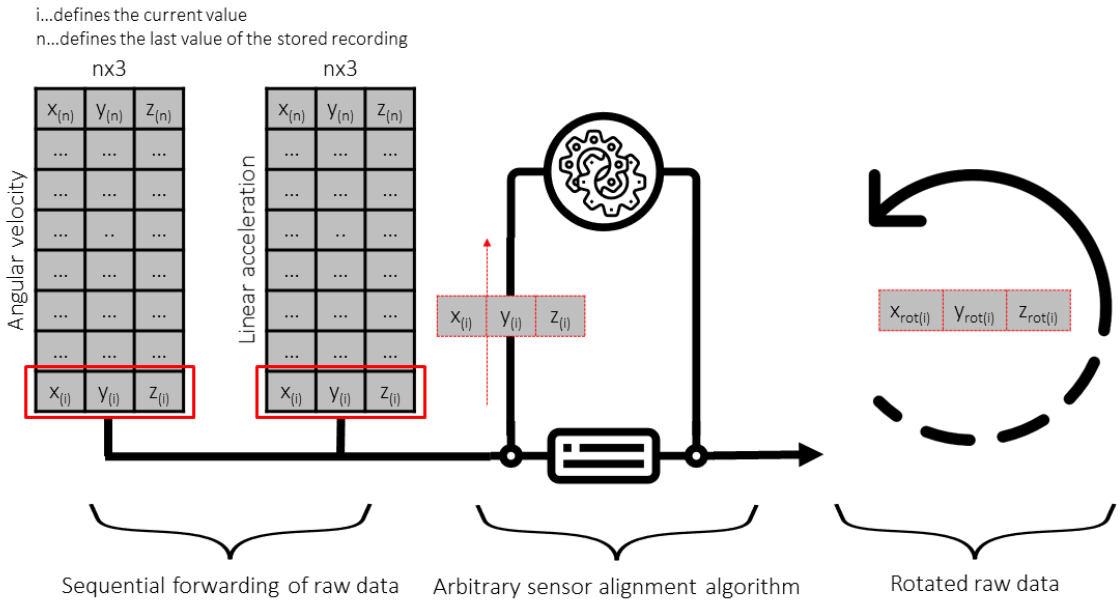

Figure 42: Data processing: Sequential forwarding of raw data—Arbitrary sensor alignment algorithm

Data visualisation: In Figure 43, the linear acceleration signals (rotated and non-rotated) of position A are visualised. For data visualisation, a resting time of five seconds was selected.

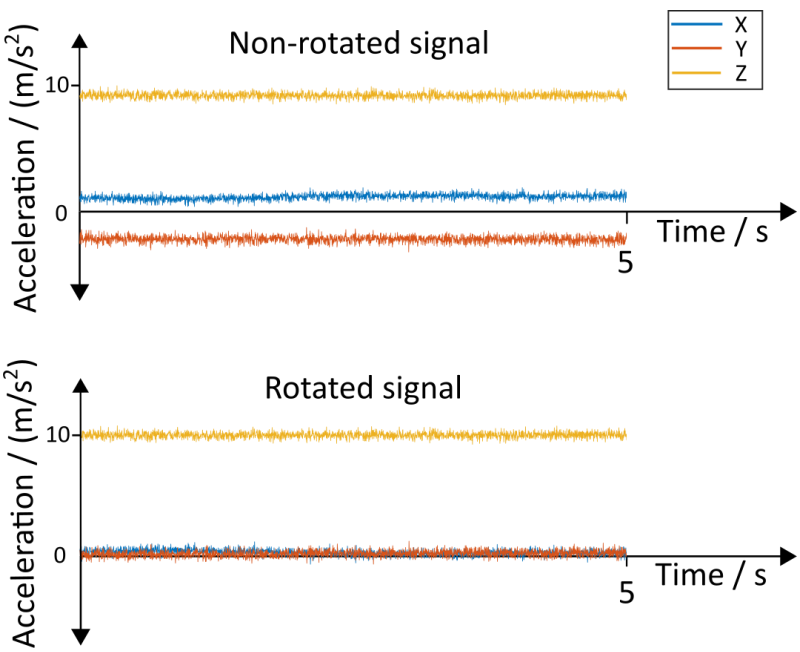

Figure 43: Linear acceleration signals.
Position A—inside of the foot.

Figure 44 shows linear acceleration signals (rotated and non-rotated) of position B. Similar to position A, a resting time of five seconds was chosen to present the functionality of the arbitrary sensor alignment algorithm.

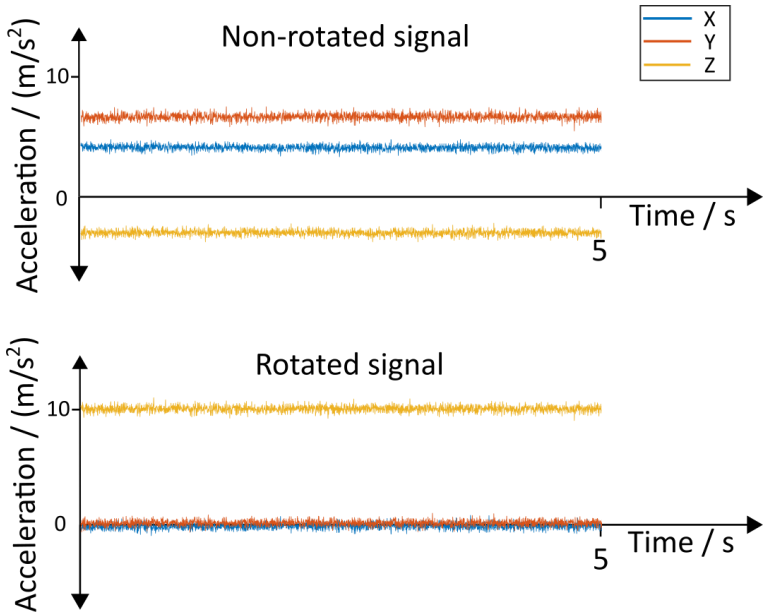

Figure 44: Linear acceleration signals.
Position B—dorsum of the foot.

The angular velocity signals (rotated and non-rotated) of the $\vec{\mathbf{y}}_{\mathbf{axis}}$ of position A are illustrated in Figure 45. For data visualisation, six gait cycles were selected.

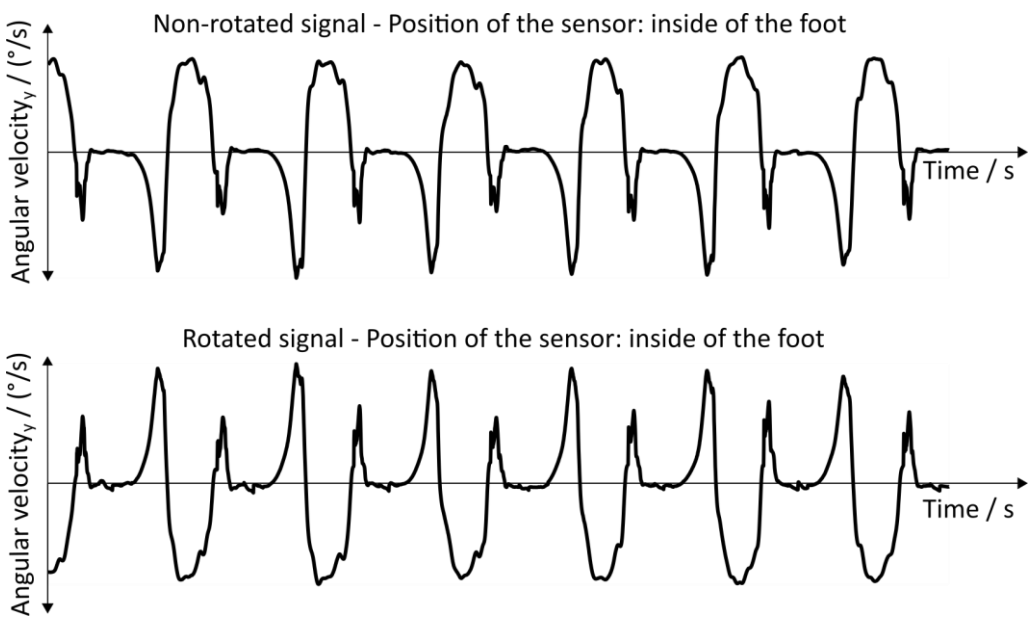

Figure 45: Angular velocity signals of the $\vec{\mathbf{y}}_{\mathbf{axis}}$
Position A—inside of the foot.

Figure 45 shows the angular velocity signals (rotated and non-rotated) of the $\vec{\mathbf{y}}_{\mathbf{axis}}$ of position B. Six gait cycles were chosen to show the functionality of the rotation process.

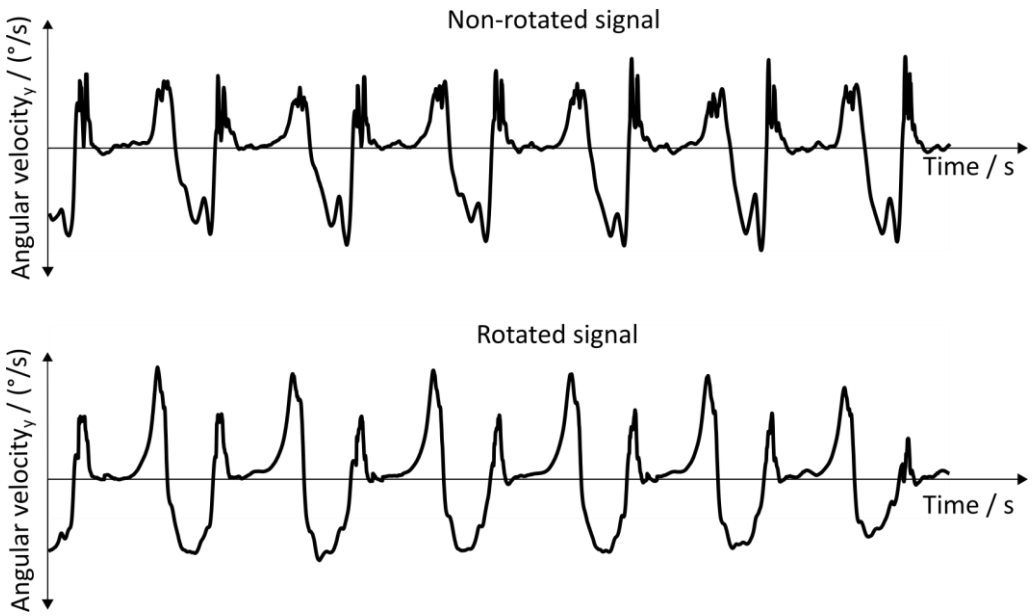

Figure 46: Angular velocity signals of the $\vec{\mathbf{y}}_{\mathbf{axis}}$.
Position B—dorsum of the foot

5.3.2 Evaluation

After data processing and visualisation, the rotated data of position A and B are evaluated using the following criteria.

Criteria 1: During resting times of the foot, the linear acceleration in the $\vec{z}_{axis}$ must represent the earth's gravitational acceleration. Therefore, the data must show a value of around 9.81m/s². Resting times are present during mid stance, respectively the full contact event. Additionally, resting times were included into the walking paradigm as shown in Figure 41.

Criteria 2: During resting times of the foot (no movement of the foot), the linear acceleration in the $\vec{x}_{axis}$ and $\vec{y}_{axis}$ must be in a low range fluctuating around zero.

Criteria 3: The waveform of the angular velocity of the $\vec{y}_{axis}$ of position A and B must have a certain similarity to the waveform of the angular velocity of the reference sensor in its $\vec{y}_{axis}$. A typical waveform of the angular velocity of two gait cycles is shown in Figure 47.

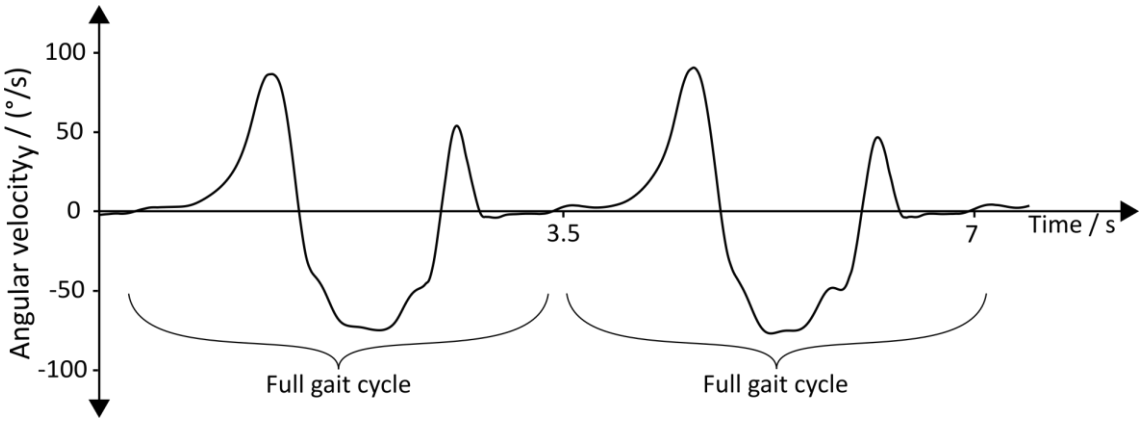

Figure 47: Angular velocity: Typical waveform of two gait cycles

Criteria 4: In this specific application, the roll axis ($\vec{x}_{axis}$) and in the yaw axis ($\vec{z}_{axis}$), of the angular velocity do not add relevant information to the subsequently used gait event detection algorithm, thus they are not examined in the evaluation.

Evaluation of criteria 1: As mentioned in section 5.1, during resting times, the foot as well as the attached IMU experience only the earth's gravitational acceleration, thus the data of the rotated signal in the $\vec{\mathbf{z}}_{\mathbf{axis}}$ of the IMU must show a value of around 9.81m/s². For evaluation of this criteria, a duration of 80 seconds for each position was considered. 80 seconds were chosen as they were the maximum number of resting times without any external disturbances such as a correction step. In Table 11, the mean value of the linear acceleration including the standard deviation is visualised.

Duration of resting time (s)	Sensor position	Axis	Mean (m/s²)	Standard deviation (m/s²)
80	A—Inside the foot	$\vec{z}_{axis}$	9.795	0.016
80	B—dorsum of the foot	$\vec{z}_{axis}$	9.782	0.022

Table 11: Rotated linear acceleration data in the $\vec{z}_{axis}$ during resting times

Evaluation of criteria 2: The rotated data in the $\vec{\mathbf{x}}_{\mathbf{axis}}$ and $\vec{\mathbf{y}}_{\mathbf{axis}}$ of the IMU must show a value of around zero as the foot itself is stationary during the full contact event. For evaluation of this criteria, the same 80 seconds as for criteria 1 were considered. In Table 12, the mean value including the standard deviation of the corresponding data is visualised.

Duration of resting time (s)	Sensor position	Axis	Mean (m/s²)	Standard deviation (m/s²)
80	A—Inside the foot	$\vec{x}_{axis}$	−0.029	0.116
80	A—Inside the foot	$\vec{y}_{axis}$	0.220	0.208
80	B—Dorsum of the foot	$\vec{x}_{axis}$	−0.337	0.213
80	B—Dorsum of the foot	$\vec{y}_{axis}$	−0.746	0.269

Table 12: Rotated linear acceleration data in the $\vec{x}_{axis}$ and y_{axis} during resting times

Evaluation of criteria 3: The evaluation of criteria 3 is focused on the shape of the angular velocity in the $\vec{\mathbf{y}}_{\mathbf{axis}}$. As the comparison of the waveform should be carried out independent from its amplitude, the signal was normalised prior to evaluation. Before normalising, the signals offset must be removed by subtracting their individual mean value. The signal can then be normalised as shown in the following formula [136] (written as MATLAB code):

$$\text{signal}_{\text{normalised}} = \frac{\text{signal}_{\text{raw}}}{\text{sqrt}\left(\max\left(\text{xcorr}(\text{signal}_{\text{raw}})\right)\right)} \tag{16}$$

The normalisation of the individual signals causes the autocorrelation function to get a value of 1 which corresponds to a similarity of 100%. This means that a value close to 1 of a cross-correlation function between the reference signal and the signals of position A and B indicates high similarity of the signals and thus indicates a successful rotation of the coordinate system. The normalised reference angular velocity signal and the normalised rotated angular velocity signal of position A can be seen in Figure 48. One gait cycle was chosen to represent the normalised signals.

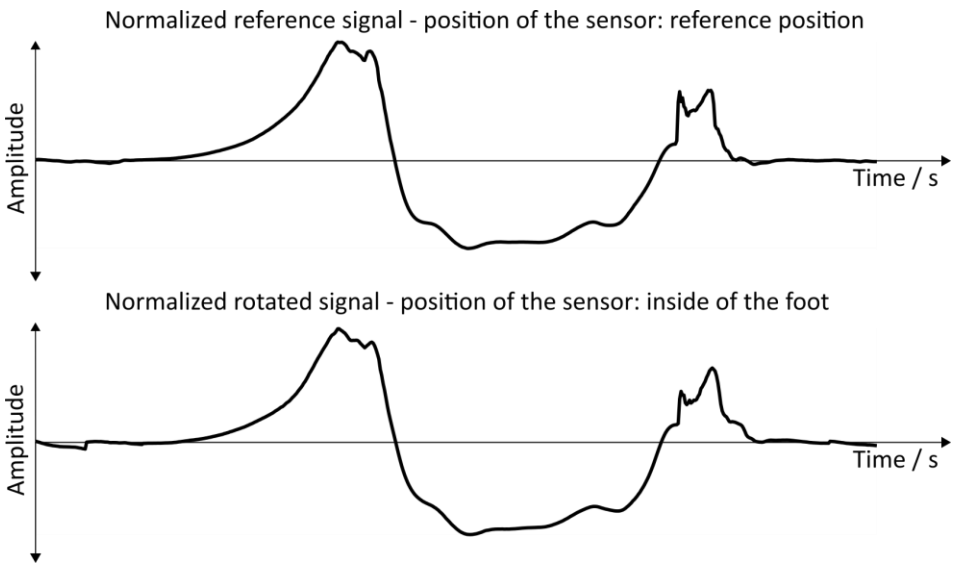

Figure 48: Angular velocity signals of the $\vec{y}_{axis}$. Position A—Inside of the foot

In Figure 49, the normalised signals of position B (rotated and reference signal) are visualised. One gait cycle was chosen to represent the normalised signals.

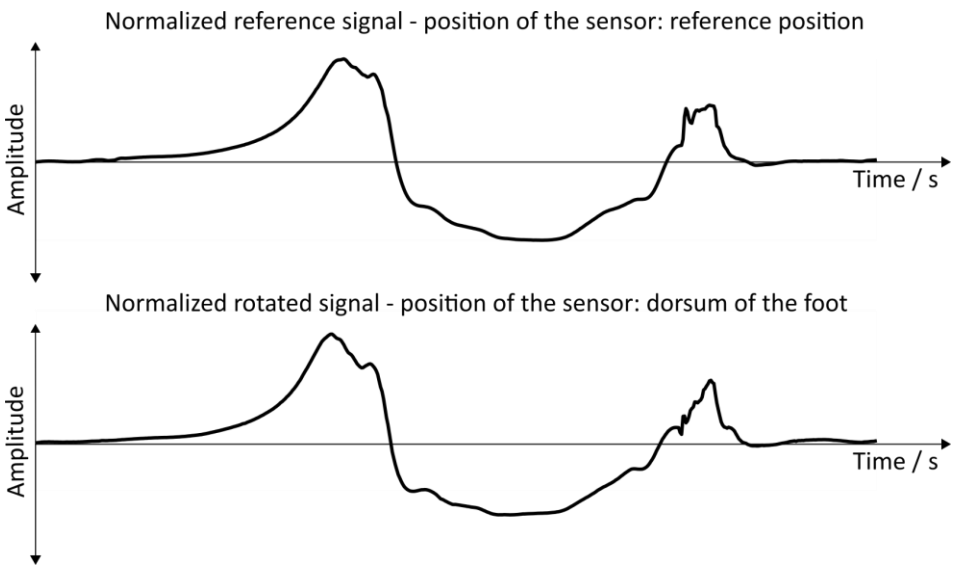

Figure 49: Angular velocity signals of the $\vec{y}_{axis}$. Position B—Dorsum of the foot

After normalising the signals, a duration of ten gait cycles each was chosen for comparison. The start and the end of this duration was defined by the according resting phases. The gait cycles of the normalised positions A and B were compared to the corresponding normalised gait cycle of the reference position. This process was repeated ten times with different gait cycles resulting in a total amount of 100 analysed gait cycles. The results of the cross-correlation can be seen in Table 13.

Number of gait cycles	Sensor position	Mean	Standard deviation
100	Inside the foot	0.998	0.001
100	Dorsum of the foot	0.988	0.002

Table 13: Cross-correlation between the angular velocity signal of the y_{axis} of position A and B and their reference signal

Discussion: The arbitrary sensor alignment algorithm contributes to the subsequently used gait detection algorithm and ensures the easy setup of the sensor. Additionally, it is one of the first calculations performed within this algorithm which later leads to a dependency of all other computations. Thus, it is an important part of the developed algorithm.

Discussion—Criteria 1: Under the assumption of ideal conditions, the linear acceleration data of the rotated $\vec{z}_{axis}$ of the IMU would show a value of 9.81m/s². Under consideration of real-life conditions, slight movements and rotations of the foot and ankle or movements of the sensor attachment are always present. Therefore, the results of the $\vec{z}_{axis}$ in Table 11 are considered satisfactory, since both the mean value of position A (9.795m/s² ± 0.016m/s²) and the mean value of position B (9.782m/s² ± 0.022m/s²) have a value close to 9.81m/s² (earth's gravitational acceleration).

Discussion—Criteria 2: Similar to criteria 1, real-life conditions have to be taken into account. As the linear acceleration data of the $\vec{x}_{axis}$ and the $\vec{y}_{axis}$ both fluctuate around zero (Table 12), the results are satisfactory.

Discussion—Criteria 3:

The evaluation shows that both cross-correlations provide values close to 1, indicating high similarity in the signals and providing a satisfactory result. In particular, the values were 0.998 ± 0.001 for the cross-correlating of the reference position and position A, and 0.988 ± 0.002 for the cross-correlation of the reference position and position B. Details can be found in Table 13.

5.4 Testing–Gait Event Detection Algorithm

The aim of the presented algorithm is to recognise four main gait events during robotic gait therapy. The following section thus aims to test its functionality and to evaluate the developed algorithm based on recorded data from healthy adults and from subjects who had a stroke. In section 5.4.1, the recording sessions with a healthy adult are elaborated. Section 5.4.2 is focussed on the conducted clinical study with stroke patients. Furthermore, experiments towards the performance of the developed algorithm were performed (sections 5.4.3).

5.4.1 Healthy Adult

Robotic gait therapy is intended for the treatment of gait disorders. In order to test and evaluate the presented algorithm and the according setup, trials with a healthy adult were conducted. The goal of these recording sessions was to prove its feasibility in a clinical environment. Furthermore, the data served as a basis to determine the detection rate and potential errors of the algorithm. The recordings were performed in the MEDIAN Neurological Rehabilitation Center Magdeburg and were supervised by professionally trained therapists. The subject was a 39-year-old healthy adult with no known gait disorders. The subject was informed about the goals of the recording sessions and has never executed a robot-assisted gait training before. The recordings were executed in two different robotic systems, Lyra and Lokomat, and prior to the first recording sessions, both the subject and the examiner were introduced into the functionalities of the robotic systems. The gait during the robotic training was measured with two IMUs attached to the foot, the setup is shown in Figure 50.

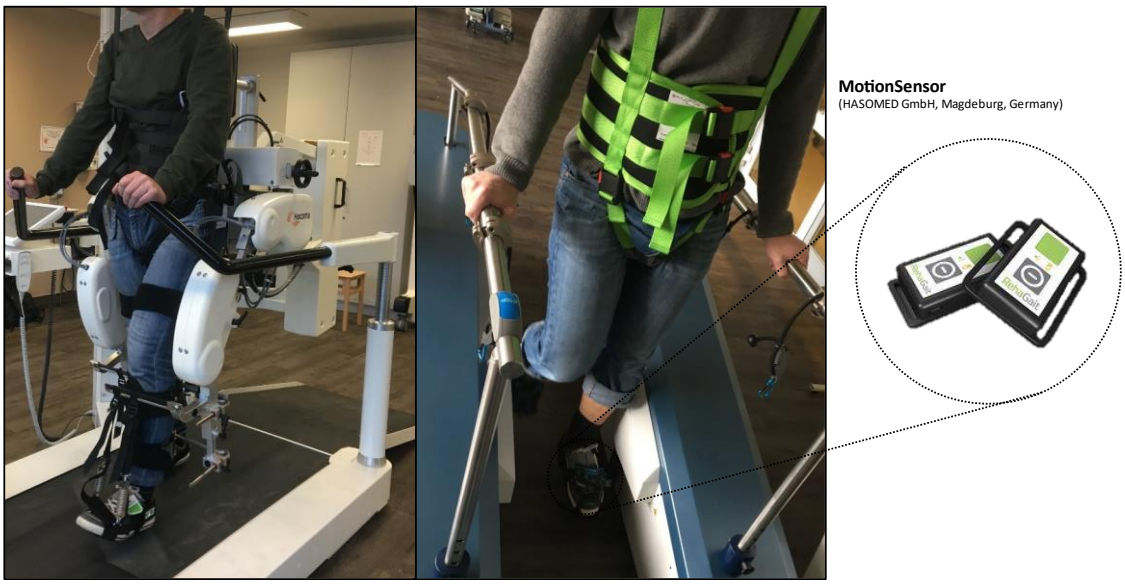

Figure 50: Setup of the recording sessions.
Left: Lokomat; Right: Lyra

Lokomat: The movement of Lokomat was induced by an orthosis attached to the subject's legs. This orthosis was adjusted to the anthropometric data of the subject and was examined by a specifically qualified physiotherapist. Furthermore, the therapist attached the harness and adapted it to the convenience of the subject. In this way, an optimal training setup was guaranteed. Since the test person was healthy and did not suffer from gait disorders, the risk of voluntarily influencing the induced gait pattern by unwanted support of the muscles was reduced. Therefore, the settings for the guidance force (section 4.1.1) were set to the maximum value. This constraint ensured that the recorded motion data reflected the walking pattern of the gait trainer and not the movement of the subject.

Lyra: The gait pattern of end-effector gait trainer Lyra was induced by movable foot plates. The subject places the feet onto the plates, the fixation was realised by fixation straps. The movable foot plates were examined and adjusted by a specifically qualified physiotherapist. Similar to Lokomat, the therapist attached the harness and adjusted it to the convenience of the subject. Lyra offers a biofeedback mode (section 4.1.2) which allows patients to influence the induced gait pattern. For this recording, the biofeedback mode was deactivated to reduce the voluntary influencing of the induced gait pattern by unwanted support of the muscles. Similar to Lokomat, this constraint ensured that the recorded motion data reflected the walking pattern of the gait trainer and not the movement of the subject.

Recordings: A total amount of six recording sessions was performed. Three recording sessions were executed with Lokomat, three with Lyra. Each recording had a total length of 60 minutes; the duration included donning time of the gait robot. The sampling frequency of the sensor was 500Hz, the measurement ranges for the linear acceleration and angular velocity were ±8g and ±1000°/s. Within the recording, three training velocities (1.2m/s, 1.5m/s, and 1.7m/s) were examined. According to the supervising therapists, these velocities represent typical values used during rehabilitation routine. The examiner started the recording with the sensors, afterwards the gait training started. In order to get reliable data, the subject was asked to accept the guidance of Lokomat and not to influence the gait pattern with voluntary movements. The software RehaGait Analyzer—for mobile gait analysis (HASOMED GmbH, Magdeburg, Germany) was used to record the data.

Analysing method: Subsequent to the acquisition, the raw data was utilised to analyse the generated algorithm. Beforehand, MATLAB was used to transfer the data into the developed algorithm. Following the import of the data, each data point was processed individually and sequentially using a customised MATLAB algorithm. A schematic representation of the sequential forwarding is visualised in Figure 51.

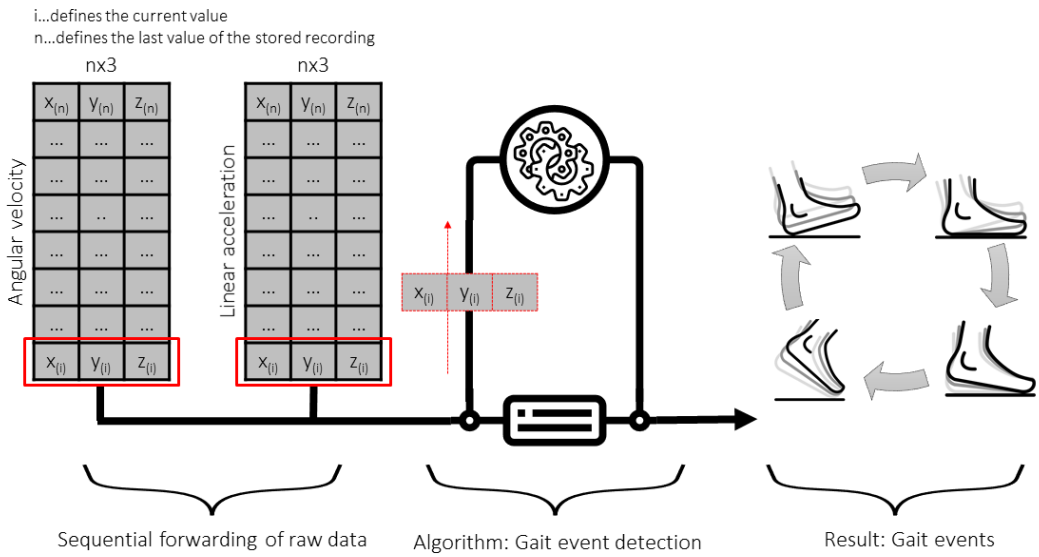

Figure 51: Sequential forwarding of raw data for the gait event detection algorithm

The custom function simulates an error-free and real-time Bluetooth connection to the sensors as it routes the samples in sequence. Thus, the gait event detection algorithm was applied to each individual datapoint in real time. The consideration of potential delays is described in section 5.4.3.

After the application of the algorithm, the data was analysed towards its functionality. A window-size of 75,000 data points (equal to 2.5 minutes) was chosen for the evaluation. The duration of 2.5 minutes was chosen as 7.5 minutes (= 3 windows) were the longest available acquisition time over all velocities. For each velocity, three windows were chosen in order to get a reliable number of datasets. As a result, nine windows (675,000 data points) were analysed for each recording. The selection method can be seen in Figure 52.

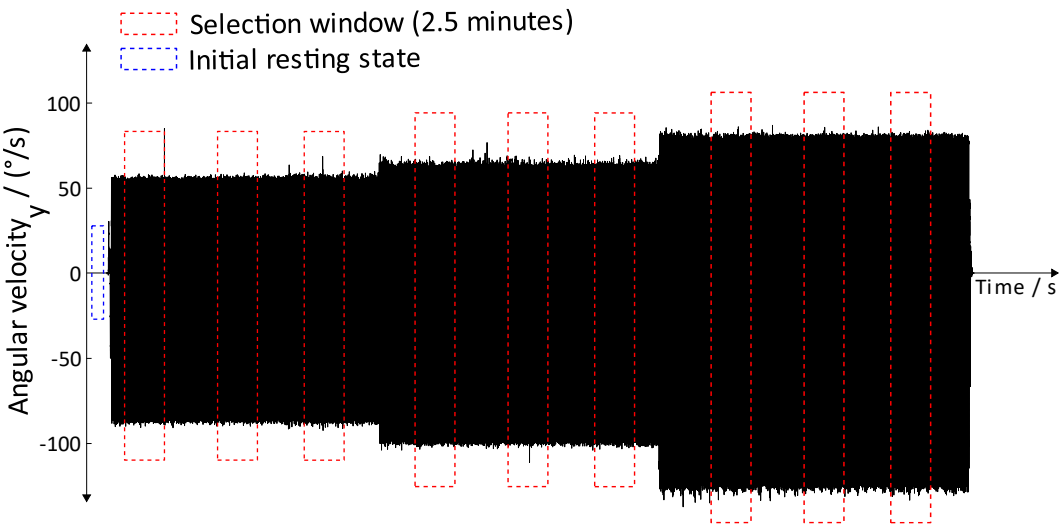

Figure 52: Selection method for Lokomat and Lyra—heathy adult

This analysing process was carried out to generate a repeatable and comparable way to evaluate the data. The analysing process was applied to the recordings of Lokomat and Lyra. The process was performed one time for each recording session. A resting period of a gait cycle was defined as the beginning of a window. The corresponding end-point of the window was defined by its size of 75,000 data points. Within those windows, the detection rate, false-positives and false-negatives as visualised in Table 14 were calculated as they represent three main outcomes for the evaluation of the gait event detection algorithm.

		Reference steps	
		True	False
Algorithm steps	True	**Correct**	**False-positive** Incorrect detected steps
	False	**False-negative** Undetected steps	**Correct**

Table 14: False-positive and false-negative

Correct detected steps within a selection window define the percentage of the detection rate. A successfully recognised step is only given if the detection sequence of gait events as described in the state diagram (Figure 32) has been fulfilled. The detection rate can thus be calculated as follows:

$$\text{Detection rate} = \frac{100}{\text{steps}_{\text{reference}}} * \text{steps}_{\text{correct detected}} \tag{17}$$

For the calculation of the detection rate, double observed steps were used as a reference ($\text{steps}_{\text{reference}}$). The correctly recognised steps of the algorithm ($\text{steps}_{\text{correct detected}}$) are determined by subtracting the incorrect detected steps from the total amount of detected steps ($\text{steps}_{\text{correct detected}} = \text{steps}_{\text{detected}} - \text{steps}_{\text{incorrect detected}}$). Incorrect detected steps are steps which fulfil the conditions of the developed algorithm, yet they appear on an incorrect position within the data and thus reflect an untypical motion behaviour during walking. In Figure 53, the difference between a correct detected an incorrect detected and an undetected step is schematically visualised. At the incorrect detected step, the sequence of the gait events is correct, yet the toe-off event is located at an incorrect position.
These incorrectly detected steps are further used to calculate the false-positives of the algorithm.

$$\text{False} - \text{positives} = \frac{100}{\text{steps}_{\text{reference}}} * \text{steps}_{\text{incorrect detected}} \tag{18}$$

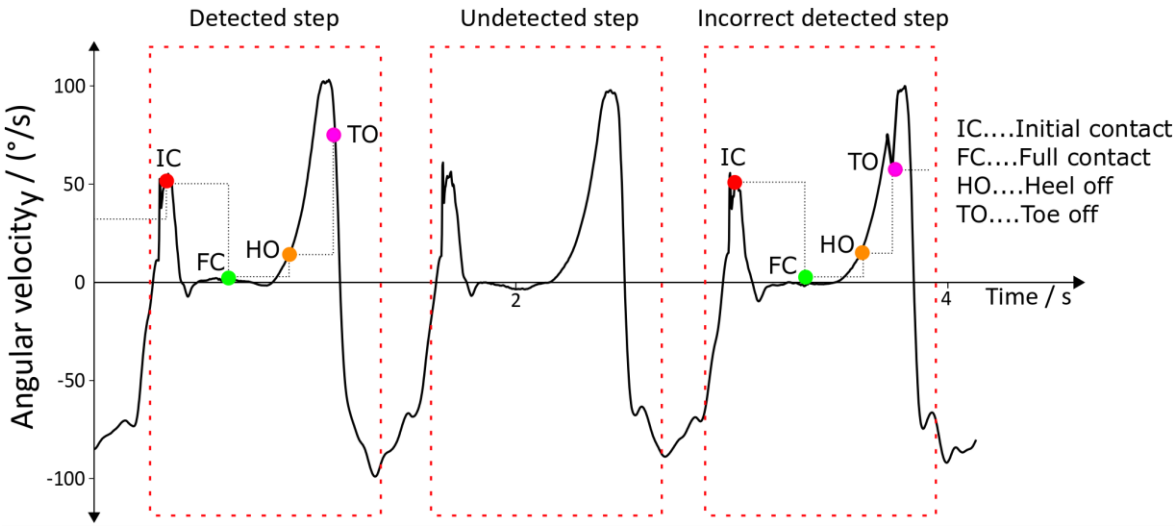

Figure 53: Difference between: Detected step, undetected steps and incorrectly detected step

For false-negatives, the amount of undetected steps ($steps_{undetected}$) is determined by subtracting the detected steps from the reference steps ($steps_{undetected} = steps_{reference} - steps_{detected}$). Based on that, false-positives are calculated as follows:

$$\text{False} - \text{negatives} = \frac{100}{steps_{reference}} * steps_{undetected} \tag{19}$$

The evaluation of the detection rate, false-positives and false-negatives including the according results are presented in section 5.5.

5.4.2 Stroke Patients

In clinical routine, robotic gait training is used to support the treatment of gait disorders. Thus, a clinical trial was conducted. The goal of this clinical study was to investigate whether the introduced algorithm including the proposed setup (Figure 50) is applicable during normal clinical rehabilitation routine of patients who suffered a stroke. Furthermore, a main priority was not to negatively influence the therapists or the patient during robot-assisted gait training. Thus, disturbances due to additional equipment (IMU and host computer) had to be reduced to a minimum by providing an easy setup.

Clinical trial: The recruitment of the participants was organised by the MEDIAN Neurological Rehabilitation Center Magdeburg. Ethical approval was granted by the Otto von Guericke University's ethics committee (section 8.3). The recruiting was split into three phases.

The first phase was executed by Prof. Dr. med. Michael Sailer (medical director and head physician of neurology) and Dr. Juliane Lamprecht (project leader at the Institute for Neurorehabilitation) who carefully screened the documents and the medical records of the patients. Based on the inclusion and exclusion criteria as stated in Figure 54, they provided a list of potential subjects who were suitable for robot-assisted gait training with Lokomat or Lyra. Phase two was executed by specially trained therapists who screened the potential subjects on the medical ward. Depending on their daily constitution (physical and mental), the therapists decided whether a robot-assisted gait training was suitable or not. After this decision, as a third phase, the subjects were asked whether or not they wanted to participate in the clinical study. The result of the recruitment was a total number of n = 10 stroke patients. All participants signed a written consent form prior to participation. The study procedure including the individual phases can be seen in Figure 54.

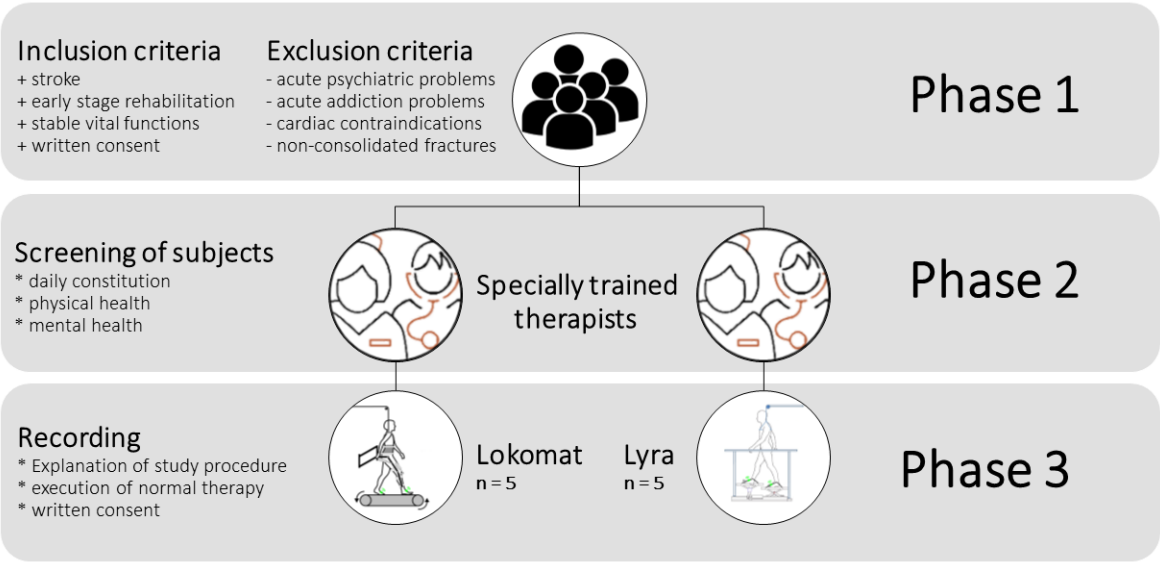

Figure 54: Procedure of the clinical study

After the subjects had been informed about the study procedure and after they had given their written consent, the therapists adjusted the robotic devices. The harness was adapted to their comfort. The orthosis of Lokomat and the foot plates of Lyra were fixed to the participant. For the fixation of the two sensors on the feet of the subject, fixation straps as shown in Figure 40 were used. As therapists coordinated the therapy and strived for an optimal rehabilitation outcome, the walking speed during the training, the guidance force of Lokomat and the biofeedback mode of Lyra were not predetermined by the study procedure. Both settings were adjusted according to the subjects' needs throughout the therapy. The total time for each therapy was 90 minutes; this time

included the screening of the participants, donning time including the explanation for the gait trainer and the description of the course of study.
This procedure ensured that the recordings could be executed during daily rehabilitation routine and thus a regular rehabilitation procedure of the participants could be ensured.
Information about the individual subjects is listed in Table 15 and Table 16. The affected side describes where the subject faced the gait disorder. The abbreviation FAC refers to the assessment of Functional Ambulation Categories which is used by therapists to find out how much support a patient needs when walking. The result is crucial—for example if it is checked whether the patient can return home after hospitalisation [137]. Whereas a FAC of 0 is the lowest scale and refers to a person who cannot walk at all or requires the assistance of two therapists, a FAC of 5 is the highest scale and refers to patients who can walk anywhere on their own, including stairs [138].

Number	Age	Sex	ICD-10-GM	Affected side	FAC
1	69	m	I63.9	Left	0
2	65	f	I63.5	Right	0
3	67	m	I63.5	Left	0
4	72	f	I69.3	Left	0
5	56	f	I61.0	Left	0

Table 15: Subjects of Lokomat

Number	Age	Sex	ICD-10-GM	Affected side	FAC
1	64	m	I63.4	Right	0
2	76	m	I61.0	Right	0
3	58	m	I63.1	Right	4
4	63	m	I61.9	Left	4
5	71	m	I63.9	Left	3

Table 16: Subjects of Lyra

Analysing method: After the application of the algorithm, the data was analysed towards the functionality of the algorithm. The analysing method is similar to the one described in 5.4.1. Yet the difference is that the selection windows were chosen differently. Due to the fact that the data was recorded during clinical routine, no specifications towards the velocity were made, thus the selection windows were not chosen within certain velocities but rather throughout the whole recording. Furthermore, the longest available acquisition

time of a participant was below eight minutes, thus a time of 3.5 minutes (= 105,000 datapoints), resulting in at least two windows for a recording, was defined as the window size. The selection method can be seen in Figure 55. Within those windows, the detection rate, false-positives and false-negatives as described in section 5.4.1 were calculated.

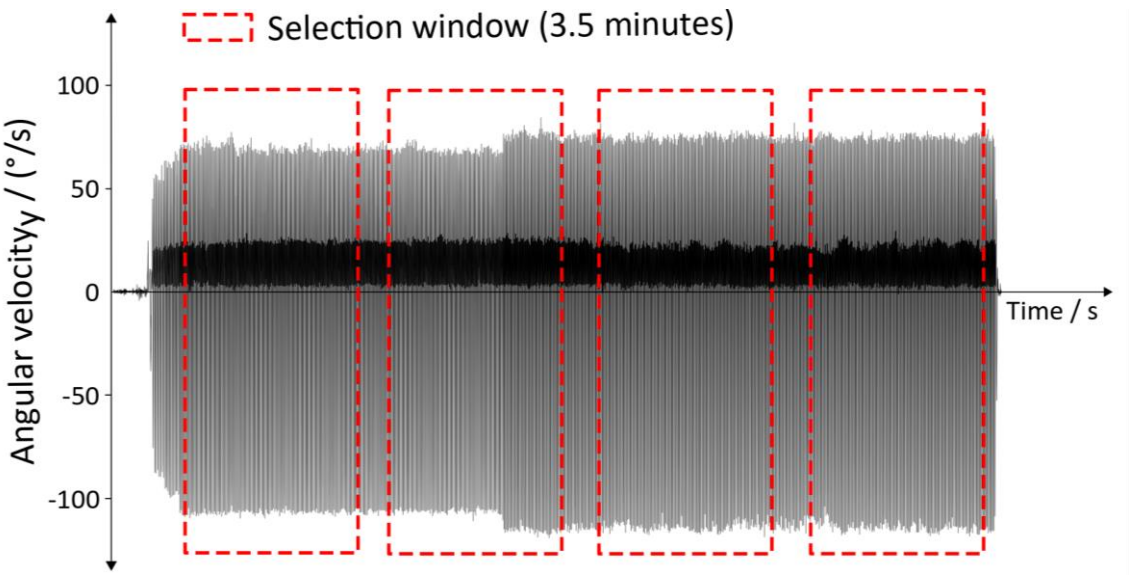

Figure 55: Selection method for Lokomat and Lyra—stroke patients

The evaluation of the detection rate, false-positives and false-negatives and the respective results are presented in section 5.5.

5.4.3 Performance

Every part of the algorithm needs a certain time for the data processing; as a result, there is a time between the incoming data stream and the output. This time delay can be called latency and refers to the performance of the algorithm. To evaluate the latency of the algorithm, each element of the gait event detection algorithm was taken into consideration for the testing procedure. The arbitrary sensor alignment including the full contact, the initial contact, the heel off and the toe off were tested individually. Furthermore, the overall latency was measured in order to be able to compare the results and to be able to detect potential flaws. Figure 56 shows the process of the latency estimation.

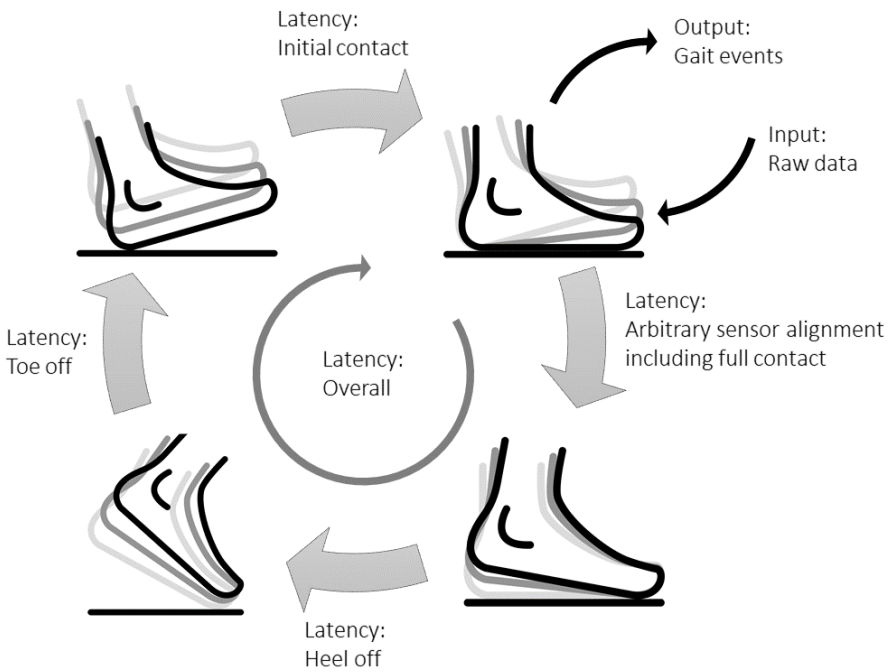

Figure 56: Latency estimation

For the estimation of the latency, the built-in MATLAB stopwatch timer (tic/toc;) was used. The tic command uses the toc function to measure the time. In detail, the tic function logs the actual time, and the toc function utilises the logged value to compute the time passed. The host computer was a LENOVO ThinkPad E590 (Windows 10) with an Intel CORE i7 8th Generation and 8GB of working memory. During the latency measurement MATLAB was the only user software actively running on the host computer and the WIFI connection was disconnected. The resolution of the stopwatch timer was determined by calling the commands tic/toc directly after each other. The data stream was provided by the aforementioned sequential forwarding of raw data (Figure 51). For the evaluation, an overground walking dataset with a duration of two minutes (=60,000 samples) was used. Each latency (Figure 56) was measured ten times and the mean and standard deviation for the elapsed time was computed, the corresponding analysis can be found in section 5.5.3.

5.5 Analysis—Gait Event Detection Algorithm

This chapter elaborates the results of the conducted recording with the healthy adult as well as the clinical trial and the performance measurements. It is split into three main parts: The first part shows the analysed data from the robotic gait training with the healthy adult, the second part presents the results of the clinical trial which focussed on gait event recognition during robotic gait therapy of patients with a stroke. The last part is focussed on the analysis of the performance of the algorithm.

5.5.1 Healthy Adult

In this section, the analysis of the testing and application from section 5.4.1 is elaborated. The detection rates of the recording session from Lokomat are shown in Figure 57. False-positives and false-negatives for Lokomat recording are shown in Figure 58 and Figure 59. The detection rate of Lyra recordings is visualised in Figure 60, the corresponding false-positives and false-negatives are shown in Figure 61 and Figure 62. Correctly recognised steps are defined by the detection rate whereas incorrectly recognised steps are defined by false-positives. False-negatives describe the undetected steps. The sensors (left/right) were evaluated separately. Furthermore, each selection window was analysed individually. Three selection windows representing one particular velocity are visualised within the dotted lines of the figures.

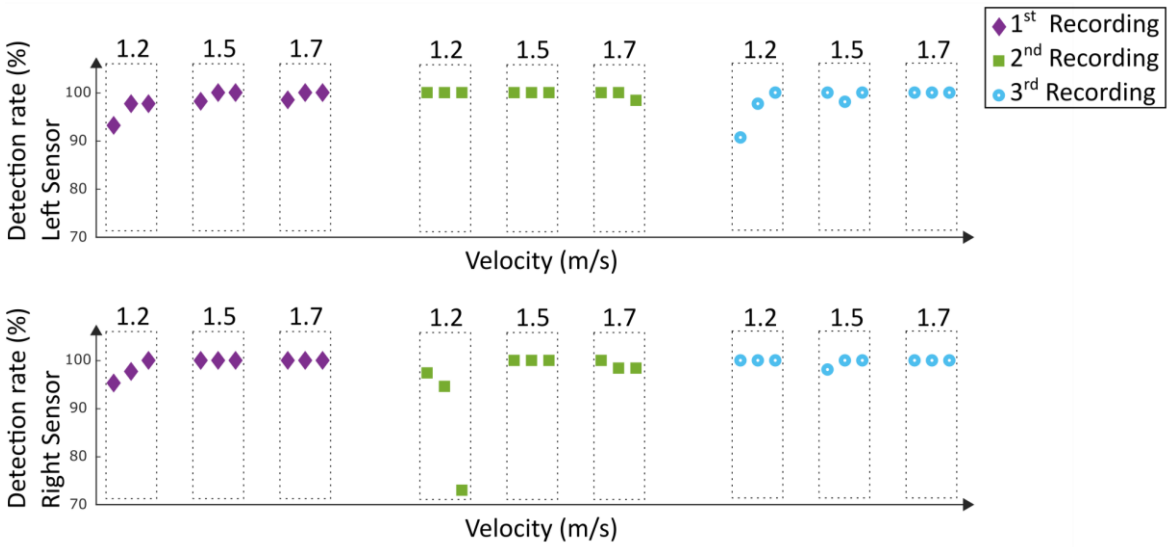

Figure 57: Detection rate: Lokomat—Healthy adult

Figure 57: Detection rate: Lokomat—Healthy adult: Within the first recording, the detection rates of the left sensor were between 93.2% and 97.7%. The detection rates of the right sensor were between 95.3% and 100%. For the second recording, one detection rate of the right sensor had a value of 98.4% whereas the rest had values of 100%. For the third recording, one value of 73% was reported for the left sensor, the remaining detection rates for this sensor were in between 94.6% and 100%. The overall detection rate for the left sensor was 99.1%, the right sensor had a detection rate value of 98.7%; overall a detection rate of 98.9%was reached. With regards to the training velocity, the following detection rates were achieved, 1.2m/s: 96.5%; 1.5m/s: 99.7%; 1.7m/s: 99.7%.

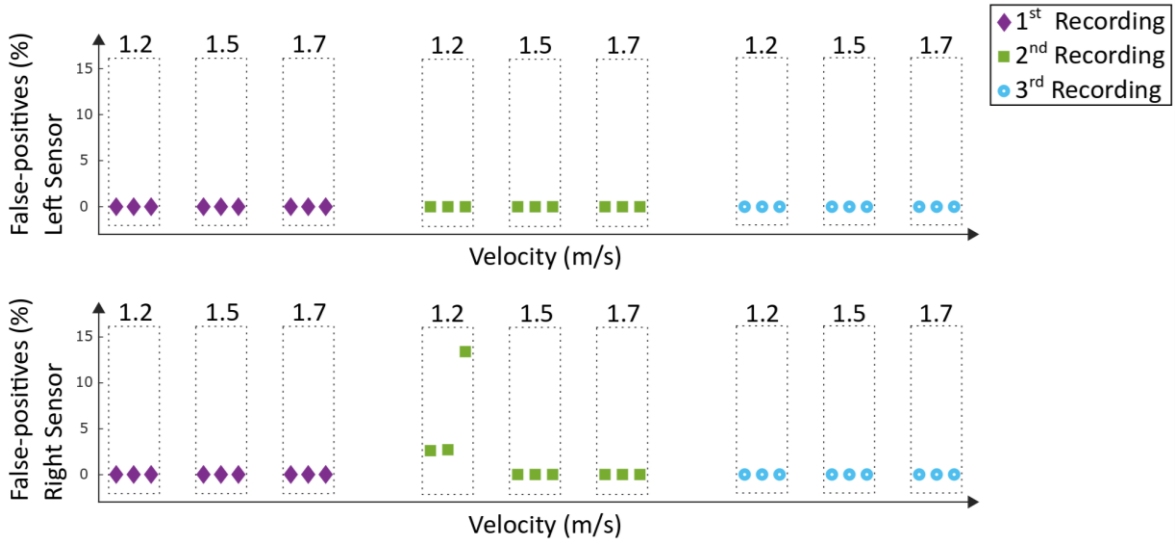

Figure 58: False-positives: Lokomat—Healthy adult

Figure 58: False-positives: Lokomat—Healthy adult: The false-positives for the majority of the velocities and their according selection windows were zero. As a result, the values for false-positives during 1.5m/s and 1.7m/s for both sensors were 0%. The same value applies for the whole left sensor. At the second recording session during 1.2m/s the right sensor had false-positives up to 15.3%. This results in an overall value for false-positives of 0.5% for the right sensor.

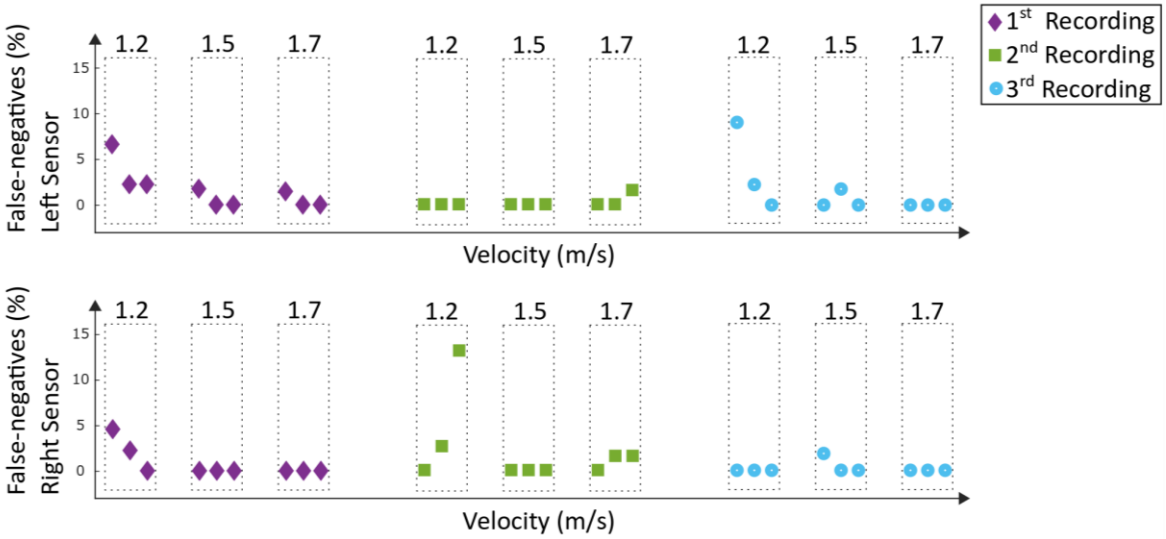

Figure 59: False-negatives: Lokomat—Healthy adult

Figure 59: False-negatives: Lokomat—Healthy adult: Except two values, the false-negatives during all recordings were below 6.8%. Higher values appeared, during the second recording with a value of 13.5% at 1.2m/s, and during the third recording with a value of 9.3% at 1.2m/s. With regards to the velocities, the value for false-negatives were 2.6% at 1.2m/s, 0.3% at 1.5m/s and 0.3% at 1.7m/s. Independently from each other, the left sensor had false-negatives of 0.9% and the right sensor had a value of 1% leading to an overall value for false-negatives of 0.9%.

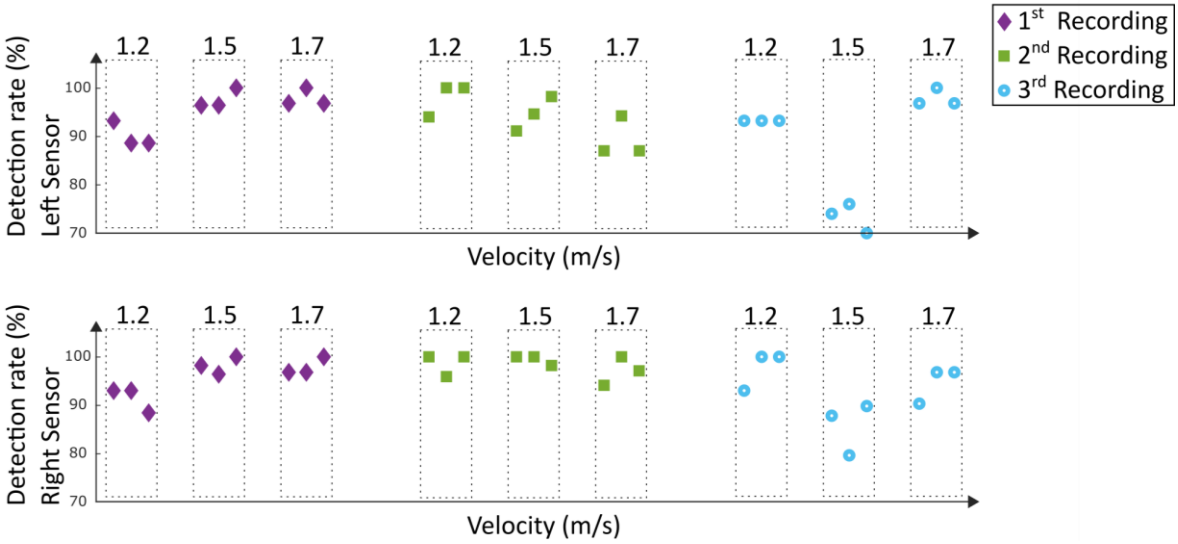

Figure 60: Detection rate: Lyra – Healthy adult

Figure 60: Detection rate: Lyra – Healthy adult**:** The detection rates from the first recording were within the minimum value of 88.6% and the maximum value of 100%. Similar

findings were obtained in the second session where the lowest detection rate was 87% and highest 100%. The third recording revealed similar rates, except four values during 1.5 m/s where detection rates were below 75%. The analysed data result in a detection rate for the left sensor of 94.2%, the right sensor had a value of 97.6%. All in all, a detection rate of 95.9% was reached. With regards to the training velocities, the following rates were achieved, 1.2m/s: 96%; 1.5m/s: 97.3; 1.7m/s: 94.7%.

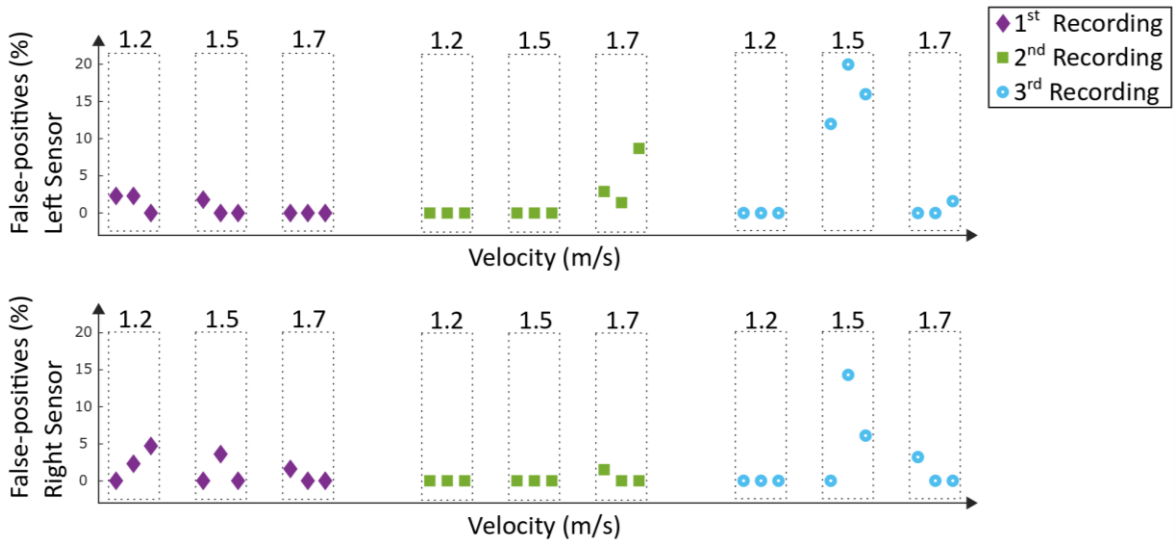

Figure 61: False-positives: Lyra – Healthy adult

Figure 61: False-positives: Lyra – Healthy adult**:** False-positives for the first recording session for both sensors were between 0% and 4.7%. The second recording had similar values for the false-positives, except one value of 8.7% during 1.7m/s at the left sensor. During the third recording session, false-positives of up to 20% at 1.5 m/s at the left sensor were reported. The overall value for false-positives was 0.9%. For the left sensor, the value for false-positives was 1.5%. The right sensor had a mean value of 0.5%. The false-positive values of the individual velocities were: 1.2m/s: 0.6%; 1.5m/s: 0.3%; 1.7m/s: 1.7%.

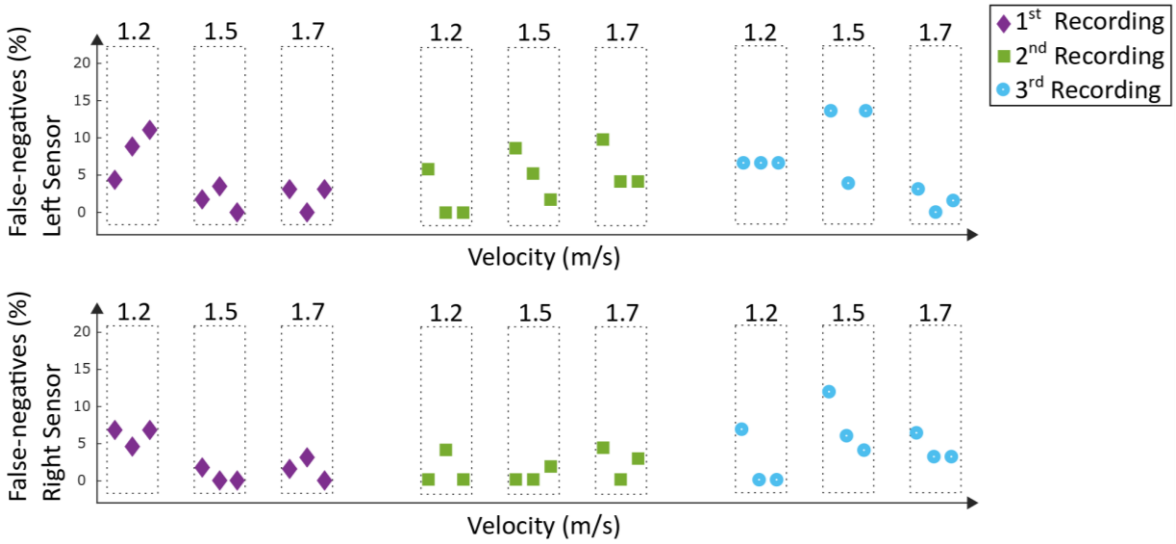

Figure 62: False-negatives: Lyra—Healthy adult

Figure 62: False-negatives: Lyra—Healthy adult: For the first recording, the false-negatives of the left sensor were up to 11.4%. For the second and third recording, the false-negatives were between 0% and 14%. False-negatives of the right sensor were between 0% and 7% for the first and second recording, the third recording had false-negatives up to 12.2%. With regards to the training velocities, the false-negatives were: 1.2m/s: 3.4%; 1.5m/s: 2.4%; 1.7m/s: 3.6%. Independently from each other, the value for false-negatives of the left sensor was 4.4%, for the right sensor, the value for false-negatives was 1.9%. As a result, an overall value for false-negatives of 3.1% can be reported.

5.5.2 Stroke Patients

In this section, the analysis of testing and application from section 5.4.2 is elaborated. Figure 63 and Figure 65 visualise the results of the detection rates, false-positives and false-negatives from the recording sessions of Lokomat. The detection rate of the Lyra recordings is shown in Figure 66, the corresponding false-positives and false-negatives can be seen in Figure 67 and Figure 68. Correctly recognised steps are defined by the detection rate whereas incorrectly recognised steps are defined by the false-positives. False-negatives describe the undetected steps. The sensors were evaluated separately. Furthermore, each selection window was analysed individually.

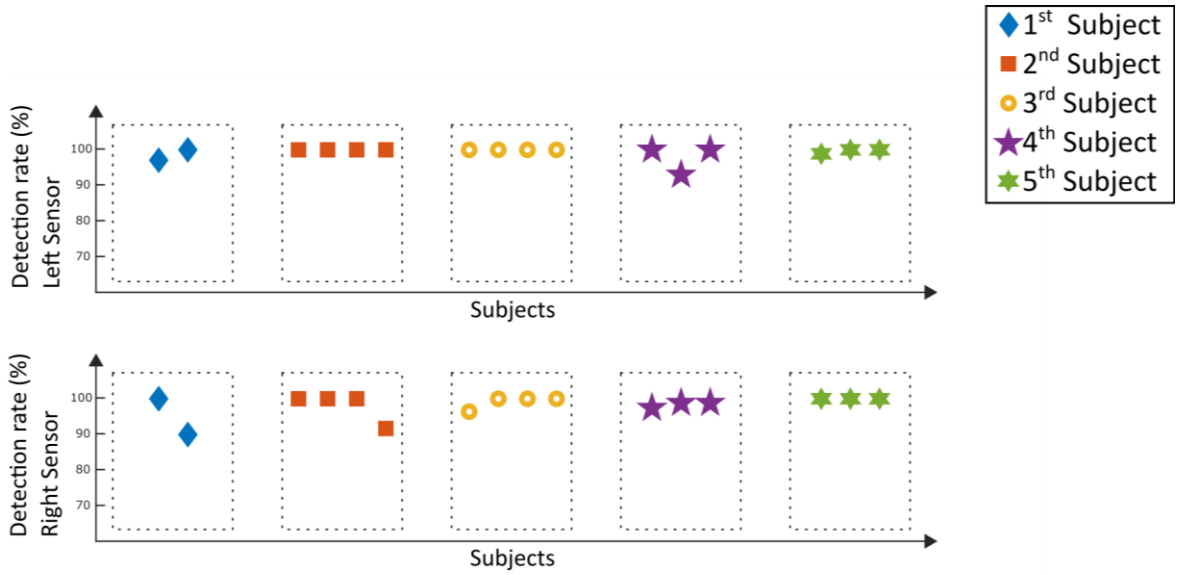

Figure 63: Detection rate: Lokomat—Stroke patients

Figure 63: Detection rate: Lokomat—Stroke patients: All detection rates of the subjects were above or equal to 90%. The detection rate for the left sensor was 99.2%, the right sensor had a value of 98.7%; overall, a detection rate of 98.9% was achieved.

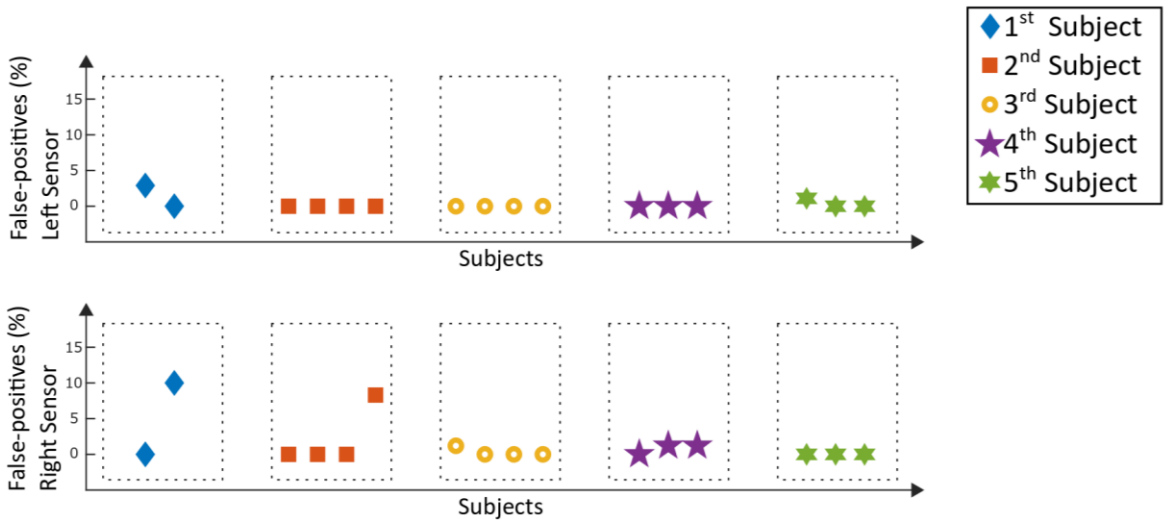

Figure 64: False-positives: Lokomat—Stroke patients

Figure 64: False-positives: Lokomat—Stroke patients: Except two values which occurred in the 1st subject (10%) and in the 2nd subject (8.3%), false-positives were between 0% and 3%. As a result, a value for false-positives for the left sensor of 0.3%, and a value for the right sensor of 1.1% was reported. All in all, the false-positive value was 0.7%.

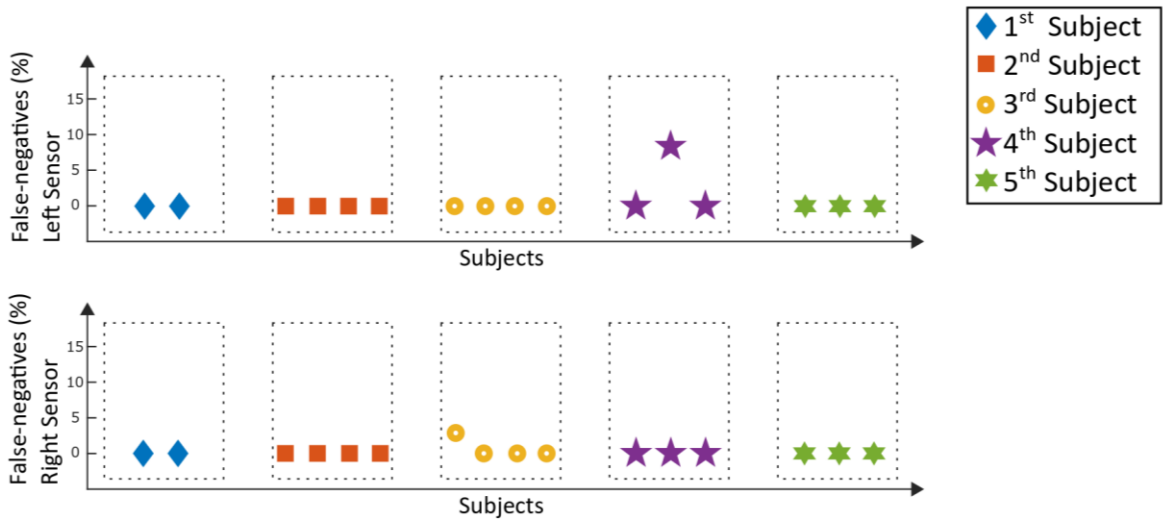

Figure 65: False-negatives: Lokomat—Stroke patients

Figure 65: False-negatives: Lokomat—Stroke patients: False-negative values were 0% for almost all analysed selection windows. Two values were above zero with the magnitude of 2.4% and 7%. The value for false-negatives for the left sensor was 0.5%, and 0.1% for the right sensor, resulting in an overall value for false-negatives of 0.3%.

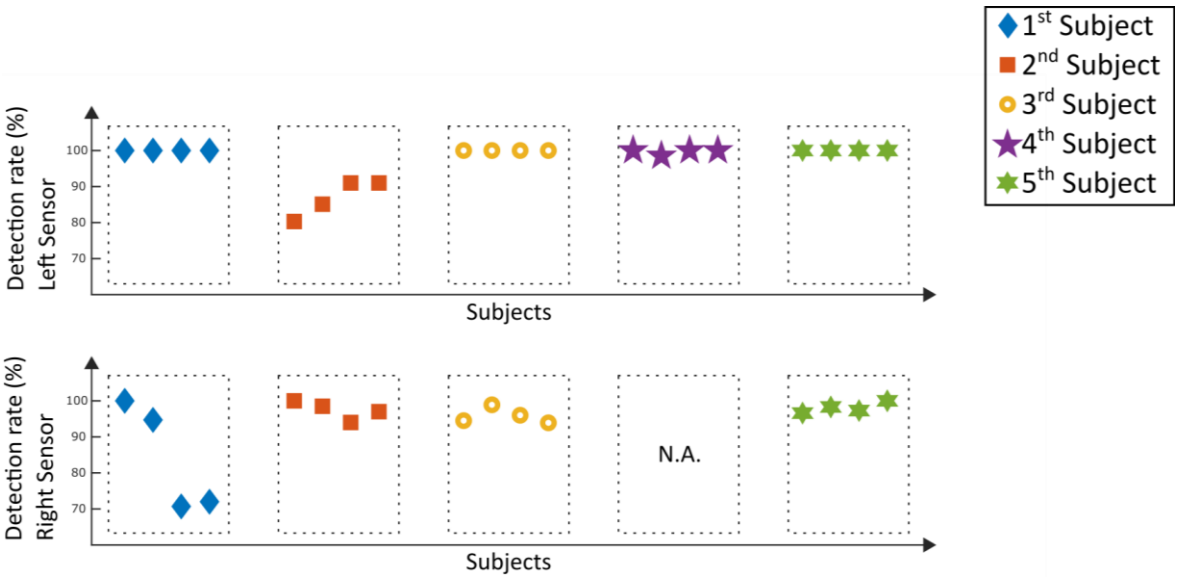

Figure 66: Detection rate: Lyra—Stroke patients

Figure 66: Detection rate: Lyra—Stroke patients: Detection rates of Lyra recording from 2nd—5th subject was between 80.3% and 100%. During the recording session of subject one, two lower values (72% and 70.7%) were reported whereas the other two detection rates were above 94%. N.A. refers to a not analysable measurement. All in all, the detection rate

was 95.9%. The individual sensors had detection rates of 97.6% (left sensor) and 93.8% (right sensor).

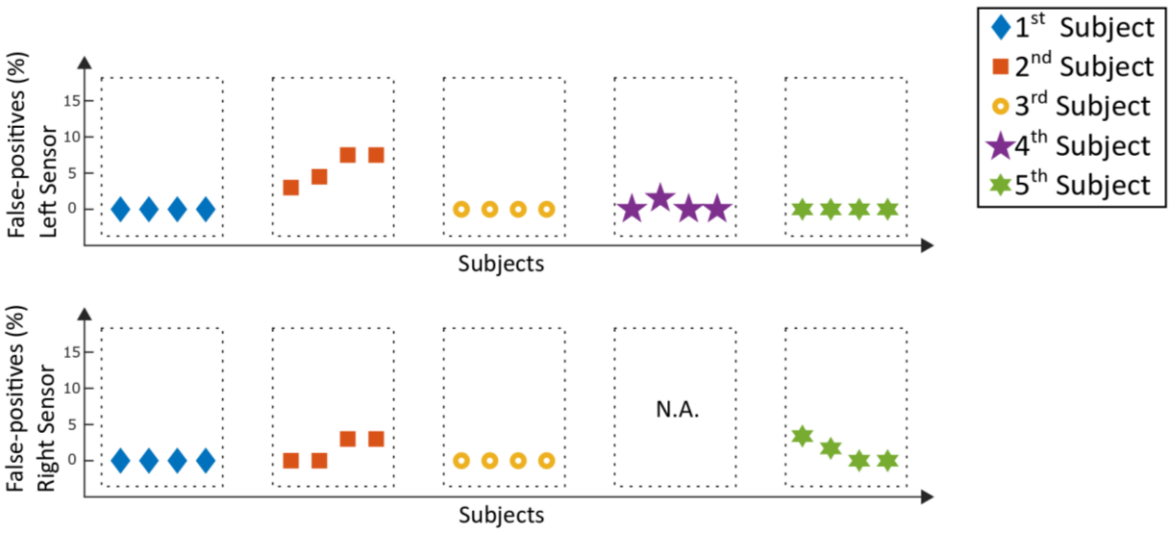

Figure 67: False-positives: Lyra—Stroke patients

Figure 67: False-positives: Lyra—Stroke patients: The false-positives for the 1st and the 3rd subjects were 0%. In the 2nd subject, values for false-positives up to 7.5% were reported. For the other subjects, the false-positives were in between 0% and 3.4%. As a result, the value for false-positives of the left sensor was 1.1%. For the right sensor, a value 0.6% was reported. This leads to an overall value for false-positives of 0.9%.

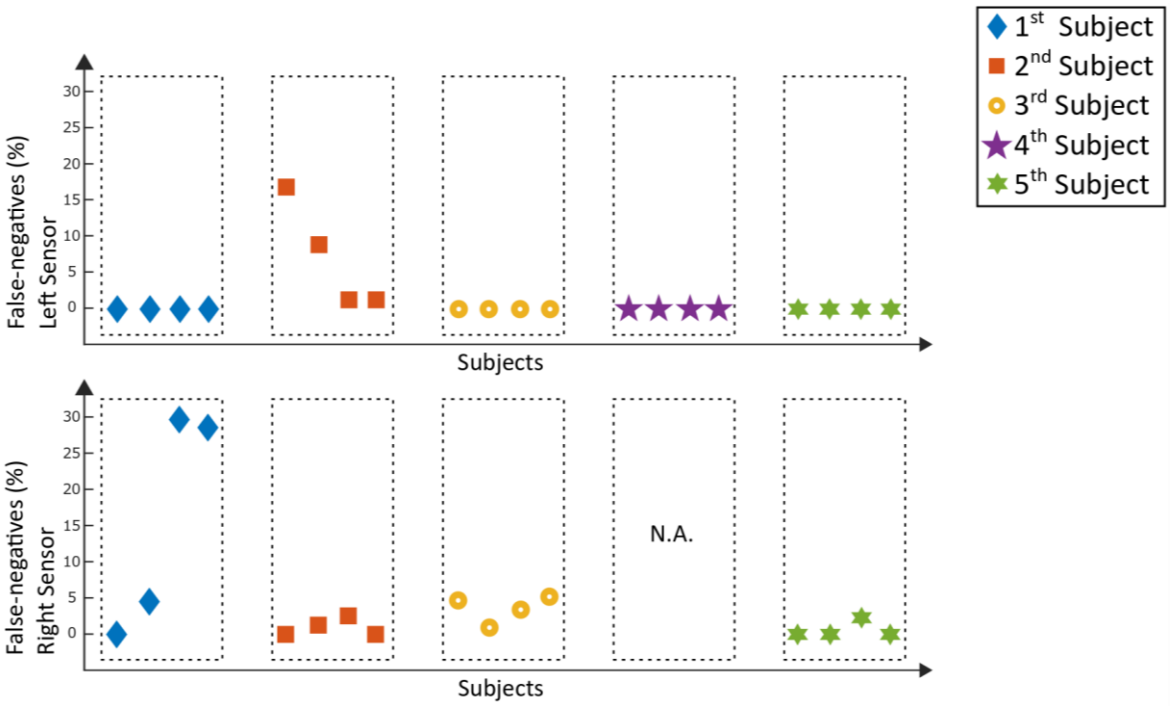

Figure 68: False-negatives: Lyra – Stroke patients

Figure 68: False-negatives: Lyra – Stroke patients**:** False-negative values for the left sensor of the 1st subject were 0%. The right sensor revealed false-negatives of up to 29.3%. The second subject had false-negatives up to 16.7% at the right sensor. For the 3rd, 4th and 5th subject the false-negatives were between 0% and 6.1%. The value for false-negatives for the left sensor was 1.3%, and 5.6% for the right sensor resulting in an overall value for false-negatives of 3.3%.

5.5.3 Performance

As mentioned in section 5.4.3, the performance was tested by estimating the latency of the individual parts of the algorithm. For the analysis of the performance, overground walking dataset with the duration of 120 seconds (60,000 samples) were used. The performance measurement was repeated ten times for each element of the algorithm, the mean and the standard deviation can be seen in Table 17.

Duration of raw data (s)	Evaluated element	Mean (µs)	Standard deviation (µs)
120	Arbitrary sensor alignment and full contact	244	13
120	Initial contact	3	0.2
120	Heel off	4	0.2
120	Toe off	16	5
120	Overall	282	17
120	Resolution (tic/toc)	0.5	0.1

Table 17: Estimated latency for gait events

The arbitrary sensor alignment algorithm induced a mean latency of 244µs ± 13µs. Initial contact and heel off both had a mean latency of below 5µs. The computation of the toe-off event results in a mean latency of 16µs ± 5µs. Overall, the gait event detection algorithm for one sensor induces a mean latency of 282µs ± 17µs. The resolution of the tic/toc function was 0.5µs ± 0.1µs.

5.6 Application—Functional Electrical Stimulation

Bench testing trials for the combination of the developed algorithm for gait event detection and functional electrical stimulation were performed and are elaborated in the following sections. Detailed information on the evaluated data and the corresponding results can be found in the corresponding analysis section.

5.6.1 Testing and Application—Trial 1

In order to further evaluate the feasibility of the concept, sub-aspects of the concept as shown in Figure 26 were considered and bench-tested.

To evaluate the capability of the algorithm to trigger FES based on the extracted gait events from the IMU data, the electrical stimulator (section 4.3) was connected to the host computer using a serial transmission via cable. Serial data transmission was realised with the ScienceMode protocol of HASOMED. ScienceMode is a communication protocol for controlling the used electrical stimulator. A host computer can be used to utilise the communication via a standard USB port. The stimulator was initiated within MATLAB in order to connect the hardware with the software. A Bluetooth connection from the sensors to the host computer was simulated as described in chapter 5.4. Furthermore, the sample frequency was taken into consideration by introducing a time delay after each sample. As mentioned in section 4.2, the sampling frequency was 500 Hz, thus the time between two samples (sampling period) is the inverse of the sampling frequency. This sampling period served as a time delay and was used to simulate the sampling frequency. Thus, real life conditions were simulated. This aspect was not taken into consideration for the previous experiments as the actual time delay of the incoming data stream was not considered relevant when analysing individual datapoints. As a representation of the stimulation electrodes, four LEDs each representing one channel were used (Figure 69). The LEDs were connected to the stimulation channels 1-4. As the LEDs represent the stimulation electrodes, their duration of illumination corresponds to the duration of the stimulation.

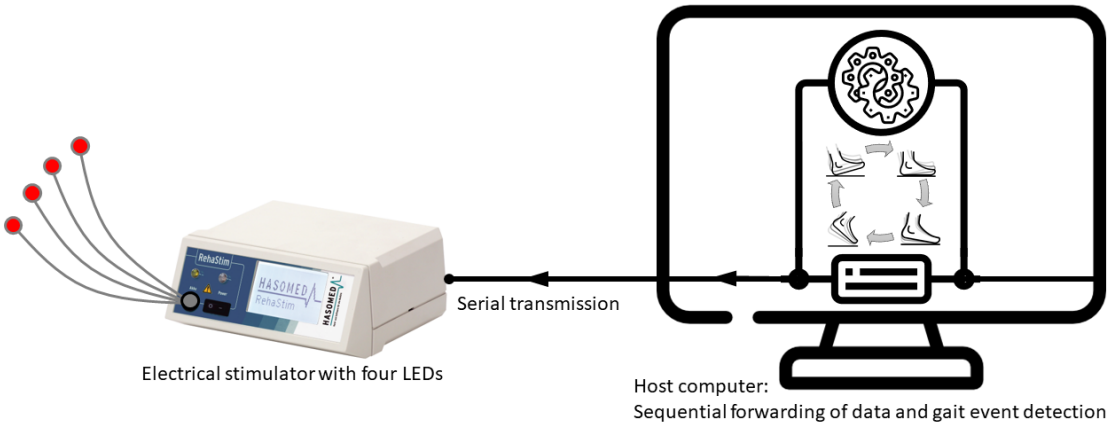

Figure 69: Setup: Bench test—Trial 1

The aforementioned communication protocol ScienceMode offers three different pulse generation modes—Single Pulse Mode, Continuous Channel List (CCL) Mode and One Shot Channel List (OSCL) Mode.

Single Pulse Mode: Using this mode, a single pulse can be created on a defined channel. Current, amplitude and pulse width can be specified for each pulse. The pulse is triggered by an external device such as a host computer and RehaStim creates the impulse immediately after the command is processed. If complex stimulation patterns are desired, more than one command can be sent sequentially. The external device (host computer) is responsible for controlling the timing.

Continuous Channel List (CCL) Mode: CCL simplifies the creation of complex templates. Doublets or triplets can be generated by defining a group of pulses which can be repeated. Altering intensity of the frequency by using doublets is a technique which can be used to influence muscle fatigue [139–143]. An example of CCL mode can be seen in Figure 70.

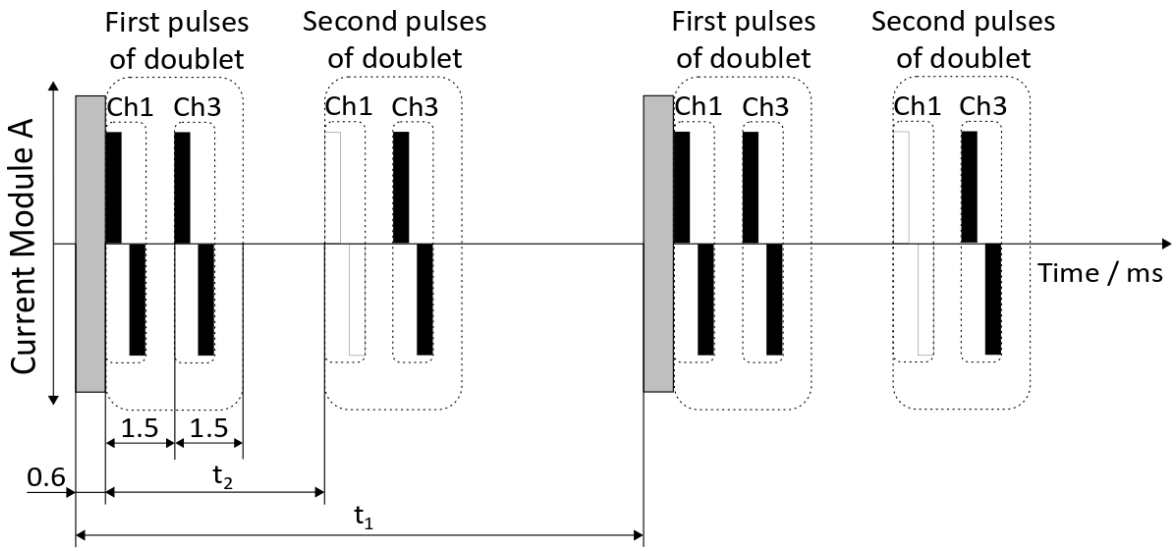

Figure 70: Continuous Channel List Mode—Example of single pulses and doublets

Channels 1 and 3 are enclosed in the channel list. $1/t_1$ defines the primary stimulation frequency. As visualised above, a doublet is created for channel 3, the stimulation frequency for that doublet is $1/t_2$. The duration of the communication between the controller and the stimulation modules is visualised as grey bars. Black bars indicate the biphasic pulses. When a channel list is created, the duration t_1 indicates the time between the repetition of the pulse list. Furthermore, a minimum time of 1.5ms must elapse between two selected channels of one module before a new stimulation can occur.

A delay of 0.6ms is in between the two modules processed in parallel. Channels 1-4 are connected to Module A, Module B (not visualised in the figure) is responsible for generating pulses on the channels 5-8. The inter-pulse time t_2 is initiated once and defines the time between the pulses of doublets and triplets. For doublets, the channel list is processed twice within this period, triplets are processed thrice, respectively. To provide more flexibility, the frequency can additionally be altered for some channels. Thus, a parameter n_{t1} can be used to lower the frequency of the selected channels accordingly. The usage of this parameter can alter the frequency within doublets and triplets. During initialisation, the used channels of the modules, the main time t_1, the time between the pulses t_2 and the maximal size of pulse groups have to be defined. The minimal possible inter-pulse time t_2 is defined as follows:

$$t_2 \geq 1.5\text{ms} * \max\left(n_{\text{Channel}_A}, n_{\text{Channel}_B}\right) \quad (1)$$

The variables n_{Channel_A} and n_{Channel_B} represent the number of selected channels

The primary stimulation frequency is defined by the duration t_1 and depends on the inter-pulse time t_2 as defined in the following condition:

$$t_1 \geq n_{\text{pulse group}} * t_2 + 1.5\text{ms} \quad (2)$$

The variable $n_{\text{pulse group}}$ defines if a single pulse ($n_{\text{pulse group}} = 1$), doublets ($n_{\text{pulse group}} = 2$) or triplets ($n_{\text{pulse group}} = 3$) are used

Taking the above-mentioned constraints into consideration, the following ranges for the primary stimulation time t_1 and inter-pulse time t_2 can be deduced.

Variable	Minimum (ms)	Maximum (ms)	Step size (ms)
Main stimulation time t_1	3	1023.5	0.5
Inter-pulse time t_2	3	16	0.5

Table 18: Main time t_1 and inter-pulse time t_2 for the channel list mode

Stimulation parameters such as pulse width, amplitude etc. can be changed as long as the CCL mode is active by sending a new external command. Deactivating the CCL mode is realised by sending a stop command to the stimulator. The primary frequency $1/t_1$ with which the channel list is handled, and the settings are managed and sent by the main processor of the RehaStim. As a result, the external device (host computer) is not blocked during this time. Thus, the host computer is able to further process data and only needs to send commands when the above-mentioned parameters need to be changed.

One Shot Channel List (OSCL) Mode: OSCL is similar to CCL; however, the processing of the main time t_1 is not automatically repeated. The channel list is only repeated if an external command is issued. Thus, the primary stimulation frequency t_1 is controlled by a command from an external device, in contrast to that the inter-pulse time t_2 is controlled with the stimulation modules.

Implementation of the CCL: For this bench testing trial, the CCL mode was assumed to be the best fit as a list of electrodes can be switched on and off by sending a command from the host computer to the stimulator and the stimulator repeats this stimulation independently from the host computer as long as no other command is sent. In order to evaluate the functionality, a stimulation sequence corresponding to the detected gait events as shown in Table 19 was used.

Gait event	LED 1	LED 2	LED 3	LED 4
Initial contact	On	Off	Off	Off
Full contact	On	On	Off	Off
Heel off	On	On	On	Off
Toe off	On	On	On	On

Table 19: Stimulation sequence for the bench testing trial

The defined stimulation sequence assures that the LEDs are switched on and off whenever the gait event detection algorithm detects a new gait event and that the gait events are visually distinguishable by the illumination of the LEDs. Simultaneously, the CCL mode guarantees that the gait event detection algorithm is not blocked while performing the stimulation.

Initialisation of the Stimulator: To realise the CCL mode and the corresponding stimulation, a connection between the host computer and the stimulator has to be established. This is realised using the MATLAB commands s = serial('port'). The command s = serial('port',Name,Value) generates an object for the serial communication port with defined properties. If invalid properties are specified, an error occurs, and the serial port object is not generated. Thus, the COM Port of the device must be determined beforehand using the device manager of the host computer. Afterwards, the serial port is opened with the MATLAB command fopen(s). The command fileID = fopen(filename) opens the file, filename, for binary read access. After performing the described process, the electrical stimulator is connected to the host computer and is opened in MATLAB which allows the communication using CCL mode.

CCL mode initialisation command: After initialising the stimulator, the CCL mode is set with the corresponding initialisation command. To realise this, the variables of Table 20 were defined.

Variable	No. of bits	Value/Range	Description
Ident	2	0	Identification number of commands 00 for the initialisation
Check	3	0–7	Checksum $\text{check} = (\text{N}_{\text{Factor}} + \text{Channel}_{\text{Stim}} + \text{Channel}_{\text{LF}} + \text{GroupTime} + \text{MainTime}) \bmod 8.$
N_Factor	3	0–7	Sets the number of times the stimulation is omitted in Channel_Lf and Channel_Stim. (never omit=0, omit once=1 … omit 7 times=7)
Channel_Stim	8	0–255	Specifies the activated channels (Bit0 = channel 1 … Bit 7 = channel 8)
Channel_Lf	8	0–255	Defines the low frequency channels (Bit0 = channel 1 … Bit 7 = channel 8)
GroupTime	5	0–31	Specifies the inter pulse-interval t_{s2} $t_{s2} \geq \text{Group_Time} * 0.5\text{ms} + 1.5\text{ms}$
MainTime	11	0–2047	Specifies the main time period t_{s1} $t_{s1} \geq \text{Main_Time} * 0.5\text{ms} + 1\text{ms}$

Table 20: Initialisation of the CCL mode: Variables

For this bench testing trial, the variable N_Factor and Channel_Lf and GroupTime were set to 0. The number of channels were four, thus Channel_Stim was set to 15 as it is the decimal value for the binary value of 1111_2. The MainTime was set to 38 in order to get a stimulation frequency of 50Hz. The checksum was calculated based on the set variables. All decimal variables were transformed to their binary value in order to generate the bytes for the initialisation command. The byte sequence can be seen in Table 21.

Bytes	Bit number	Variable	Bits with respect to variable	Value
Byte_1	7	-	-	1
	6	Ident	1	0
	5	Ident	0	0
	4	Check	2	1
	3	Check	1	0
	2	Check	0	1
	1	N_Factor	2	0
	0	N_Factor	1	0
Byte_2	7	-	-	0
	6	N_Factor	0	0
	5	Channel_Stim	7	0
	4	Channel_Stim	6	0
	3	Channel_Stim	5	0
	2	Channel_Stim	4	0
	1	Channel_Stim	3	1
	0	Channel_Stim	2	1
Byte_3	7	-	-	0
	6	Channel_Stim	1	1
	5	Channel_Stim	0	1
	4	Chanel_Lf	7	0
	3	Chanel_Lf	6	0
	2	Chanel_Lf	5	0
	1	Chanel_Lf	4	0
	0	Chanel_Lf	3	0
Byte_4	7	-	-	0
	6	Chanel_Lf	2	0
	5	Chanel_Lf	1	0
	4	Chanel_Lf	0	0
	3	-	-	0
	2	-	-	0
	1	GroupTime	4	0
	0	GroupTime	3	0
Byte_5	7	-	-	0
	6	GroupTime	2	0
	5	GroupTime	1	0
	4	GroupTime	0	0
	3	MainTime	10	0
	2	MainTime	9	0
	1	MainTime	8	0
	0	MainTime	7	0
Byte_6	7	-	-	0
	6	MainTime	6	0
	5	MainTime	5	1
	4	MainTime	4	0
	3	MainTime	3	0
	2	MainTime	2	1
	1	MainTime	1	1
	0	MainTime	0	0

Table 21: Initialisation of CCL mode: Byte sequence

After the generation of the bytes, the initialisation command can be sent via the serial connection to the stimulator using the MATLAB command fwrite(s,[Byte_1,Byte_2,Byte_3,Byte_4_,Byte_5,Byte_6]);.

CCL mode updating command: The update command initiates or alters a stimulation as soon as the command is sent. Similar to the initialisation command, variables need to be sent in the correct order to define the sequence of stimulation (Table 22).

Variable	Bits	Value/Range	Description
Ident	2	1	Identification number of commands 00 for the initialisation
Check	5	0 – 31	Checksum $\text{check} = (\text{Mode} + \text{PulseWidth} + \text{PulseCurrent}) \bmod 32.$
Mode	2	0 – 2	Defines the stimulation mode. (Single pulse=0, doublet=1, triplet=2)
PulseWidth	9	0 – 500	Defines the pulse width in
PulseCurrent	7	0 – 127	Current in mA (Bit0 = channel 1 … Bit 7 = channel 8)

Table 22: Update of CCL mode: Variables

For this bench testing trial, the variable Mode was set 0 as no doublets or triplets were required. The pulse width and the current influence, the brightness of the LEDs, both values were chosen to be close to the maximum values (pulse width = 400µs and current = 100mA) to generate a bright illumination. The checksum was calculated based on the set variables for each update command. All decimal variables were transformed to their binary value in order to generate the bytes for the update command. The sequence of the byte sequence can be seen in Table 23.

Bytes	Bits	Variable	Bits with respect to variable
Byte_1	7	-	-
	6	Ident	1
	5	Ident	0
	4	Check	4
	3	Check	3
	2	Check	2
	1	Check	1
	0	Check	0
For each activated channel, three bytes are sent to the stimulator in ascending order with regard to the channel number			
Bytes	**Bits**	**Variable**	**Bits with respect to variable**
Byte_2	7	-	-
	6	N_Factor	1
	5	Channel_Stim	0
	4	-	-
	3	-	-
	2	-	-
	1	PulseWidth	8
	0	PulseWidth	7
Byte_3	7	-	-
	6	PulseWidth	6
	5	PulseWidth	5
	4	PulseWidth	4
	3	PulseWidth	3
	2	PulseWidth	2
	1	PulseWidth	1
	0	PulseWidth	0
Byte_4	7	-	-
	6	PulseCurrent	6
	5	PulseCurrent	5
	4	PulseCurrent	4
	3	PulseCurrent	3
	2	PulseCurrent	2
	1	PulseCurrent	1
	0	PulseCurrent	0

Table 23: Update of CCL mode: Byte sequence

Depending on the gait event, the CCL mode triggers the LED (Table 19). Thus, four update commands each consisting of 13 bytes were generated. These 13 bytes incorporate the Ident and Check-Bits and the individual binary configuration depending on the stimulated channel as described in Table 23. The values of the bytes during the corresponding gait event can be seen in Table 24.

Gait phase	Byte	Value		Gait phase	Byte	Value	
Initial contact	1	10110100		Full contact	1	10101000	
	2	00000011	Channel 1		2	00000011	Channel 1+2
	3	00010000			3	00010000	
	4	01100100			4	01100100	
	5	00000000			5	00000011	
	6	00000000			6	00010000	
	7	00000000			7	01100100	
	8	00000000			8	00000000	
	9	00000000			9	00000000	
	10	00000000			10	00000000	
	11	00000000			11	00000000	
	12	00000000			12	00000000	
	13	00000000			13	00000000	
Heel off	1	10101000		Toe off	1	10101000	
	2	00000011	Channel 1+2+3		2	00000011	Channel 1+2+3+4
	3	00010000			3	00010000	
	4	01100100			4	01100100	
	5	00000011			5	00000011	
	6	00010000			6	00010000	
	7	01100100			7	01100100	
	8	00000011			8	00000011	
	9	00010000			9	00010000	
	10	01100100			10	01100100	
	11	00000000			11	00000011	
	12	00000000			12	00010000	
	13	00000000			13	01100100	

Table 24: Update of CCL mode: Byte sequence for the individual gait events

After the generation of the bytes, the update command can be sent. Depending on the gait events, the bytes as defined in Table 24 must be sent using the MATLAB command fwrite(s,[Byte_1….,Byte13]);.

CCL mode stop command: The CCL mode runs until the stimulator receives a stop command or the electrodes lose skin contact and cause an electrode failure. Similar to the initialisation and update command, variables need to be sent in order to define the sequence of stimulation (Table 25).

Variable	Bits	Value/Range	Description
Ident	2	1	Identification number of commands
Check	5	0 – 31	Checksum; $\text{check} = (0) \bmod 32 = 0$.

Table 25: Stop of CCL mode: Variables

The stop command stays the same for all channels and stops the stimulation. By using the MATLAB command fwrite(s,[Byte_1]), the stop command is sent, the corresponding Byte_1 can be seen in Table 26.

Bytes	Bits	Variable	Bits with respect to variable	Value
Byte_1	7	-	-	1
	6	Ident	1	1
	5	Ident	0	0
	4	Check	4	0
	3	Check	3	0
	2	Check	2	0
	1	Check	4	0
	0	Check	0	0

Table 26: Stop of CCL mode: Byte sequence

After implementation of the CLL mode to trigger the LEDs according to the gait events, the latency was determined. As described in section 5.4.3, the tic/toc function was used to estimate the time needed for executing the function. The latency estimation for the bench testing was done similarly to Figure 56 but instead of the latency of the gait events, the *fwrite(s,[…])* function needed to send the update commands after each gait event to the stimulator were considered. For the evaluation, an overground walking dataset with a duration of two minutes (=60,000 samples) was used. The latency for each command was evaluated ten times. Mean and standard deviation for the elapsed time were calculated and can be seen in section 5.6.4.

5.6.2 Testing and Application—Trial 2

After the first bench testing and evaluating the algorithms capability to trigger the stimulator according to the gait events, the LEDs representing the stimulation channels were replaced by self-adhering neurostimulation electrodes for electrical stimulation. The RehaTrode stimulation electrodes (HASOMED GmbH, Magdeburg, Germany) were

connected to the stimulator and the device was connected to the host computer using a serial connection. The initialisation of the stimulator was done as described in Bench testing—Trial 1. In order to generate a walking pattern, the involved muscles were defined. As there are only limited stimulation channels (8 stimulation channels, section 4.3), not all muscles involved in walking as described in section 2.2.1 can be activated with electrical stimulation. Furthermore, the accessibility of muscles must be considered, meaning that superficial and more prominent muscles are easier to access compared to underlying muscles or muscles which might be covered with clothes during therapy. As a result, four main muscles for each lower extremity as visualised in Figure 71 were considered for functional electrical stimulation. In the upcoming paragraphs, the applied method is described for one leg. For the second leg, the same method would be applied.

Muscle	Side	Color	Start (%)	Peak (%)	End (%)
Rectus femoris	Right	Red	57	59	65
Rectus femoris	Left	Red	7	9	15
Biceps femoris (long head)	Right	Blue	82	93	5
Biceps femoris (long head)	Left	Blue	32	42	55
Tibialis anterior	Right	Black	56	0	13
Tibialis anterior	Left	Black	6	50	63
Gastrocnemius	Right	White	9	40	50
Gastrocnemius	Left	White	59	90	0

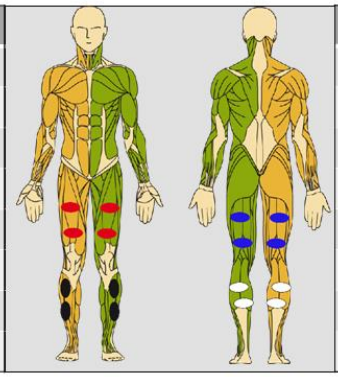

Figure 71: Four main muscles considered for functional electrical stimulation

For the creation of the update commands (as described in detail in section 5.6.1), the start and the end of the activation period is of importance. Taking into account the muscle activation sequences with respect to the events of the human gait cycle as described in section 2.2.1 and considering the gait cycle as a dynamic and consecutive sequence of eight events starting from the initial contact at 0% of the gait cycle and ending at the next initial contact at 100% of the gait cycle, a muscle activation sequence for functional electrical stimulation as shown in Figure 72 can be derived.

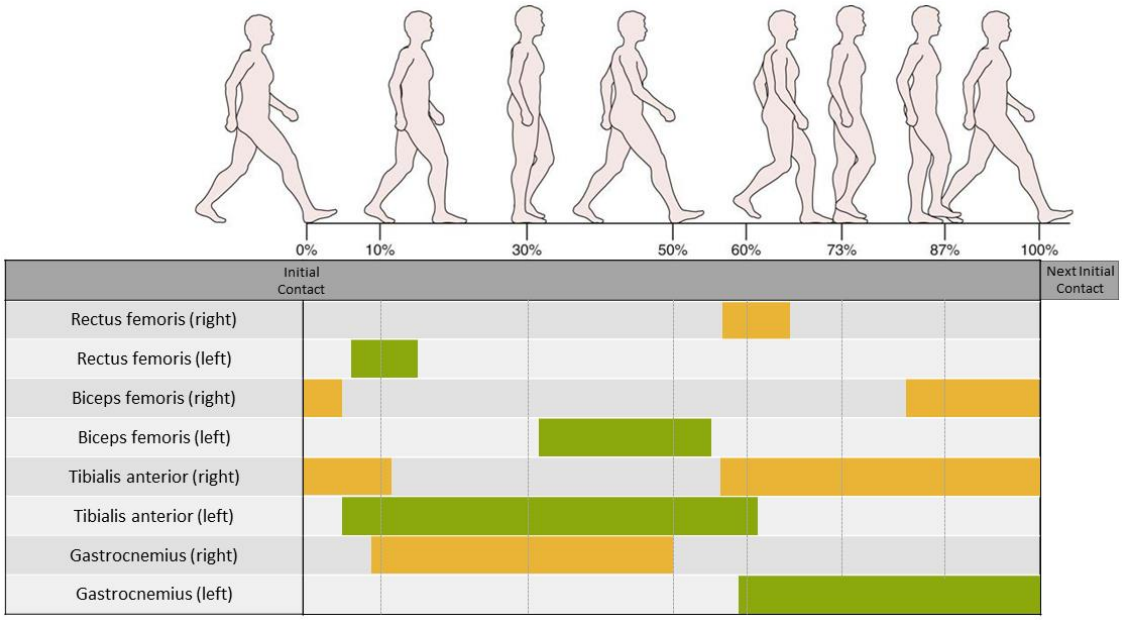

Figure 72: Muscle activation sequence for functional electrical stimulation

The duration of the whole gait cycle must be known in order to apply the activation sequence as described in Figure 72. Based on that, a first approach for the generation of the stimulation was derived:

As robot-assisted gait training provides a cyclic movement and as the gait velocity is subject to only small changes throughout the therapy, the duration of the previous step can be considered as the stimulation duration for the next step. In order to realise that the duration of the previous step must be known. Based on that information, the duration of the individual periods can be calculated according to the percentages of stimulation as visualised in Figure 71. Considering a robot-assisted gait training of a stroke patients (section 5.4.2), an exemplary duration as shown in Figure 73 can be assumed.

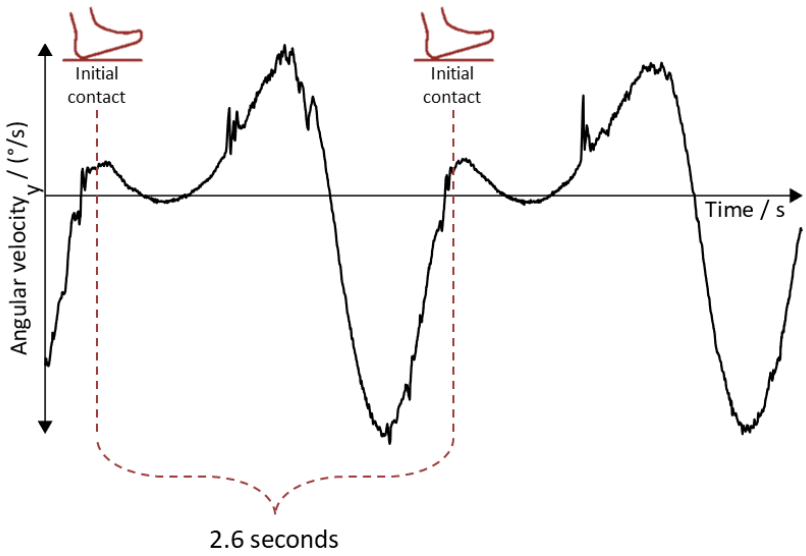

Figure 73: Typical duration of a gait cycle during robotic gait training

An update of the step duration can be done repeatedly, and a stimulation can be triggered at every initial contact which allows the algorithm to alter the stimulation times after every step. An example of the stimulation times combining the step duration of 2.6 seconds (Figure 73) and the activation percentages (Figure 72) can be seen in Table 27.

Muscle	Start #1 (ms)	End #1 (ms)	Start #2 (ms)	End #2 (ms)
Rectus femoris	1482	1690	-	-
Biceps femoris	0	130	2132	2600
Tibialis anterior	0	338	1456	2600
Gastrocnemius	234	1300	-	-

Table 27: Start and stop times for the activation of the muscles during one gait cycle with the duration of 2.6 seconds (Bench test—Trial 2)

The stimulation times of the individual muscles overlap at certain points and lead to the fact that up to two channels need to be activated simultaneously. Furthermore, there is a time between the heel off and the toe off where none of the chosen muscles is active. During this period, all channels must be deactivated. The combination of activation and deactivation of muscles and the amount of needed update commands for one gait cycle are visualised in Figure 74.

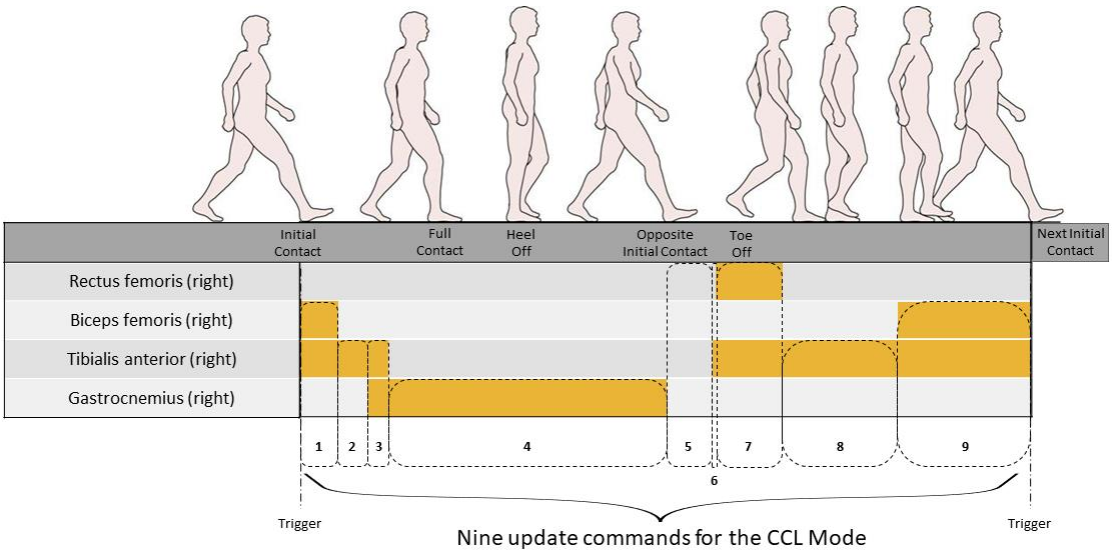

Figure 74: Amount of update commands of the CCL mode during one gait cycle (Bench test—Trial 2)

As a result, nine update commands are needed to activate/deactivate four muscles throughout the gait cycle, whereas each muscle is activated by its own channel. Channel 1: rectus femoris, channel 2: biceps femoris, channel 3: tibialis anterior and channel 4: gastrocnemius. The update commands could also be reduced as some activate the same muscle groups, yet for a better overview and for an easier implementation into the algorithm, a detailed clustering of commands was chosen. As a next step, the parameters frequency, pulse width and amplitude for the stimulation must be defined.

Frequency: The used frequencies for electrical stimulation can be very different depending on the aim of the treatment , most clinical applications however tend to use frequencies of 20-50Hz for the therapy [144,145]. Constant low frequency stimulation can be used to avoid fatigue and discomfort [146] but could also lead to a lack of muscle activation which, in turn, leads to non-efficient contraction and low force generation [147]. In general, higher frequencies are supposed to be more pleasant compared to lower frequencies as they elicit a smoother force response (tetanic contraction) and have a less tingling/sparkling effect. Lower frequencies rather generate a tapping/twitching effect where the single pulses can be differentiated [148].

Pulse width: For biphasic pulses (Figure 25), the pulse accounts for one positive phase coupled with one negative phase, the pulse width or pulse duration refers to the duration of the positive or negative phase [149]. For FES cycling where dynamic quadriceps

extensions are wanted, pulse widths between 300µs-600µs [147,150–152] are used. Lower frequency stimulation which provides pulse durations of 500µs-1000µs can result in a lower fatigue index. Furthermore, short pulse widths (10µs-50µs) can influence the recruitment of muscular fibres which can lead to a higher torque recruiting a lower amount of fibres before generating an activation of a different muscle [153]. A comparison of pulse widths with values of 50—1000µs at a frequency of 20 Hz showed, that longer pulse durations produced stronger contractions in the soleus muscle generating a greater plantarflexion and additionally increased general contractile properties [154]. Typically, when a deeper penetration is wanted, longer pulse durations are recommended [155].

Amplitude: The higher the pulse amplitude, the greater the depolarising effect in the regions beneath the stimulation electrodes [156]. Increased intensities will lead to increased strength. However, gains in muscle strength are often present after training with electrical stimulation [157–160]. The pulse amplitude also influences the patients' comfort whereas higher amplitudes are typically less tolerated compared to lower amplitudes. Overall, the combination of frequency and amplitude will determine the quality of muscle contraction [155].

Summary: Summing up all the above-mentioned information of the individual parameters and their effect on muscle contraction, an overview as provided in Table 28 can be derived. Yet it is important to mention that the combination of parameters has to be evaluated for each application and for each subject working with electrical stimulation. Furthermore, a gradual increase of the amplitude achieves an optimal contraction within tolerable levels. If no contraction can be generated, the parameters can be manipulated and adjusted for each patient.

Parameter	Adjustment	Effect
Frequency	Low: 1Hz-10Hz	Muscle twitch, can be less comfortable but less fatigue.
	Medium: 20Hz-60Hz	Tetanic muscle contraction causing a smoother force response.
	High: > 60Hz	Tetanic contraction might diminish gradually, sensory response becomes stronger.
Pulse width	Low: 10μs -200μs	Superficial contraction, less likely to activate other muscle fibres. Can be good for smaller muscle groups
	Medium: 200μs -500μs	Stronger contraction, recruiting more motor fibres, higher risk for activating other muscles.
	High: 500μs-1000μs	Powerful contraction, can be good for larger groups of muscles
Amplitude	Low	Causes a weak response: Tends to be a more comfortable contraction
	High	Causes a strong response: Less tolerable compared to low amplitudes.

Table 28: Parameters for electrical stimulation

Considering the above-mentioned information, the following parameters were chosen for this experiment: frequency: 50Hz; pulse width: 100μs; amplitude: 30mA. As a result, the following update commands can be generated.

Byte	Value		Byte	Value		Byte	Value	
1	10100100	Command 1	1	10100100	Command 2	1	10100100	Command 3
2	00000000		2	00000000		2	00000000	
3	00000000		3	00000000		3	00000000	
4	00000000		4	00000000		4	00000000	
5	00000000		5	00000000		5	00000000	
6	01100100		6	00000000		6	00000000	
7	00011110		7	00000000		7	00000000	
8	00000000		8	00000000		8	00000000	
9	01100100		9	01100100		9	01100100	
10	00011110		10	00011110		10	00011110	
11	00000000		11	00000000		11	00000000	
12	00000000		12	00000000		12	01100100	
13	00000000		13	00000000		13	00011110	
1	10100100	Command 4	1	10100100	Command 5	1	10100100	Command 6
2	00000000		2	00000000		2	00000000	
3	00000000		3	00000000		3	00000000	
4	00000000		4	00000000		4	00000000	
5	00000000		5	00000000		5	00000000	
6	00000000		6	00000000		6	00000000	
7	00000000		7	00000000		7	00000000	
8	00000000		8	00000000		8	00000000	
9	00000000		9	00000000		9	01100100	
10	00000000		10	00000000		10	00011110	
11	00000000		11	00000000		11	00000000	
12	01100100		12	00000000		12	00000000	
13	00011110		13	00000000		13	00000000	
1	10100100	Command 7	1	10100100	Command 8	1	10100100	Command 9
2	00000000		2	00000000		2	00000000	
3	01100100		3	00000000		3	00000000	
4	00011110		4	00000000		4	00000000	
5	00000000		5	00000000		5	00000000	
6	00000000		6	00000000		6	01100100	
7	00000000		7	00000000		7	00011110	
8	00000000		8	00000000		8	00000000	
9	01100100		9	01100100		9	01100100	
10	00011110		10	00011110		10	00011110	
11	00000000		11	00000000		11	00000000	
12	00000000		12	00000000		12	00000000	
13	00000000		13	00000000		13	00000000	

Table 29: Update of CCL mode: Byte sequence as described in Figure 74 (Bench test—Trial 2)

After defining the parameters and generating the byte sequence, the update commands can be implemented. As mentioned before, the initial contact is used for triggering the stimulation, the detected duration from the previous step is considered to be the stimulation time for the upcoming step and the segmentation of the commands is realised by using the muscle activation sequence shown in Figure 71. The individual gait events such as initial contact, full contact, heel off and toe off are used for gait event detection, thus they are essential for defining the total duration of the step, yet they do not influence the stimulation pattern directly. This concept is schematically shown in Figure 75.

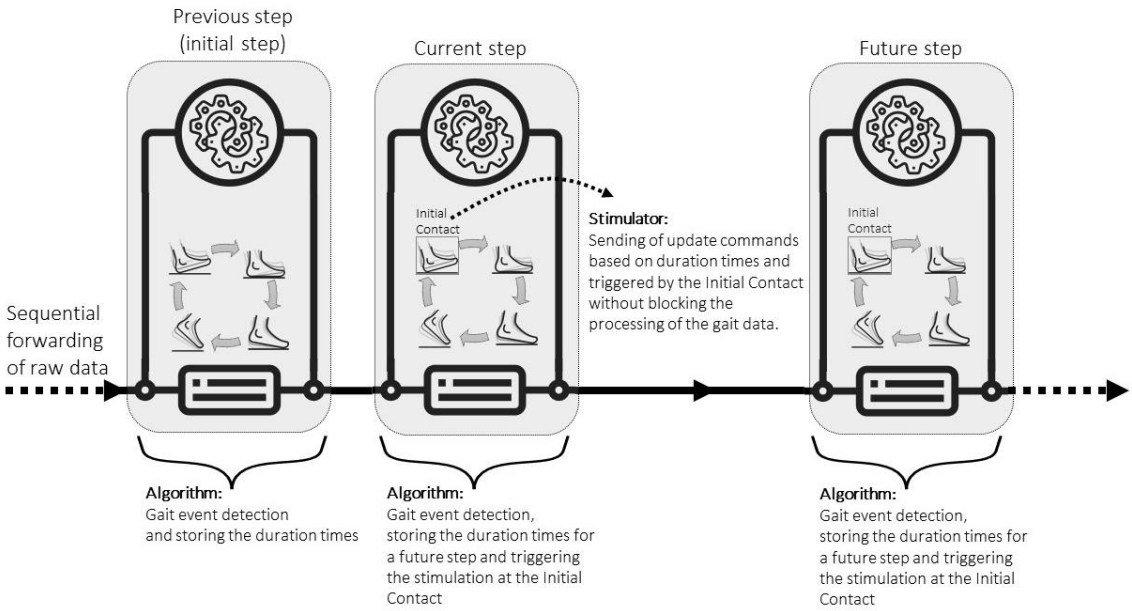

Figure 75: Concept: Bench test—Trial 2

5.6.3 Testing and Application–Trial 3

As mentioned in section 5.6.2, the individual gait events were used for defining the step time but did not directly influence the stimulation pattern. In order to allow a faster response to changes in the gait pattern, all four gait events can be actively utilised to alter the stimulation pattern. For the realisation of that approach, a more detailed elaboration of the distribution of the individual gait events is needed. Thus, gait events can be organised as follows [95,161]: Initial contact—0% Foot flat (respectively full contact) —8%, heel off—40%, toe off—60% and next initial contact—100%, with the boundary condition that the gait cycle is a dynamic and consecutive sequence of eight events starting from the initial contact at 0% of the gait cycle and ending at the next initial contact at 100% of the gait cycle. Implementing this into the existing concept of section 5.6.2, a new pattern of update commands as visualised in Figure 76 can be derived.

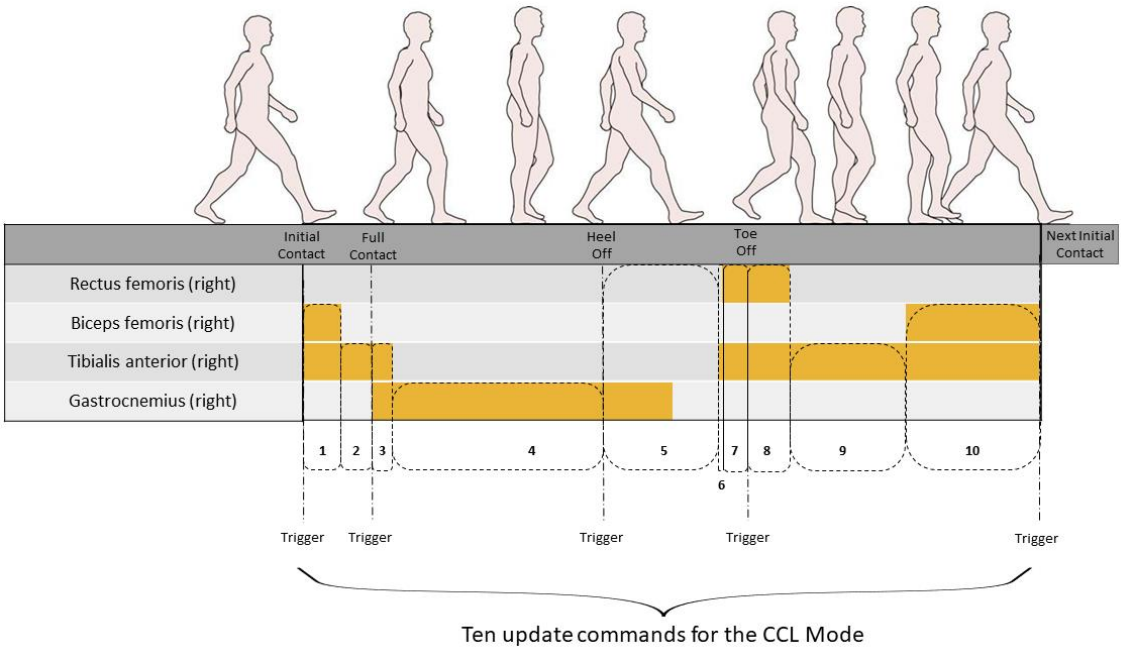

Figure 76: Amount of update commands of the CCL mode during one gait cycle (Bench test—Trial 3)

As a result, ten update commands are needed to activate/deactivate four muscles throughout the gait cycle. Parameters like frequency, pulse width, amplitude for the stimulation and the allocation of channels were the same as in 5.6.2. Furthermore, the initialisation command and the stop command are kept identical as four channels were used for stimulation. The update commands could also be reduced as some activate the same muscle groups; yet for a better overview and for an easier implementation into the algorithm, a detailed clustering of commands was chosen. The newly defined update commands are shown in Table 30.

Byte	Value		Byte	Value		Byte	Value	
1	10100100	Command 1	1	10100100	Command 2	1	10100100	Command 3
2	00000000		2	00000000		2	00000000	
3	00000000		3	00000000		3	00000000	
4	00000000		4	00000000		4	00000000	
5	00000000		5	00000000		5	00000000	
6	01100100		6	00000000		6	00000000	
7	00011110		7	00000000		7	00000000	
8	00000000		8	00000000		8	00000000	
9	01100100		9	01100100		9	01100100	
10	00011110		10	00011110		10	00011110	
11	00000000		11	00000000		11	00000000	
12	00000000		12	00000000		12	01100100	
13	00000000		13	00000000		13	00011110	
1	10100100	Command 4	1	10100100	Command 5	1	10100100	Command 6
2	00000000		2	00000000		2	00000000	
3	00000000		3	00000000		3	00000000	
4	00000000		4	00000000		4	00000000	
5	00000000		5	00000000		5	00000000	
6	00000000		6	00000000		6	00000000	
7	00000000		7	00000000		7	00000000	
8	00000000		8	00000000		8	00000000	
9	00000000		9	00000000		9	00000000	
10	00000000		10	00000000		10	00000000	
11	00000000		11	00000000		11	00000000	
12	01100100		12	01100100		12	00000000	
13	00011110		13	00011110		13	00000000	
1	10100100	Command 7	1	10100100	Command 8	1	10100100	Command 9
2	00000000		2	00000000		2	00000000	
3	01100100		3	01100100		3	00000000	
4	00011110		4	00011110		4	00000000	
5	00000000		5	00000000		5	00000000	
6	00000000		6	00000000		6	00000000	
7	00000000		7	00000000		7	00000000	
8	00000000		8	00000000		8	00000000	
9	01100100		9	01100100		9	01100100	
10	00011110		10	00011110		10	00011110	
11	00000000		11	00000000		11	00000000	
12	00000000		12	00000000		12	00000000	
13	00000000		13	00000000		13	00000000	

	1	10100100	Command 10
	2	00000000	
	3	00000000	
	4	00000000	
	5	00000000	
	6	01100100	
	7	00011110	
	8	00000000	
	9	01100100	
	10	00011110	
	11	00000000	
	12	00000000	
	13	00000000	

Table 30: Update of CCL mode: Byte sequence as described in Figure 76 (Bench test—Trial 3)

After defining the parameters and generating the byte sequence, the update commands can be implemented. In contrast to Trial 2 from Section 5.6.2 where the initial contact was the only trigger for starting and changing the stimulation, in this trial, all gait events (initial contact, full contact, heel off and toe off) are capable of changing the stimulation in real time. The duration in between the gait events, for the duration of the update commands, is derived from the previous step. Yet, every gait event alters the stimulation as soon as it is detected, thus a faster adaption to possible alterations in the gait pattern of the robotic gait training can be realised. This concept is schematically shown in Figure 77.

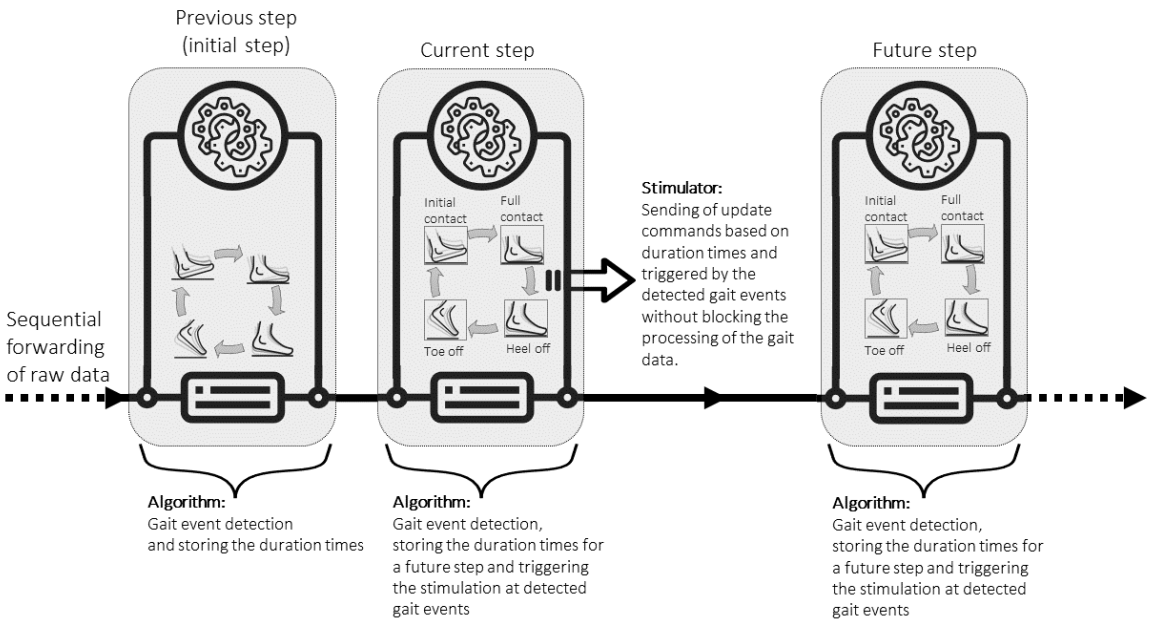

Figure 77: Concept: Bench test—Trial 3

5.6.4 Performance

After investigating the performance of algorithm, the latency of the update commands was tested (section 5.6.1). For the analysis of the latency of the commands, an overground walking dataset with the duration of 120 seconds (60,000 samples) was used. The latency estimation was repeated ten times for each update command; the mean and the standard deviation can be seen in Table 31.

Duration of raw data (s)	Evaluated update command	Mean (μs)	Standard deviation (μs)
120	Initial contact	1.79	0.64
120	Full contact	1.69	0.61
120	Heel off	1.74	0.49
120	Toe off	1.72	0.58

Table 31: Estimated latency for the update commands

The mean latency of the update commands was 1.74μs ± 0.58μs. The resolution of the tic/toc function was evaluated in section 5.4.3 and was 0.5μs ± 0.1μs.

As the duration of the gait cycle is a key factor for the timing of the stimulation, the step duration was measured to evaluate the performance and the applicability of the concept (section 6.3). To define a typical step duration during robotic therapy, the steps from stroke patients during Lokomat and Lyra therapy were investigated. For the evaluation, 50 steps per robotic device consisting of various walking velocities were used. Each duration was measured by calculating the time in between two initial contacts as shown in Figure 78.

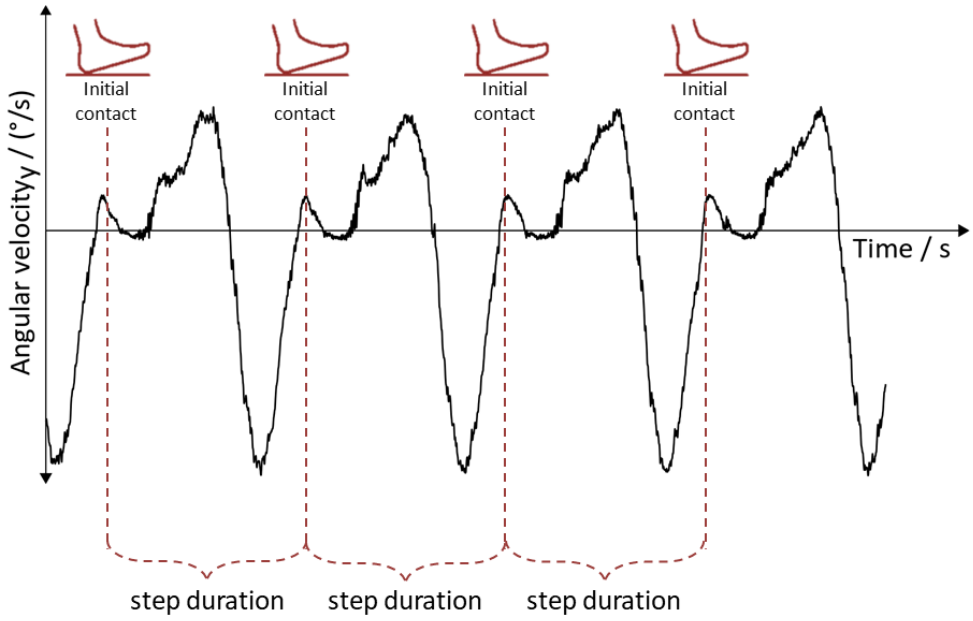

Figure 78: Step duration for four steps

To diversify the results, these 50 steps were distributed to five subjects and 10 steps were measured for each subject. The five subjects were the same subjects which were tested in section 5.4.2. The step duration of Lokomat datasets can be seen in Table 32. Table 33 represents the step duration of the datasets of Lyra recordings.

Subject	Number of steps	Mean (ms)	Standard deviation (ms)
1	10	2825	476
2	10	3207	24
3	10	2641	5
4	10	2380	14
5	10	3335	9

Table 32: Step duration during Lokomat training

The step duration for all subjects during Lokomat training is in between 2380ms and 3335ms, the mean step duration of Lokomat over five subjects for ten steps per subject (left leg) was 2878ms ± 417ms.

Subject	Number of steps	Mean (ms)	Standard deviation (ms)
1	10	2661	37
2	10	2997	45
3	10	2394	687
4	10	3003	5
5	10	2669	45

Table 33: Step duration during Lyra training

The step duration for all subjects during Lyra training was in between 2661 and 3003. Overall, the mean step duration of Lyra over five subjects for ten steps per subject (left leg) was 2745ms ± 384ms. As a result, the mean step duration over all subjects (Lyra and Lokomat) was 2811ms ± 450ms.

6 Discussion and Conclusion

The following paragraphs aim to discuss and explain the results from the conducted clinical trials, the bench testing and the performance testing. Furthermore, already existing and similar works will be discussed in this context. Additionally, limitations and boundary conditions will be elaborated. Every conducted experiment will be discussed independent from each other. Additionally, a conclusion for each experiment is provided within the individual section.

6.1 Gait Event Detection—Healthy Adult

The results from the conducted experiments in section 5.5 are discussed within this section. Furthermore, they will be compared to related works within the conclusion. The results from the arbitrary sensor alignment algorithm which contributes to the results of the gait event detection algorithm as it ensures the correct rotation of the gathered data is not discussed within this section. The corresponding discussion for the arbitrary sensor alignment algorithm can be found in section 5.3.

6.1.1 Discussion

For the evaluation of the analysed Lokomat recordings, the detection rate, false-positives and false-negatives (Figure 57 - Figure 59) were considered. As visualised in Table 14, false-positives represent incorrectly detected steps and are a potential hazard as they could initiate a stimulation command which is not synchronised with the present gait cycle. False-negatives represent undetected steps, they lower the detection rate and are considered not to be hazardous as they would not trigger an electrical impulse. Looking at the conducted experiment, nearly all results of the false-positives achieved a value of 0% and the values for the detection rate reached values of 90.7% up to 100%. Only one recording at 1.2 m/s revealed a lower detection rate with a value of 73%. During this recording, also the highest false-positives within the whole recording with a value of 13.4% at the right sensor was found. High values for false-positives might not be tolerable during robotic gait training as the amount of incorrect stimulation would be too high to guarantee a valuable therapy. High values for false-positives only occurred during one recording session. One reason for this may be that the subject changed the setup during training.

Specifically, the subject adjusted the harness during the training as one of the belts carrying the weight of the subject moved and resulted in discomfort. This adjustment resulted in a movement of the upper and lower body or the legs, respectively, and thus could have influenced the robotic movement and the gathered data. Another reason for high false-positives could be that an evasive movement of the participant was triggered by the discomfort of the harness which might have influenced the walking pattern of the robotic gait trainer. Similar to the evaluation of Lokomat, for Lyra recordings, the detection rates, false-positives and false-negatives were taken into consideration (Figure 60-Figure 62). During the first recording of Lyra, detection rates reached values of 88.6% up to 100%. False-positives ranged within 0% to 4.7%. As previously noted, false-positives might initiate harmful electrical impulses as they represent incorrectly detected step; nevertheless, a small number of false-positives might be acceptable. Furthermore they can be reduced by developing complementary techniques for error recognition. Comparable results could be achieved during the second recording. Except for one outlier, the third measurements provide acceptable results as well. While the subject was walking with 1.5 m/s, the worst results for Lyra training were observed. Values of 70% were obtained for the detection rate, additionally the highest value for false-positives was 20%. Yet, the acceptable range of false-positives from a medical perspective with regards to electrical stimulation was not investigated and should be subject of future research. Similar to Lokomat, one possible cause for the outliers could be re-adjustments of the body weight support system. The adjustments could have caused swinging of the trunk of the subject leading to unwanted movements in the lower extremities. End-effector gait trainers as Lyra mostly provide a very rigid fixation of the subject's foot. Nevertheless, torso movements might alter the motion of the subject's leg and could affect the trajectory of the induced walking pattern of the robotic device.

6.1.2 Conclusion

Based on the results discussed in section 6.1.1, a setup which uses IMUs for the recognition of gait events during gait training with robots like Lokomat and Lyra is feasible. Furthermore, the results allow the conclusion that a system as conceptually shown in Figure 26. with the goal of supporting robotic gait training with FES is realisable.

The donning time of two inertial measurement units is rather small compared to the setup time of Lokomat or Lyra, thus it marginally influences the net therapy time. Furthermore, the arbitrary sensor alignment algorithm offers a high degree of flexibility in the positioning of the sensors, allowing the therapist to vary the position at which they want

to attach the sensor to the foot of the patient. Additionally, it partly avoids incorrect data recording due to faulty positioning of the IMU or due to slight shifts of the sensor during training. Yet, some boundary conditions such as tightly fixing the sensor on the foot of the subject must be fulfilled for proper functioning of the proposed setup.

High values for false-positives might be caused by unforeseen movements of the subject; thus, to avoid high false-positives, further methods of troubleshooting need to be established. One limitation of this conducted experiment was that the recordings were made with one healthy adult under several boundary conditions such as using the maximum guidance force of Lokomat and switching off the biofeedback mode of Lyra. Despite the boundary conditions, it could have happened that the subject unconsciously modified the robotic walking as a guided gait movement might be a completely new experience for a healthy person. In order to test these assumptions, recordings with stroke patients were performed (section 5.4.2). The corresponding results are discussed in section 6.2.

Approaches using IMUs for the detection of gait events during walking achieved similar results [122,162]. Yet, the main goal of these methods was the recognition of human gait and not the recognition of a walking pattern performed by a robotic gait trainer, thus the comparability is limited to the outcome measures and not to the implemented algorithms. Inertial measurement units as used within this work measure angular velocity and linear acceleration. Based on this data, the gait events are detected. Neurological patients however present unexpected muscular events caused by spasticity or other pathologies which can disrupt the smooth movement of the robotic device and can jeopardise the electrical trigger instant. This issue was addressed before the recording session by testing the capability of the robot to detect voluntary movement. Robotic gait trainers can record the load of a patient [163]. This patient output can be used to evaluate induced movement such as spasticity of a leg. Once spasticity is detected, the induced gait pattern of the device is stopped so that no injury is caused. As a result, the data from the inertial measurement units would not correspond to a walking pattern and the troubleshooting methods would discard the gait events, and no trigger for an electrical stimulation would be sent to the stimulator. For these recordings, the occurrence of spasticity was simulated by applying a voluntary force against the robotic movement. Furthermore, a careful evaluation of the risk factors for robot-assisted gait training such as joint contractures and limitations in the range of motion must be conducted from health care professionals prior to a treatment. The described concept offers the possibility to detect four main gait events and to stimulate the corresponding muscles within them. Thus, slight changes of the timing of gait events within the gait cycle are recognised, and the initiation of stimulation commands can be

altered accordingly. There are different approaches that do not offer this flexibility as the initiation of stimulation commands is triggered by the initial contact [25], the initial and the final stage of the stance period [27] or initiated by a human controlled finger switch [33]. Furthermore, the presented approach can be expanded for the application with a variety of robotic gait trainers as the use of inertial measurement units makes it autonomous from the data delivered by the gait trainers. Concepts as described in [27,33] rely on robot-specific information and thus might be less extendable to other robots.

The presented algorithm functions according to its intendent purpose; nevertheless it is must be noted that the algorithm has not been validated against gold standards for motion capturing such as an optical marker system. The main reason for that is that an optical marker system requires direct visual contact to their markers (active or passive) and robotic gait trainers can easily block the direct view with their mechanical structure. Furthermore, during clinical routine the therapist has to supervise the training of the patient. Doing so, they move around the gait trainer, sit on the base plate of the gait trainer and adjust the training according to the needs of the patient. This movement around the feet would constantly obscure the markers, causing the analysis of the motion to be erroneous and inaccurate. Nevertheless, for future research a different region of interest such as the knee joint or the hips allowing easier positioning and visibility of the optical markers should be investigated. Although there were some limitations, the described approach offers a feasible and novel setup with the capability to serve as an additional tool for robotic gait trainers to enhance rehabilitation with functional electrical stimulation.

6.2 Gait Event Detection — Stroke Patients

Within this section, the results of the conducted clinical trail are discussed; additionally, they will be compared to related works within the conclusion. The recordings of stroke patients during robotic gait training with Lokomat and Lyra are discussed and compared to the conducted experiments with a healthy adult. Furthermore, related works will be addressed within the conclusion.

6.2.1 Discussion

Similar to the experiment conducted with the healthy adult, the detection rate (Lokomat: Figure 63, Lyra: Figure 66), false-positives (Lokomat: Figure 64, Lyra: Figure 67) and false-negatives (Lokomat: Figure 65, Lyra: Figure 68) were considered. A mean detection rate 98.7% for Lokomat was achieved. Compared to the experiment performed from a healthy adult, the mean values of the detection rates are similar (98.6%). Similar results were achieved for Lyra recordings. The mean value for the detection rates of patients with a stroke was 95.8% and for the healthy adult, the mean value for the detection rate was 94.1. Also, false-positives for both gait trainers within the clinical trial and the experiment with the healthy adult are within the same range.
Lokomat: False-positives for stroke patients: 0.9%; false-positives for the healthy adult 0.3%. Lyra: False-positives for stroke patients: 1%; false-positives for the healthy adult: 2%. The same applies for the false-negative values where all results are within a comparable range. Lokomat: False-negatives for stroke patients: 0.3%; false-negatives for the healthy adult: 4%. Lyra: False-negatives for stroke patients: 3.2%; false-negatives for the healthy adult: 4%. Nonetheless, also higher values for false-positives of about 11% and higher values for false-negatives of about 15% were found. Higher false-positive values as during Lokomat training of subject one (Figure 64), and higher false-negative values as during Lyra training of subject two (Figure 68) could be caused by various factors. One factor could be that the settings of the Lokomat exoskeleton induced vibrations and disrupted the sensor signals. This might happen when the therapists adjust the exoskeleton during the therapy in order to optimise the exoskeleton to the patient's comfort. For Lyra therapy, this could happen when the therapists adjust the foot fixation during the training. Another factor could be that the sensor loosened its attachment during the gait training and caused jittered signals, resulting in incorrect gait event detection.

6.2.2 Conclusion

Within this clinical trial, the developed gait event detection algorithm was tested and evaluated during robotic gait therapy with stroke patients. The feasibility, acceptability and robustness of the concept could be demonstrated. The setup of the IMUs was done within the donning time of the robotic gait trainers, thus the patients could execute their therapy as planned within their schedule. Therefore, the participants were not exposed to adverse effects in the course of the rehabilitation process. The achieved results lead to the conclusion that the algorithm is robust towards motion induced by the patients or potential lack of movement due to their affected legs. The developed methods to enhance confidence of the algorithm including the unsupervised adaptability (section 5.2) improved the gait event detection algorithm and were sensitive towards discarding incorrect gait events such as detecting a wrong initial contact caused by jittering of the jerk (Figure 37 and Figure 38). The feedback from the participating subjects and therapists was largely positive. Only one patient reported discomfort caused by the IMU as the sensor was positioned on an already existing painful pressure mark. Therefore, one measurement which is marked as "N.A." in Figure 66 and Figure 67 was not analysable. Nevertheless, despite introducing a new technology (IMUs) to the rehabilitation process, no further problems occurred. Overall, the patients and the subject showed great interest and acceptance for the concept and the potential use in the rehabilitation process.

With regard to the net therapy time of the subjects, not all completely exploited the full time. Some subjects had their first robotic gait training which led to longer donning time as the orthosis of Lokomat or the adjustments of the foot plates of Lyra had to be defined for the first time for these patients. Additionally, the subjects had more questions towards the therapist and the rehabilitation technique was explained in detail to the patients. Another main factor was the patients' physical and mental condition which largely influenced the therapy time as a tired and unmotivated patient tends to exhaust earlier compared to a motivated person. As a result, the amount of gathered data varied and some analyses were limited to fewer analysed windows.

The rehabilitation approach of Lokomat and Lyra covers level-ground walking, thus other movements such as backwards walking or stair climbing which are provided by other robots such as the G-EO (section 3.4.5) were not taken into consideration and the algorithm is not intended to be used for these motions. Nevertheless, future developments with other gait trainers might address more walking patterns.

The developed algorithm covers a variety of techniques to enhance the confidence of the algorithm which aim to detect incorrect gait events and discard them. However, only a

particular amount of training velocities and training setups was tested, thus a variation towards very high or very slow velocities which could also be part of a therapy routine might cause situations which have not been taken into consideration so far. Although the algorithm is able to adapt within certain bounds, more data with a broader range of training velocities is needed to eliminate potential error cases and to provide prove for the effectiveness of the developed techniques to enhance the confidence of the algorithm.

The data was analysed within certain time windows. This process was chosen to generate an analysing process which is repeatable and comparable. The smallest usable acquisition period was less than eight minutes (1st subject in Figure 64 and Figure 65). Thus, a window size of 3.5 minutes to generate at least two analysed time windows for each subject was chosen. Variations in the window size (larger or shorter) should not have a high impact on the detection rate as walking, and especially walking within a guided movement during robotic gait training is a highly repetitive motion. Nevertheless, specific movements of patients outside a chosen time window might influence the data leading to a slightly better or worse overall detection rate.

The gait detection technology is a very mature field and has been investigated a lot within the past years. The IMU-based or sEMG-based gait sensing techniques as described in [164] and the machine learning-based gait detection algorithms such as support vector machine, classification via regression and other methods are used in the field of gait detection. Due to some limiting factors such as limited amount of reference signals for sEMG patterns especially for specific robot-assisted gait trainers (most signals are collected for walking on a treadmill [165–167] or during normal walking [164,168,169]) sEMG was not considered a valid option for the specific approach within this work. One reasons for that was, that reference signals for sEMG patterns during robotic gait training are limited; furthermore, the devices used for the recording of sEMG signals can interfere with the signals of a prospectively used FES device. In addition, the donning time of IMUs is less compared to sEMG devices as the fixation strap can be applied to the subject without any further preparation, such as removing clothing to position the device on the muscle or cleaning the skin for good adhesion of the sEMG sensor. Especially for patients, this short donning time of IMUs is a major advantage as net therapy time is less influenced.

An approach using long short-term memory deep neural network (LSTM-DNN) for gait event detection during treadmill walking resulted in accuracy rates up to 95.1% for gait recognition [79]. In this approach, linear acceleration signals from three IMUs attached to distinct locations on the subject's foot were recorded and two gait phases were detected. Despite similar result in the gait recognition, the comparability is limited as the main goal

of this approach was the recognition of gait during treadmill walking and not the recognition of a robotic gait trainer with its system-dependent characteristics of movement. Approaches which minimised the setup time with utilising one sensor on the lower back are promising as well [170]. Nevertheless, for the application within this work, one IMU on the lower back was not applicable as the body weight support system of Lokomat and Lyra would cover the sensor and might influence its behaviour due to limiting the movement of the subject and due to constant shear forces between the lower back of the subject, of the sensor and the body weight support system.

Approaches using deep neural networks for gait event detection with optical motion capture systems achieved recognition values of up to 99% depending on the desired gait phase (99% for foot-contact, 95% for foot off) [120]. These results are based on optical measurement systems which do not seem feasible for the proposed concept as their usage during clinical routine is not applicable due to the fact that the mechanical structure of the gait trainer and the movement of the therapist would constantly obscure the markers. Additionally, the application of optical markers requires time and expertise. As the aim of the suggested setup is to be applied by the therapists during normal rehabilitation routine, it must be easy and fast.

The reported results in [79] are based on four individuals (three sensors per leg), each walking 120 seconds three times at different speeds, resulting in a time of 6 minutes per subject. The analysed dataset within this work has similar recording time per subject (minimum amount of data is 7 minutes). In order to keep the setup as simple as possible, especially under the consideration that the recordings were executed during normal clinical routine, the aim was to reduce the number of sensors and to develop an easy setup with fast donning times which has the potential for further usage in a practical field. A total amount of ten subjects (5 subjects per gait trainer) were recorded resulting in more than 5,000 analysed steps. The deep learning models as mentioned above are data-intensive, require lot of training, and their deployment in the real-life scenario needs specialised equipment due to high processing power. Nevertheless, they are very powerful in their specific fields and provide good and valuable results.

Comparing the results from this work to the approaches mentioned above, the results of the detection rates are similar, yet not fully comparable as the approaches aim for the recognition of different movements. Furthermore, the approach within this work provides a lightweight algorithm which has the potential to be implemented within a wearable device. Nevertheless, a larger number of participants must be evaluated in order to prove the results.

To sum up, the achieved results within this study are promising and show the feasibility of the proposed concept. The developed algorithm and the developed techniques to enhance the confidence of the algorithm seem to provide robust setting for the usage during the robotic gait therapy of stroke patients. The proposed concept provides a lightweight algorithm which enables an easy attachment of the sensor due to possibility of an arbitrary sensor alignment, thus an application in the clinical routine seems feasible. Despite the limited amounts of subjects, the results showed that gait event detection during clinical routine does not add more burden for the therapists, moreover the therapists and the patients showed large interest in the technology. Nevertheless, unwanted outliers need to be diminished by implementing more error handling methods or by introducing more boundary conditions for the setup of the sensors.

6.3 Performance and Applicability of the Concept

The performance of the gait event detection algorithm including the performance of the electrical stimulation will be discussed and evaluated within this section. Furthermore, a potential Bluetooth connection for future use will be introduced and discussed. Related works and the applicability of the concept within a clinical setting will be addressed in the conclusion.

6.3.1 Discussion

To evaluate performance of the proposed concept, the whole measurement and execution chain including the physiological process during muscle contraction was considered. Thus, four main components as shown in Figure 79 were analysed within this work.

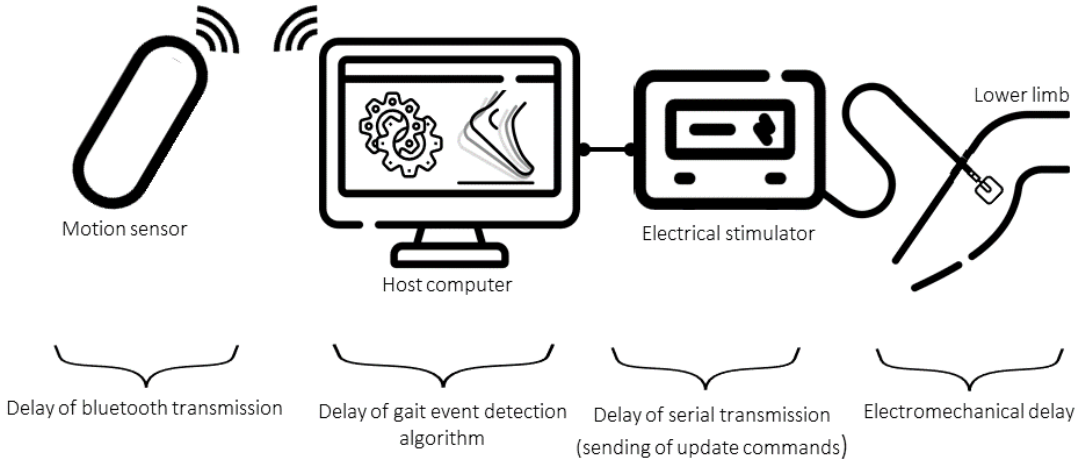

Figure 79: Schematic representation of the measurement and execution chain of the proposed concept

Each component induces a delay between the actual movement of the subject in the gait trainer and the resulting stimulation. The performed tests and measurements aimed to investigate these delays; the results will be discussed in the following paragraphs.

Delay of Bluetooth transmission:

For the future use of a Bluetooth connection, the transmission between the inertial measurement unit and the host computer (delay of the data transfer) must be taken into

consideration. For Bluetooth devices, a maximum delay below 46ms can be obtained [171]. The Bluetooth connection was chosen as it is a standard communication protocol which is widely used in medical and consumer devices for gait recognition.

Delay of gait event detection algorithm: In addition, the delay of the gait event detection algorithm was investigated (section 5.5.3). As the algorithm runs on a host computer, the specifications of the computer might influence the runtime of the individual parts; thus, the specifications of the host computer were defined in section 5.4.3 as LENOVO ThinkPad E590 with an intel CORE i7 8th Generation and 8GB of working memory; additionally, during the latency testing, MATLAB was the only software actively running on the host computer and the WIFI connection was disconnected in order to avoid interferences. A mean latency of the whole gait event detection algorithm of 282µs ± 17µs was derived whereas the resolution of the measurement function was tic/toc was 0.5µs ± 0.1µs. As a result, the gathered data cannot be generalised to other host computers as no investigations towards other computer specifications were done. However, in future works this might be improved when developing a concept which incorporates the detection algorithm and the stimulation model in one embedded device.

Delay of serial transmission: As a next step, the serial transmission between the host computer and the electrical stimulator was considered in section 5.6.4. Similar to the delay of the gait event detection algorithm, this aspect depends on the specifications of the host computer. For the evaluation, the same host computer as mentioned above was used. The mean latency of the serial transmission (sending update commands to the stimulator) was 1.74µs ± 0.58µs. Furthermore, a maximum delay of 2ms of the stimulator itself (section 2.3) must be taken into consideration.

Electromechanical delay: As a last step, physiological processes during muscle contraction were considered. The so-called electromechanical delay (EMD) of the muscles is defined as the time lag between the (initial) stimulation of a muscle at the neuromuscular junction and a measurable change in force output [172]. EMD seems to be influenced by various factors such as the angle of the moved joint, motor unit recruitment, and the properties of the considered tissue [172–174]. Additionally, physical activity, gender, age, muscle exhaustion and temperature, and other factors can influence the EMD [175–178].
Experimental studies in humans conducted with different methods showed EMD varying between 8ms up to more than 100ms [179–181]. An investigation towards the EMD of leg flexors and extensors on young and old healthy pre and post a fatigue-inducing protocol

adults showed mean EMD for leg extensors for young men of 97.66ms and 110.8ms for old men [182]. As a result, an EMD of 100ms was assumed for further discussion.

Delay of the proposed concept: Summing up all relevant information of the components with their individual induced latencies, an overall delay as shown in can be derived.

Component	Approx. delay (ms)
Bluetooth transmission	46
Gait event detection algorithm	0.28
Serial transmission	0.002
Stimulator	2
EMD	100
Overall	148.282

Table 34: Approximate overall delay of the proposed concept

As result, an overall induced latency of 148.282ms needs to be considered for the performance and the applicability whereas the electromechanical delay of the muscle plays the major role within this consideration.

6.3.2 Conclusion

Concepts as described in [25–33,130] did not consider the delay of a Bluetooth transmission as their operating principle is based on information provided directly by the robot. Within this work, the delay of the Bluetooth connection was evaluated theoretically as the connection to a Bluetooth device was not realised. Nevertheless, the consideration of the delay was part of the analysis for the applicability of the concept as it contributes to overall delay of the concept.

According to [25] in order generate a feasible stimulation, the latency of the stimulation must be short enough to ensure that the stance muscles are activated prior to loading more than 50% of body weight onto the stance limb. For healthy adults, the acceptance of 50% of the weight is reached after 5% of the gait cycle [129]. Thus, the duration of the actual gait cycle must be known as it is the main factor which influences the timing of the electrical stimulation and muscle activation. In order to define a typical step duration during robot-assisted gait training, the steps from stroke patients during Lokomat and Lyra therapy were investigated. For the evaluation, 50 steps per robotic device consisting of various walking velocities were used. Each duration was measured by calculating the time in

between two initial contacts as shown in Figure 75. The mean step duration over all subjects and gait trainers was 2,811ms ± 450ms (section 5.6.4). The gathered step duration is comparable with the step duration of 2.6 seconds as reported in [25]. Considering the upper bound of the mean step duration (3,261ms), 50% of the body weight are accepted after 163.05ms, thus the overall delay of 148.282ms would be short enough to ensure a feasible stimulation. Considering the lower bound of the step duration (2,361ms), 50% of the body weight are accepted after 118.05ms, thus the steps would be would be slightly too short (30.232ms) to overcome the overall delay. Yet within the afore-mentioned publication [25], EMD was not considered at all for evaluating the feasibility of the stimulation. Concepts as described in section 3 often do not take EMD into account, yet most of them consider the concept as feasible. A reason for that could be that the exact determination of EMD is not always possible for all patient groups due to a lack of clinical data or lack of assessments to define EMD. In addition, the delayed reaction between the initiation of the stimulation and the generation of muscle power may increase in cases of muscle fatigue [183]. Muscle fatigue is defined as a decrease in force or power production in response to contractile activity [184], and is highly dependent on the stimulation parameters as described in section 5.6.2. Furthermore, various other factors such as metabolic factors and fatigue reactants affect the muscle fatigue [185]. Thus, nutrition, the individual training, diseases such as stroke and the daily constitution of the patients are likely to affect EMD.

Taking all the above-mentioned information into account, a big matrix of positively and negatively influencing factors for EMD arises. Some of them such as nutrition are controllable, some of them such as daily constitution and individual training are less controllable leading to the result that EMD during clinical routine is likely to vary widely throughout all patients. One option to overcome this uncertainty is to determine EMD for each individual subject before FES treatment. In clinics, technologies such as electromyography or biomarkers for the diagnosis of muscle fatigue can be used. Furthermore, potential high muscle fatigue can be avoided before the treatment by omitting improper exercise and good nutrition. However, currently there are no official or semi-official guidelines for the management of muscle fatigue [185].

In fact, taking the lower bound of the gathered step data into account, the delay would be slightly too long to be able to stimulate the muscles before shifting 50% of body weight onto the stance leg, yet the body weight support system which is provided by the gait robots additionally support the patient's lower limbs during gait training and prevents the full body weight to be shifted onto the legs. Thus, the proposed concept of a gait event detection algorithm which gathers data from an inertial sensor to initiate FES during

robotic gait training seems feasible and applicable during clinical routine and might be a valuable additional therapy for people with gait disorders.

7 Outlook and Future Works

As mentioned in section 6, the reported results underlie some limitations. While some of them such as the motivation and daily constitution of a patient are only partially solvable by technical developments, several other aspects can be addressed in future works. Within this section, a selection of possible refinements and future approaches is presented.

Miniaturisation of the concept

The proposed concept as shown in Figure 26 consists of the robotic gait trainer, two IMUs, a stimulator and a host computer. For the daily use in a clinical routine, it would be necessary to miniaturise the proposed concept to fewer parts. As the develop threshold-based algorithm is lightweight and can be transformed from MATLAB Code to C Code, the algorithm itself could be integrated into the stimulator, omitting the host computer. A concept of an embedded device incorporating all the mentioned functionalities is shown in Figure 80.

Figure 80: Miniaturised concept (host computer including stimulation modules)

Flexibility of stimulation paradigms

So far, the proposed concept aims to communicate with RehaStim I electrical stimulator (Figure 24). For the daily use in a clinic, the application of eight surface electrodes might be too complex and time-consuming, thus a higher flexibility in the number of used electrodes would be desirable. In order to realise that, a graphical user interface can be

implemented to define the targeted muscles on demand. A concept as shown in Figure 81 and Figure 82 would allow the user to easily select the required muscles. In the interface of Figure 81, the user would be able to select the wanted sides of the lower limbs; furthermore, there could be the option to add the upper limbs in case the subject requires further stabilisation of the upper body.

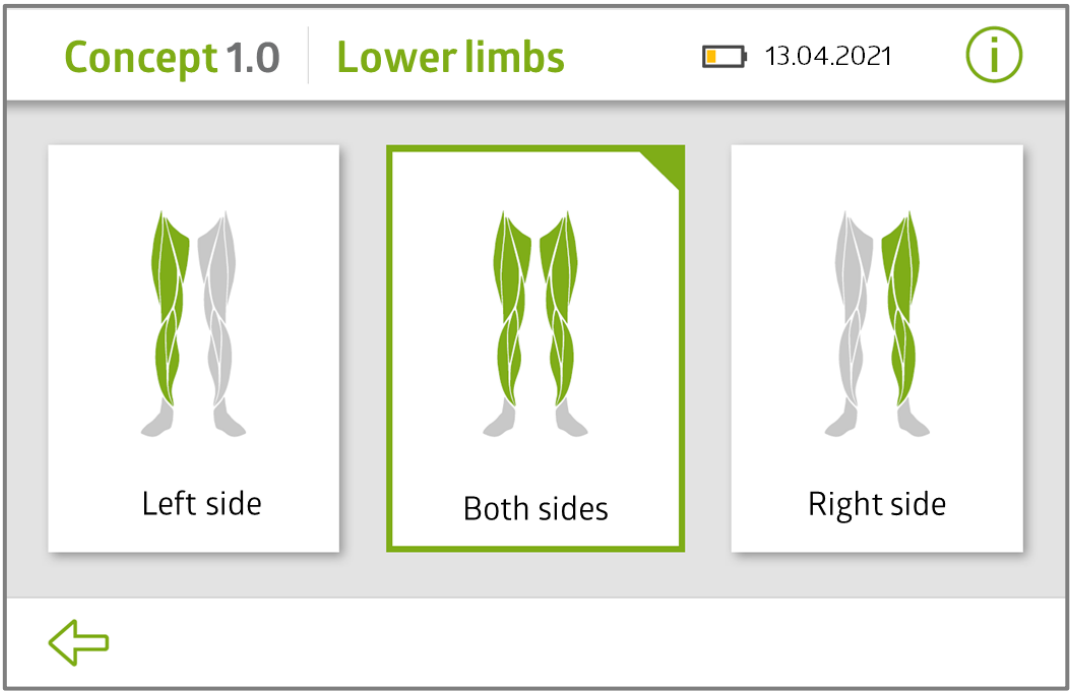

Figure 81: Graphical user interface—Page 1

After selecting the wanted side, the user can select the specific muscles to further individualise the treatment (Figure 82). This individualisation would allow the therapist to adapt the treatment easily throughout the training session.

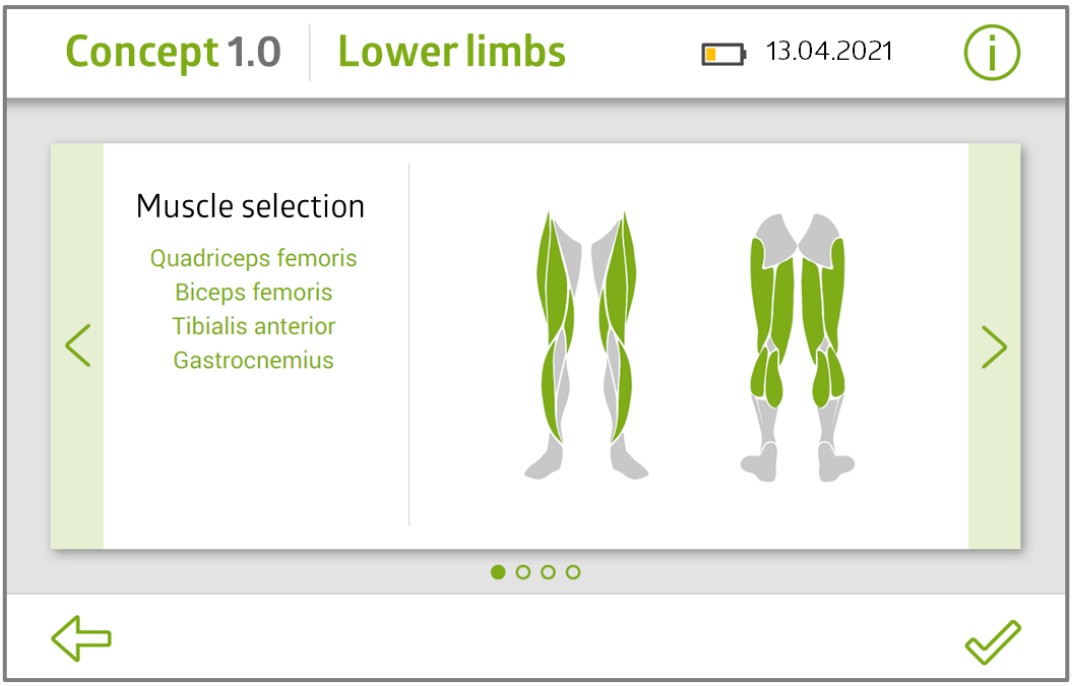

Figure 82: Graphical user interface—Page 2

Validation of the algorithm

The developed algorithm provides good results in terms of detection rate, false-positives and false-negatives. Nevertheless, no validation with gold standards has been performed. Pressure sensitive walkways might not be a good option as some of the gait trainers such as Lyra do not have direct contact of the foot with the ground. Thus, a validation study could only be made with optical marker systems. However, this could be very time and money-consuming as rehabilitation clinics most likely do not have an optical motion capture system in a room where robotic treatment is executed. Moreover, the technical design of some gait trainers may hide anatomical landmarks of the patient which would be necessary for the recognition of the movement. One approach could be to place the markers on a different region of interest such as the knee joint which would make the optical motion capturing easier but would limit the comparability. Another possibility could be to synchronise the gathered IMU data with the data provided by the robots itself such as number of steps. Yet, similar to the optical markers systems with different positions of the markers, the comparability would be limited and might not fulfill the validation aspect.

Medical efficacy

The advantages of robotic gait therapy and functional electrical stimulation for the treatment of gait disorders or other pathologies is well researched [6,7]. Furthermore,

investigations towards the combination of both techniques have only risen within the last years. Especially with the improvement of gait event detection, timing of the stimulation and thus neural plasticity and motor learning could be improved. However, it seems that there is no clear evidence that a better accuracy and better timing of functional electrical stimulation is a driving factor for good rehabilitation results. Thus, more research towards the medical efficacy of a combination of these rehabilitation methods and of the individual methods should be executed to show the potential of these applications.

Detection methods

The algorithm is threshold-based and lightweight, different approaches such as machine learning methods for gait event detection could be a valuable addition to enhance robustness and performance of the algorithm. So far, many studies conducted with machine learning methods show excellent offline results, yet when applied for real-time gait event detection, machine learning methods do not provide as good results as offline methods [79,121,125]. Furthermore, as the robotic gait cycle is a highly repetitive movement, the integration of an iterative learning control as described in [186] could be a valuable asset for error minimisation. Another interesting aspect of research would be the inter-comparability of the presented detection method within this work and detection methods for human walking. So far, the recorded robotic gait data within this work was bench test with commercially available software tools for offline gait recognition with unsatisfactory results. Thus, a new approach specifically developed to detect the robotic gait with all its robot-specific particularities as presented within this work was developed. Nevertheless, in future works this aspect could be investigated to optimise the detection methods. Additionally, the presented concept could also be tested with large datasets of human walking (like the evaluation of the arbitrary sensor alignment algorithm in section 5.4) to expand the field of application or to adapt it to a different purpose.

Electrode arrays

The location of the electrodes is a crucial part of using FES and depending on the intended purpose of the treatment, the placement can vary which can consume a lot of time in clinical routine. When using electrode arrays, the placement process can be automated , and fatigue can be reduced [187,188]. Additionally, smaller muscle groups can be active by adjusting the shape and size of the array [189,190]. Thus, in future investigations, replacing single pad electrodes with electrode arrays might be a benefit when testing the medical efficacy of the proposed setup.

Latency optimisation

The latency of the concept as reported in the performance analysis results from the measurement and execution chain and is subject to change as a variation in the setup (host computer, IMU etc.) can influence the outcome of the latency. Therefore, an embedded device as shown in Figure 80 could be used to standardise the latency. Moreover, a specific communication protocol could be developed in order to minimise the transmission latency.

Gait event prediction

Gait event prediction algorithms can detect steps or gait events before an actual event happens [191,192]. In the context of triggering FES, this would allow the stimulation algorithm to correct for transmission delay and EMD. The earlier and more detailed a step (or gait event) can be predicted, the better the triggering algorithm can adjust the stimulation pattern in order to support the next step in the robot. In future works, a prediction algorithm might be considered as it could be a big asset for the latency optimisation.

8 Appendix

8.1 Measurement Protocols–Healthy Adult

Number	Gait trainer	Duration (min)	Velocities (m/s)	Comment
1	Lokomat	60	1.3, 1.5, 1.7	First measurement with Lokomat. Fitting of the exoskeleton was determined initially.
2	Lokomat	60	1.3, 1.5, 1.7	-
3	Lokomat	60	1.3, 1.5, 1.7	-
5	Lokomat	60	1.3, 1.5, 1.7	-
1	Lyra	60	1.3, 1.5, 1.7	First measurement with Lokomat. Fitting of the foot fixation was determined initially.
2	Lyra	60	1.3, 1.5, 1.7	-
3	Lyra	60	1.3, 1.5, 1.7	-
4	Lyra	60	1.3, 1.5, 1.7	-
5	Lyra	60	1.3, 1.5, 1.7	-
General comment: The duration of 60 minutes included the setup time. During the recordings, adjustments of the exoskeleton were done. The guidance force was set to 100% and the BWSS (body weight support system) was adjusted to the comfort of the subject.				

Table 35: Measurement protocols of Lokomat and Lyra recordings of the healthy adult.

8.2 Measurement Protocols–Stroke Patients

1st Subject (Lokomat)			
Start (hh:mm):	11:13	Duration (min):	10
Stop (hh:mm):	11:24	Hip fixation (Yes/No):	No
Velocity (m/s):	1.2-1.3		
Additional comment:	Adjustments of the exoskeleton were done during recording. The guidance force was varied throughout the measurement. BWSS (Body weight support system) was adjusted to 35kg (49% according to the display of Lokomat)		
2nd Subject (Lokomat)			
Start (hh:mm):	11:32	Duration (min):	10
Stop (hh:mm):	11:42	Hip fixation (Yes/No):	No
Velocity (m/s):	1.2		
Additional comment:	Adjustments of the exoskeleton were done during recording. The guidance was varied throughout the measurement. BWSS was adjusted to 35kg (52% according to the display of Lokomat). Exhausted and tired subject. Therapy was shorter than planned.		
3rd Subject (Lokomat)			
Start (hh:mm):	09:13	Duration (min):	20
Stop (hh:mm):	09:33	Hip fixation (Yes/No):	No
Velocity (m/s):	1.5		
Additional comment:	Adjustments of the exoskeleton were done during recording. The guidance was varied throughout the measurement. BWSS was adjusted to 42.3kg (49% according to the display of Lokomat).		
4th Subject (Lokomat)			
Start (hh:mm):	11:15	Duration (min):	30
Stop (hh:mm):	11:45	Hip fixation (Yes/No):	No
Velocity (m/s):	1.5-1.7		
Additional comment:	The guidance was varied throughout the measurement. BWSS was adjusted to 34kg (48% according to the display of Lokomat). Exhausted and tired subject. Therapy was shorter than planned.		
5th Subject (Lokomat)			
Start (hh:mm):	09:21	Duration (min):	20
Stop (hh:mm):	09:50	Hip fixation (Yes/No):	No
Velocity (m/s):	1.3-1.4		
Additional comment:	Adjustments of the exoskeleton were done during recording. The therapy was stopped shortly and continued afterwards. The guidance was varied throughout the measurement. BWSS was adjusted to 44kg (49% according to the display of Lokomat). Exhausted and tired subject. Therapy was shorter than planned.		

Table 36: Measurement protocols of Lokomat recordings

1st Subject (Lyra)			
Start (hh:mm):	14:16	Duration (min):	20
Stop (hh:mm):	14:37	Hip fixation (Yes/No):	Yes
Velocity (m/s):	1.5		
Additional comment:	BWSS was adjusted to 20kg (the total weight of the participant was not documented within the recording).		
2nd Subject (Lyra)			
Start (hh:mm):	09:20	Duration (min):	20
Stop (hh:mm):	09:41	Hip fixation (Yes/No):	Yes
Velocity (m/s):	1.3		
Additional comment:	BWSS was adjusted to 60kg (the total weight of the participant was not documented within the recording). Foot fixation was slightly loose.		
3rd Subject (Lyra)			
Start (hh:mm):	09:50	Duration (min):	25
Stop (hh:mm):	10:20	Hip fixation (Yes/No):	No
Velocity (m/s):	1.5		
Additional comment:	BWSS was adjusted to 20kg (the total weight of the participant was not documented within the recording). Therapy was executed with biofeedback mode.		
4th Subject (Lyra)			
Start (hh:mm):	09:11	Duration (min):	20
Stop (hh:mm):	09:40	Hip fixation (Yes/No):	No
Velocity (m/s):	1.3		
Additional comment:	BWSS was adjusted to 30kg (the total weight of the participant was not documented within the recording). Pain on the right ankle. Sensor was removed and replaced several times. Data from right sensor cannot be evaluated.		
5th Subject (Lyra)			
Start (hh:mm):	10:45	Duration (min):	20
Stop (hh:mm):	11:05	Hip fixation (Yes/No):	No
Velocity (m/s):	1.2-1.5		
Additional comment:	BWSS was adjusted to 30kg (the total weight of the participant was not documented within the recording).		

Table 37: Measurement protocols of Lyra recordings

8.3 Ethical Approval

UNIVERSITÄTSKLINIKUM MAGDEBURG A.ö.R.

OTTO VON GUERICKE UNIVERSITÄT MAGDEBURG

TOP NATIONALES KRANKENHAUS 2019 FOCUS

Ethik-Kommission, Medizinische Fakultät / Universitätsklinikum, Leipziger Str. 44 Haus 28, 39120 Magdeburg

Frau Dr. J. Lamprecht
MEDIAN Klinik
Neurologisches Rehabilitationszentrum (NRZ) Magdeburg
Gustav-Ricker-Str. 4
39120 Magdeburg

Ethik-Kommission der Otto-von-Guericke-Universität an der Medizinischen Fakultät und am Universitätsklinikum Magdeburg A.ö.R.

Univ.-Prof. Dr. med. Christof Huth
Vorsitzender

Dr. med. Norbert Beck
Geschäftsführer

Telefon: +49 391 67-14314
Telefax: +49 391 67-14354
elektr.Fax: +49 391 67-290185
eMail: ethikkommission@ovgu.de

Datum
15.10.2019

139/19

Erhebung von Bewegungsdaten mittels Inertialsensoren während robotergestütztem Gangtraining mit Lokomat® und Lyra®

Sehr geehrte Frau Dr. Lamprecht,
sehr geehrte Kolleginnen und Kollegen,

die Ethik-Kommission der Otto-von-Guericke-Universität an der Medizinischen Fakultät und am Universitätsklinikum Magdeburg hat die übergebenen Unterlagen zur o. g. Studie überprüft, in der letzten Kommissionssitzung eingehend erörtert und ist zu der Auffassung gekommen, dass gegen die Durchführung keine ethischen Bedenken bestehen.
Diese **zustimmende Bewertung** ergeht unter dem Vorbehalt gleichbleibender Gegebenheiten.

Die Verantwortlichkeit des jeweiligen Prüfwissenschaftlers / behandelnden Prüfarztes bleibt in vollem Umfang erhalten und wird durch diese Entscheidung nicht berührt. Alle zivil- oder haftungsrechtlichen Folgen, die sich ergeben könnten, verbleiben uneingeschränkt beim Projektleiter und seinen Mitarbeitern.
Beim Monitoring sind die Bestimmungen des Bundes- und Landesdatenschutzgesetzes sowie die sich aus der ärztlichen Schweigepflicht ergebenden Einschränkungen zu beachten, was eine Aushändigung kompletter Patientenakten zum Monitoring ausschließt.
Ein Monitoring personen- und studienbezogener Daten wird dadurch nicht beeinträchtigt.
Hinsichtlich der EU-Datenschutzgrundverordnung (DSGVO), welche ab 25.05.2018 Wirksamkeit entfaltet, werden folgende Hinweise gegeben: Datenschutzrechtliche Aspekte von Forschungsvorhaben werden durch die Ethikkommission grundsätzlich nur kursorisch geprüft. Diese Bewertung ersetzt mithin nicht die Konsultation des zuständigen Datenschutzbeauftragten.
Um die Übersendung von studienbezogenen Jahresberichten / Abschlussberichten / Publikationen wird unter Nennung unserer Registraturnummer gebeten.

Mit freundlichen Grüßen

(i. A. Dr. med. Norbert Beck, Geschäftsführer)
Prof. Dr. med. C. Huth
Vorsitzender der Ethik-Kommission

Ethik-Kommission
der Otto-von-Guericke-Universität an der Medizinischen Fakultät
und am Universitätsklinikum Magdeburg A.ö.R.
Vorsitzender: Univ.-Prof. Dr. med. C. Huth

Anlage zum Votum der Studie 139/19 vom 15.10.2019

Zum Zeitpunkt der Bewertung der vorstehenden Studie waren folgende Damen und Herren Mitglied der Ethik-Kommission der Otto-von-Guericke-Universität an der Medizinischen Fakultät und am Universitätsklinikum Magdeburg:

Herr Prof. Dr. med. Norbert Bannert	Medizinische Fakultät / Universitätsklinikum, Pädiater
Frau Prof. Dr. phil. Eva Brinkschulte	Medizinische Fakultät / Universitätsklinikum, Bereich Geschichte, Ethik und Theorie der Medizin
Herr Prof. Dr.-Ing. Rolf Findeisen	Fakultät für Elektrotechnik und Informationstechnik, Institut für Automatisierungstechnik
Herr Prof. Dr. med. Christof Huth	Medizinische Fakultät / Universitätsklinikum, Universitätsklinik für Herz- und Thoraxchirurgie
Frau Assessorin Ute Klanten	Medizinische Fakultät / Universitätsklinikum, Stabsstelle Recht
Herr Prof. Dr. rer. nat. Siegfried Kropf	Medizinische Fakultät / Universitätsklinikum, Mathematiker, Biometriker
Herr Dr. med. Werner Kuchheuser	Medizinische Fakultät / Universitätsklinikum, Institut für Rechtsmedizin
Herr Prof. Dr. med. Frank Peter Meyer	Medizinische Fakultät / Universitätsklinikum, Klinischer Pharmakologe
Herr Prof. Dr. med. Jens Schreiber	Medizinische Fakultät / Universitätsklinikum, Universitätsklinik für Pneumologie
Herr Prof. Dr.-Ing. Klaus Tönnies	Fakultät für Informatik, Institut für Simulation und Graphik, AG Bildverarbeitung/Bildverstehen

Mitglieder der Ethik-Kommission, die in eine Studie eingebunden sind, haben für die Votierung der betreffenden Studie kein Stimmrecht.

Die Ethik-Kommission der Otto-von-Guericke-Universität an der Medizinischen Fakultät und am Universitätsklinikum Magdeburg ist unter Beachtung entsprechender internationaler Richtlinien (ICH, GCP) und nationaler Richtlinien (AMG, GCP-V, MPG, MPKPV) tätig, nach Landesrecht (Hochschulmedizingesetz des Landes Sachsen-Anhalt § 25a, Verordnung über Ethik-Kommissionen zur Bewertung klinischer Prüfungen von Arzneimitteln - Ethik-Kom-VO LSA - i. d. akt. Fassung) legitimiert. Weiterhin besteht eine Registrierung der Ethik-Kommission beim Bundesamt für Strahlenschutz nach § 205 (4) StrlSchG sowie beim Office for Human Research Protections, reg. no. IRB00006099, Rockville, MD, U.S.A..

Dr. med. Norbert Beck
Geschäftsführer der Ethik-Kommission

8.4 Own Publications incorporated within this Work

Peer-reviewed journal publications

Schicketmueller, A.; Rose, G.; Hofmann, M. Feasibility of a Sensor-Based Gait Event Detection Algorithm for Triggering Functional Electrical Stimulation during Robot-Assisted Gait Training. Sensors (Basel) 2019, doi: 10.3390/s19214804.

Schicketmueller, A.; Lamprecht, J.; Hofmann, M.; Sailer, M.; Rose, G. Gait Event Detection for Stroke Patients during Robot-Assisted Gait Training. Sensors 2020, 20, doi:10.3390/s20123399.

Conference contributions

Schicketmueller, A.; Rose, G.; Hofmann, M. Gait Event Detection for Functional Electrical Stimulation during Lokomat Training, RehabWeek 2019, Toronto, 24-28 June 2019.

Schicketmueller, A.; Rose, G.; Hofmann, M. Sensor-based movement detection for Functional Electrical Stimulation during End-effector Gait Rehabilitation. 13th Vienna International Workshop on Functional Electrical Stimulation, Vienna, 23-25 September 2019.

Schicketmueller, A.; Hofmann, M.; Rose, G. IMU triggered FES for Robotic Gait Training, RehabWeek 2021, Virtual Event, 23-25 September 2021.

9 List of Figures

Figure 1: Structure of the nervous system 5
Figure 2: Brain—simplified segmentation [38] 6
Figure 3: Cross-section of the spinal cord [38] 7
Figure 4: Spinal cord segments (left) and corresponding dermatomes (right) [39] 7
Figure 5: Structure and function of a neuron [40] 8
Figure 6: Schematical representation of an action potential [40] 9
Figure 7: Chemical synapse [40] 10
Figure 8: Seven components that form the functional basis for walking [56]. 13
Figure 9: Human gait cycle [57] 14
Figure 10: Schematic representation of a surface FES system 18
Figure 11: Strength-duration curve of a denervated cat tibialis anterior muscle [61] 18
Figure 12: Body-weight-supported treadmill training (BWSTT), adapted from [64] 20
Figure 13: Left: Lokomat (Hocoma, Volketswil, Switzerland) 21
Figure 14: Left: Lyra (Thera Trainer, Hochdorf, Germany) 22
Figure 15: Left: LEXO® (Tyromotion, Graz, Austria) 22
Figure 16: Development of learned non-use phenomenon [73] 23
Figure 17: Left: FLOAT (Reha-Stim Medtec, Schlieren, Switzerland) 24
Figure 18: Left: EksoNR™ (Ekso Bionics, Richmond, USA) 24
Figure 19: Global and local coordinate system 25
Figure 20: Strapdown system 26
Figure 21: Left: MotionMaker (Swortec, Monthey, Switzerland) Right: WalkTrainer (Swortec, Monthey, Switzerland) 35
Figure 22: RT 600 (Restorative Therapies, Baltimore, USA) 37
Figure 23: MotionSensor with its local coordinate system 40
Figure 24: Electrical stimulator (RehaStim) 41
Figure 25: Biphasic rectangular pulse 42
Figure 26: Concept: Robotic gait training with IMUs to trigger FES 43
Figure 27: Flowchart of the algorithms 45
Figure 28: Schematic representation of an IMU attached to the left foot 46
Figure 29: Visualisation of an IMU during full contact in the sagittal plane 48
Figure 30: Rotation of the foot after the mid stance 49
Figure 31: Angular velocities during heel off, whereas (i) denotes the current sample and refers to condition (4). 50
Figure 32: State diagram of gait events during robotic gait training, adapted from [122] 51
Figure 33: Angular velocity during the full contact event 53
Figure 34: Angular velocity within the yaxis during the toe-off event 55
Figure 35: Detection sequence of the gait event detection algorithm 57
Figure 36: Detection of initial contact: Floating threshold and angular velocity band 59

Figure 37: Angular velocity signal and jerk signal during robotic gait training (sagittal plane) 60
Figure 38: Angular velocity signal and jerk signal during robotic therapy (stroke patient) 60
Figure 39: Left: Position A—Inside of the foot Right: Position B—Dorsum of the foot 62
Figure 40: Reference position 63
Figure 41: Walking paradigm for the evaluation of the arbitrary sensor alignment algorithm 63
Figure 42: Data processing: Sequential forwarding of raw data—Arbitrary sensor alignment algorithm 64
Figure 43: Linear acceleration signals. 64
Figure 44: Linear acceleration signals. 65
Figure 45: Angular velocity signals of the **yaxis** 65
Figure 46: Angular velocity signals of the **yaxis**. 66
Figure 47: Angular velocity: Typical waveform of two gait cycles 67
Figure 48: Angular velocity signals of the yaxis. Position A—Inside of the foot 69
Figure 49: Angular velocity signals of the yaxis. Position B—Dorsum of the foot 69
Figure 50: Setup of the recording sessions. 72
Figure 51: Sequential forwarding of raw data for the gait event detection algorithm 73
Figure 52: Selection method for Lokomat and Lyra—heathy adult 74
Figure 53: Difference between: Detected step, undetected steps and incorrectly detected step 76
Figure 54: Procedure of the clinical study 77
Figure 55: Selection method for Lokomat and Lyra—stroke patients 79
Figure 56: Latency estimation 80
Figure 57: Detection rate: Lokomat—Healthy adult 81
Figure 58: False-positives: Lokomat—Healthy adult 82
Figure 59: False-negatives: Lokomat—Healthy adult 83
Figure 60: Detection rate: Lyra – Healthy adult 83
Figure 61: False-positives: Lyra – Healthy adult 84
Figure 62: False-negatives: Lyra—Healthy adult 85
Figure 63: Detection rate: Lokomat—Stroke patients 86
Figure 64: False-positives: Lokomat—Stroke patients 86
Figure 65: False-negatives: Lokomat—Stroke patients 87
Figure 66: Detection rate: Lyra—Stroke patients 87
Figure 67: False-positives: Lyra—Stroke patients 88
Figure 68: False-negatives: Lyra – Stroke patients 88
Figure 69: Setup: Bench test—Trial 1 91
Figure 70: Continuous Channel List Mode—Example of single pulses and doublets 92
Figure 71: Four main muscles considered for functional electrical stimulation 101
Figure 72: Muscle activation sequence for functional electrical stimulation 102
Figure 73: Typical duration of a gait cycle during robotic gait training 103

Figure 74: Amount of update commands of the CCL mode during one gait cycle (Bench test—Trial 2) 104
Figure 75: Concept: Bench test—Trial 2 108
Figure 76: Amount of update commands of the CCL mode during one gait cycle (Bench test—Trial 3) 109
Figure 77: Concept: Bench test—Trial 3 111
Figure 78: Step duration for four steps 113
Figure 79: Schematic representation of the measurement and execution chain of the proposed concept 124
Figure 80: Miniaturised concept (host computer including stimulation modules) 129
Figure 81: Graphical user interface—Page 1 130
Figure 82: Graphical user interface—Page 2 131

Permission to use the referenced images/graphs has kindly been granted by the authors, publishers, or manufacturers.

10 List of Tables

Table 1: Muscle activation sequence during stance, adapted from [58] 15
Table 2: Muscle activation sequence during swing, adapted from [58] 16
Table 3: Muscle activation sequence of the foot joints, adapted from [58]..... 16
Table 4: Online and offline algorithms for gait event detection. 30
Table 5: Lokomat: Hybrid robotic rehabilitation system 33
Table 6: Gangtrainer GT II: Hybrid robotic rehabilitation system 34
Table 7: WalkTrainer: Hybrid robotic rehabilitation system 35
Table 8: MotionMaker: Hybrid robotic rehabilitation system 36
Table 9: G-EO: Hybrid robotic rehabilitation system 36
Table 10: RT 600: Hybrid robotic rehabilitation system 37
Table 11: Rotated linear acceleration data in the zaxis during resting times 67
Table 12: Rotated linear acceleration data in the xaxis and yaxis during resting times..... 68
Table 13: Cross-correlation between the angular velocity signal of the yaxis of position A and B and their reference signal 70
Table 14: False-positive and false-negative..... 75
Table 15: Subjects of Lokomat 78
Table 16: Subjects of Lyra 78
Table 17: Estimated latency for gait events..... 89
Table 18: Main time t_1 and inter-pulse time t_2 for the channel list mode 93
Table 19: Stimulation sequence for the bench testing trial 94
Table 20: Initialisation of the CCL mode: Variables 95
Table 21: Initialisation of CCL mode: Byte sequence 96
Table 22: Update of CCL mode: Variables..... 97
Table 23: Update of CCL mode: Byte sequence 98
Table 24: Update of CCL mode: Byte sequence for the individual gait events 99
Table 25: Stop of CCL mode: Variables 100
Table 26: Stop of CCL mode: Byte sequence 100
Table 27: Start and stop times for the activation of the muscles during one gait cycle with the duration of 2.6 seconds (Bench test—Trial 2) 103
Table 28: Parameters for electrical stimulation 106
Table 29: Update of CCL mode: Byte sequence as described in Figure 74 (Bench test—Trial 2) 107
Table 30: Update of CCL mode: Byte sequence as described in Figure 76 (Bench test—Trial 3) 111
Table 31: Estimated latency for the update commands 112
Table 32: Step duration during Lokomat training 113
Table 33: Step duration during Lyra training..... 114
Table 34: Approximate overall delay of the proposed concept 126

Table 35: Measurement protocols of Lokomat and Lyra recordings of the healthy adult. 134
Table 36: Measurement protocols of Lokomat recordings 135
Table 37: Measurement protocols of Lyra recordings 136

11 References

1. Johnson, W.; Onuma, O.; Owolabi, M.; Sachdev, S. Stroke: a global response is needed. Bull. World Health Organ. **2016**, 94, 634-634A, doi:10.2471/BLT.16.181636.
2. Jørgensen, H.S.; Nakayama, H.; Raaschou, H.O.; Olsen, T.S. Recovery of walking function in stroke patients: The copenhagen stroke study. Arch. Phys. Med. Rehabil. **1995**, 76, 27–32, doi:10.1016/S0003-9993(95)80038-7.
3. Algurén, B.; Lundgren-Nilsson, A.; Sunnerhagen, K.S. Functioning of stroke survivors - A validation of the ICF core set for stroke in Sweden. Disabil. Rehabil. **2010**, 32, 551–559, doi:10.3109/09638280903186335.
4. Dobkin, B.H. Clinical practice. Rehabilitation after stroke. N. Engl. J. Med. **2005**, 352, 1677–1684, doi:10.1056/NEJMcp043511.
5. Iosa, M.; Morone, G.; Fusco, A.; Bragoni, M.; Coiro, P.; Multari, M.; Venturiero, V.; Angelis, D. de; Pratesi, L.; Paolucci, S. Seven Capital Devices for the Future of Stroke Rehabilitation. Stroke Research and Treatment **2012**, 2012, 1–9, doi:10.1155/2012/187965.
6. Mehrholz, J.; Thomas, S.; Werner, C.; Kugler, J.; Pohl, M.; Elsner, B. Electromechanical-assisted training for walking after stroke. Cochrane Database Syst. Rev. **2017**, 5, CD006185, doi:10.1002/14651858.CD006185.pub4.
7. Mehrholz, J.; Thomas, S.; Kugler, J.; Pohl, M.; Elsner, B. Electromechanical-assisted training for walking after stroke. Cochrane Database Syst. Rev. **2020**, 10, CD006185, doi:10.1002/14651858.CD006185.pub5.
8. Hidler, J.M.; Wall, A.E. Alterations in muscle activation patterns during robotic-assisted walking. Clin. Biomech. (Bristol, Avon) **2005**, 20, 184–193, doi:10.1016/j.clinbiomech.2004.09.016.
9. Hesse, S. Lokomotionstherapie: Ein praxisorientierter Überblick; Hippocampus-Verl.: Bad Honnef, Germany, 2007, ISBN 978-3936817270.
10. Yoshida, Y.; Ikuno, K.; Shomoto, K. Comparison of the Effect of Sensory-Level and Conventional Motor-Level Neuromuscular Electrical Stimulations on Quadriceps Strength After Total Knee Arthroplasty: A Prospective Randomized Single-Blind Trial. Arch. Phys. Med. Rehabil. **2017**, 98, 2364–2370, doi:10.1016/j.apmr.2017.05.005.
11. Matsuse, H.; Hashida, R.; Takano, Y.; Omoto, M.; Nago, T.; Bekki, M.; Shiba, N. Walking Exercise Simultaneously Combined With Neuromuscular Electrical Stimulation of Antagonists Resistance Improved Muscle Strength, Physical Function, and Knee Pain in Symptomatic Knee Osteoarthritis: A Single-Arm Study. Journal of strength and conditioning research **2017**, 31, 171–180, doi:10.1519/JSC.0000000000001463.
12. Embrey, D.G.; Alon, G.; Brandsma, B.A.; Vladimir, F.; Silva, A.; Pflugeisen, B.M.; Amoroso, P.J. Functional electrical stimulation improves quality of life by reducing intermittent claudication. International journal of cardiology **2017**, 243, 454–459, doi:10.1016/j.ijcard.2017.05.097.

13. Knutson, J.S.; Gunzler, D.D.; Wilson, R.D.; Chae, J. Contralaterally Controlled Functional Electrical Stimulation Improves Hand Dexterity in Chronic Hemiparesis: A Randomized Trial. Stroke **2016**, 47, doi:10.1161/STROKEAHA.116.013791.
14. Springer, S.; Khamis, S.; Laufer, Y. Improved ankle and knee control with a dual-channel functional electrical stimulation system in chronic hemiplegia. A case report. European journal of physical and rehabilitation medicine **2014**, 50, 189–195.
15. Pool, D.; Blackmore, A.M.; Bear, N.; Valentine, J. Effects of short-term daily community walk aide use on children with unilateral spastic cerebral palsy. Pediatric physical therapy : the official publication of the Section on Pediatrics of the American Physical Therapy Association **2014**, 26, 308–317, doi:10.1097/PEP.0000000000000057.
16. O'Dell, M.W.; Dunning, K.; Kluding, P.; Wu, S.S.; Feld, J.; Ginosian, J.; McBride, K. Response and prediction of improvement in gait speed from functional electrical stimulation in persons with poststroke drop foot. PM R **2014**, 6, 587-601; quiz 601, doi:10.1016/j.pmrj.2014.01.001.
17. Sampson, P.; Freeman, C.; Coote, S.; Demain, S.; Feys, P.; Meadmore, K.; Hughes, A.-M. Using Functional Electrical Stimulation Mediated by Iterative Learning Control and Robotics to Improve Arm Movement for People With Multiple Sclerosis. IEEE Trans. Neural Syst. Rehabil. Eng. **2016**, 24, 235–248, doi:10.1109/TNSRE.2015.2413906.
18. Functional Electrical Stimulation (FES) for Stroke Rehabilitation; Tong, R.K.-Y., Ed.; John WIley & Sons Inc.: New Jersey.
19. Howlett, O.A.; Lannin, N.A.; Ada, L.; McKinstry, C. Functional electrical stimulation improves activity after stroke: a systematic review with meta-analysis. Arch. Phys. Med. Rehabil. **2015**, 96, 934–943, doi:10.1016/j.apmr.2015.01.013.
20. Springer, S.; Khamis, S. Effects of functional electrical stimulation on gait in people with multiple sclerosis - A systematic review. Mult. Scler. Relat. Disord. **2017**, 13, 4–12, doi:10.1016/j.msard.2017.01.010.
21. Sharif, F.; Ghulam, S.; Malik, A.N.; Saeed, Q. Effectiveness of Functional Electrical Stimulation (FES) versus Conventional Electrical Stimulation in Gait Rehabilitation of Patients with Stroke. J. Coll. Physicians Surg. Pak. **2017**, 27, 703–706.
22. Martin, R.; Sadowsky, C.; Obst, K.; Meyer, B.; McDonald, J. Functional electrical stimulation in spinal cord injury: from theory to practice. Top. Spinal Cord Inj. Rehabil. **2012**, 18, 28–33, doi:10.1310/sci1801-28.
23. Shariat, A.; Najafabadi, M.G.; Ansari, N.N.; Cleland, J.A.; Singh, M.A.F.; Memari, A.-H.; Honarpishe, R.; Hakakzadeh, A.; Ghaffari, M.S.; Naghdi, S. The effects of cycling with and without functional electrical stimulation on lower limb dysfunction in patients post-stroke: A systematic review with meta-analysis. NeuroRehabilitation **2019**, 44, 389–412, doi:10.3233/NRE-182671.
24. Bruni, M.F.; Melegari, C.; Cola, M.C. de; Bramanti, A.; Bramanti, P.; Calabrò, R.S. What does best evidence tell us about robotic gait rehabilitation in stroke patients: A systematic review and meta-analysis. J. Clin. Neurosci. **2018**, 48, 11–17, doi:10.1016/j.jocn.2017.10.048.

25. Dohring, M.E.; Daly, J.J. Automatic synchronization of functional electrical stimulation and robotic assisted treadmill training. IEEE Trans. Neural Syst. Rehabil. Eng. **2008**, 16, 310–313, doi:10.1109/TNSRE.2008.920081.
26. Spaich, E.G.; Bøg, M.F.; Erkocevic, E.; Smidstrup, A.; Andersen, O.K.; Nielsen, J.F. Gait Orthosis Lokomat Combined with Functional Electrical Stimulation for Foot Drop Correction: A Feasibility Study. In Replace, Repair, Restore, Relieve – Bridging Clinical and Engineering Solutions in Neurorehabilitation; Jensen, W., Andersen, O.K., Akay, M., Eds.; Springer International Publishing: Cham, 2014; pp 751–757, ISBN 978-3-319-08071-0.
27. Laursen, C.B.; Nielsen, J.F.; Andersen, O.K.; Spaich, E.G. Feasibility of Using Lokomat Combined with Functional Electrical Stimulation for the Rehabilitation of Foot Drop. Eur. J. Transl. Myol. **2016**, 26, 6221, doi:10.4081/ejtm.2016.6221.
28. Tong, R.K.Y.; Ng, M.F.W.; Li, L.S.W.; So, E.F.M. Gait training of patients after stroke using an electromechanical gait trainer combined with simultaneous functional electrical stimulation. Phys. Ther. **2006**, 86, 1282–1294, doi:10.2522/ptj.20050183.
29. Bouri, M.; Stauffer, Y.; Schmitt, C.; Allemand, Y.; Gnemmi, S.; Clavel, R.; Metrailler, P.; Brodard, R. The WalkTrainer: A Robotic System for Walking Rehabilitation. In 2006 IEEE International Conference on Robotics and Biomimetics. 2006 IEEE International Conference on Robotics and Biomimetics, Kunming, China, 17–20 Dec. 2006; IEEE, 2006 - 2006; pp 1616–1621, ISBN 1-4244-0570-X.
30. Stauffer, Y.; Allemand, Y.; Bouri, M.; Fournier, J.; Clavel, R.; Metrailler, P.; Brodard, R.; Reynard, F. The WalkTrainer--a new generation of walking reeducation device combining orthoses and muscle stimulation. IEEE Trans. Neural Syst. Rehabil. Eng. **2009**, 17, 38–45, doi:10.1109/TNSRE.2008.2008288.
31. Yves, S.; Bouri, M.; Clavel, R.; Allemand, Y.; Brodard, R. A Novel Verticalized Reeducation Device for Spinal Cord Injuries: the WalkTrainer, from Design to Clinical Trials. In Robotics 2010 Current and Future Challenges; Abdellatif, H., Ed.; InTech, 2010, ISBN 978-953-7619-78-7.
32. Metrailler, P.; Blanchard, V.; Perrin, I.; Brodard, R.; Frischknecht, R.; Schmitt, C.; Fournier, J.; Bouri, M.; Clavel, R. Improvement of rehabilitation possibilities with the MotionMaker TM. In The First IEEE/RAS-EMBS International Conference on Biomedical Robotics and Biomechatronics, 2006. BioRob 2006. The First IEEE/RAS-EMBS International Conference on Biomedical Robotics and Biomechatronics, 2006. BioRob 2006, Pisa, Italy, February 20-22, 2006; IEEE, 2006; pp 359–364, ISBN 1-4244-0040-6.
33. McCabe, J.P. Feasibility of combining gait robot and multichannel functional electrical stimulation with intramuscular electrodes. JRRD **2008**, 45, 997–1006, doi:10.1682/JRRD.2007.08.0124.
34. Schwesig, R.; Kauert, R.; Wust, S.; Becker, S.; Leuchte, S. Reliability of the novel gait analysis system RehaWatch. Biomed. Tech. (Berl) **2010**, 55, 109–115, doi:10.1515/bmt.2010.025.
35. Donath, L.; Faude, O.; Lichtenstein, E.; Nüesch, C.; Mündermann, A. Validity and reliability of a portable gait analysis system for measuring spatiotemporal gait

characteristics: comparison to an instrumented treadmill. J. Neuroeng. Rehabil. **2016**, 13, 6, doi:10.1186/s12984-016-0115-z.
36. Mariani, B.; Rouhani, H.; Crevoisier, X.; Aminian, K. Quantitative estimation of foot-flat and stance phase of gait using foot-worn inertial sensors. Gait Posture **2013**, 37, 229–234, doi:10.1016/j.gaitpost.2012.07.012.
37. Mariani, B.; Hoskovec, C.; Rochat, S.; Büla, C.; Penders, J.; Aminian, K. 3D gait assessment in young and elderly subjects using foot-worn inertial sensors. J. Biomech. **2010**, 43, 2999–3006, doi:10.1016/j.jbiomech.2010.07.003.
38. Appell, H.-J.; Stang-Voss, C. Funktionelle Anatomie: Grundlagen sportlicher Leistung und Bewegung, 4. Aufl.; Springer-Verlag: s.l., 2008, ISBN 978-3-540-74862-5.
39. Poeck, K.; Hacke, W. Neurologie, 12., aktualisierte und erweiterte Auflage; Springer Medizin Verlag Heidelberg: Berlin, Heidelberg, 2006, ISBN 9783540299974.
40. Clauss, W.; Clauss, C. Humanbiologie kompakt, 2. Auflage; Springer Spektrum: Berlin, Heidelberg, 2018, ISBN 9783662558492.
41. Robertson, V. Electrotherapy Explained: Principles and Practice, 4th ed.; Elsevier Health Sciences UK: Saintt Louis, 2006, ISBN 978-0-7506-8843-7.
42. Faller, A.; Schünke, M.; Schünke, G. Der Körper des Menschen: Einführung in Bau und Funktion ; 4 Poster mit Übersichten Skelett, Gefäße, Nerven, Muskeln, 16., überarb. Aufl.; Georg Thieme Verlag KG: Stuttgart, 2012, ISBN 9783133297165.
43. Hennerici, M.G.; Binder, J.; Szabo, K. Stroke; OUP Oxford: Oxford, 2012, ISBN 9780199582808.
44. Jia, X.; Kowalski, R.G.; Sciubba, D.M.; Geocadin, R.G. Critical care of traumatic spinal cord injury. J. Intensive Care Med. **2013**, 28, 12–23, doi:10.1177/0885066611403270.
45. Ahuja, C.S.; Wilson, J.R.; Nori, S.; Kotter, M.R.N.; Druschel, C.; Curt, A.; Fehlings, M.G. Traumatic spinal cord injury. Nat. Rev. Dis. Primers **2017**, 3, 17018, doi:10.1038/nrdp.2017.18.
46. Roberts, T.T.; Leonard, G.R.; Cepela, D.J. Classifications In Brief: American Spinal Injury Association (ASIA) Impairment Scale. Clin. Orthop. Relat. Res. **2017**, 475, 1499–1504, doi:10.1007/s11999-016-5133-4.
47. Carranza, M. Parkinson's disease: A guide to medical treatment, First edition; SEEd: Torino, Italy, 2013, ISBN 8897419429.
48. Scolding, N.; Wilkins, A. Multiple sclerosis; Oxford University Press: Oxford, 2012, ISBN 9780199603251.
49. Nelles, G. Rehabilitation von sensomotorischen Störungen: S2k-Leitlinie. Leitlinien für Diagnostik und Therapie in, 2018.
50. Platz, T. Therapie des spastischen Syndroms: S2k-Leitlinie. Leitlinien für Diagnostik und Therapie in der Neurologie., 2018.
51. Zilles, K. Neuronal plasticity as an adaptive property of the central nervous system. Annals of Anatomy - Anatomischer Anzeiger **1992**, 174, 383–391, doi:10.1016/S0940-9602(11)80255-4.
52. Demarin, V.; Morović, S.; Béné, R. Neuroplasticity. Periodicum biologorum **2014**, 116, 209–211.

53. Ackermann, H.; Nelles, G. Neurologische Rehabilitation: 115 Tabellen; Thieme: Stuttgart, 2004, ISBN 3131362618.
54. Ackermann, H. Neurorehabilitation: Ein Praxisbuch für interdisziplinäre Teams ; mit 92 Tabellen; Springer: Berlin u.a., 2010, ISBN 978-3-642-12914-8.
55. Hebb, D.O. The organization of behavior: A neuropsychological theory; L. Erlbaum Associates: Mahwah, N.J, 2002, ISBN 0805843000.
56. Vaughan, C.L.; Davis, B.L.; O'Connor, J.C. Gait analysis laboratory: An interactive book & software package; Human Kinetics Publishers: Champaign, Ill., 1992, ISBN 9780873223683.
57. Neumann, D.A.; Rowan, E.E. Kinesiology of the musculoskeletal system: Foundations for physical rehabilitation; Mosby: St. Louis, Mo., 2008, ISBN 0815163495.
58. Perry, J. Gait analysis: Normal and pathological function (Second edition); Slack: Thorofare, New Jersey, 2010, ISBN 9781556427664.
59. Alon, G. Functional Electrical Stimulation (FES): Transforming Clinical Trials to Neuro-Rehabilitation Clinical Practice- A Forward Perspective. J Nov Physiother **2013**, 03, doi:10.4172/2165-7025.1000176.
60. Popovic, M.R.; Masani, K.; Micera, S. Functional Electrical Stimulation Therapy: Recovery of Function Following Spinal Cord Injury and Stroke. In Neurorehabilitation Technology; Dietz, V., Nef, T., Rymer, W.Z., Eds.; Springer London: London, 2012; pp 105–121, ISBN 978-1-4471-2276-0.
61. Peckham, P.H.; Knutson, J.S. Functional electrical stimulation for neuromuscular applications. Annu. Rev. Biomed. Eng. **2005**, 7, 327–360, doi:10.1146/annurev.bioeng.6.040803.140103.
62. Bijak, M.; Mödlin, M.; Hofer, C.; Rakos, M.; Kern, H.; Mayr, W. FES treatment of lower extremities of patients with upper / lower motor neuron lesion: A comparison of rehabilitation strategies and stimulation equipment. In 11th Mediterranean Conference on Medical and Biomedical Engineering and Computing 2007; Jarm, T., Kramar, P., Zupanic, A., Eds.; Springer Berlin Heidelberg: Berlin, Heidelberg, 2007; pp 658–660, ISBN 978-3-540-73043-9.
63. French, B.; Thomas, L.H.; Coupe, J.; McMahon, N.E.; Connell, L.; Harrison, J.; Sutton, C.J.; Tishkovskaya, S.; Watkins, C.L. Repetitive task training for improving functional ability after stroke. Cochrane Database Syst. Rev. **2016**, 11, CD006073, doi:10.1002/14651858.CD006073.pub3.
64. Dietz, V.; Colombo, G.; Jensen, L. Locomotor activity in spinal man. The Lancet **1994**, 344, 1260–1263, doi:10.1016/s0140-6736(94)90751-x.
65. Mehrholz, J.; Pohl, M.; Elsner, B. Treadmill training and body weight support for walking after stroke. Cochrane Database Syst. Rev. **2014**, CD002840, doi:10.1002/14651858.CD002840.pub3.
66. van Hedel, H.J.A.; Dietz, V. Rehabilitation of locomotion after spinal cord injury. Restor. Neurol. Neurosci. **2010**, 28, 123–134, doi:10.3233/RNN-2010-0508.
67. Kwakkel, G.; van Peppen, R.; Wagenaar, R.C.; Wood Dauphinee, S.; Richards, C.; Ashburn, A.; Miller, K.; Lincoln, N.; Partridge, C.; Wellwood, I.; et al. Effects of

augmented exercise therapy time after stroke: a meta-analysis. Stroke **2004**, 35, 2529–2539, doi:10.1161/01.STR.0000143153.76460.7d.

68. Brütsch, K.; Schuler, T.; Koenig, A.; Zimmerli, L.; -Koeneke, S.M.; Lünenburger, L.; Riener, R.; Jäncke, L.; Meyer-Heim, A. Influence of virtual reality soccer game on walking performance in robotic assisted gait training for children. J. Neuroeng. Rehabil. **2010**, 7, 15, doi:10.1186/1743-0003-7-15.
69. Maggioni, S.; Melendez-Calderon, A.; van Asseldonk, E.; Klamroth-Marganska, V.; Lünenburger, L.; Riener, R.; van der Kooij, H. Robot-aided assessment of lower extremity functions: a review. J. Neuroeng. Rehabil. **2016**, 13, 72, doi:10.1186/s12984-016-0180-3.
70. Kim, Y.-H. Robotic assisted rehabilitation therapy for enhancing gait and motor function after stroke. Precis Future Med **2019**, 3, 103–115, doi:10.23838/pfm.2019.00065.
71. Marchal-Crespo, L.; Riener, R. Robot-assisted gait training. Rehabilitation Robotics; Elsevier, 2018; pp 227–240, ISBN 9780128119952.
72. Israel, J.F.; Campbell, D.D.; Kahn, J.H.; Hornby, T.G. Metabolic costs and muscle activity patterns during robotic- and therapist-assisted treadmill walking in individuals with incomplete spinal cord injury. Phys. Ther. **2006**, 86, 1466–1478, doi:10.2522/ptj.20050266.
73. Taub, E.; Uswatte, G.; Mark, V.W.; Morris, D.M.M. The learned nonuse phenomenon: implications for rehabilitation. Eura. Medicophys. **2006**, 42, 241–256.
74. Dobkin, B.H.; Duncan, P.W. Should body weight-supported treadmill training and robotic-assistive steppers for locomotor training trot back to the starting gate? Neurorehabil. Neural Repair **2012**, 26, 308–317, doi:10.1177/1545968312439687.
75. van den Brand, R.; Heutschi, J.; Barraud, Q.; DiGiovanna, J.; Bartholdi, K.; Huerlimann, M.; Friedli, L.; Vollenweider, I.; Moraud, E.M.; Duis, S.; et al. Restoring voluntary control of locomotion after paralyzing spinal cord injury. Science **2012**, 336, 1182–1185, doi:10.1126/science.1217416.
76. Haslwanter, T. 3D Kinematics; Springer International Publishing: Cham, 2018, ISBN 978-3-319-75276-1.
77. Rueterbories, J.; Spaich, E.G.; Andersen, O.K. Gait event detection for use in FES rehabilitation by radial and tangential foot accelerations. Med. Eng. Phys. **2014**, 36, 502–508, doi:10.1016/j.medengphy.2013.10.004.
78. Mo, S.; Chow, D.H.K. Accuracy of three methods in gait event detection during overground running. Gait Posture **2018**, 59, 93–98, doi:10.1016/j.gaitpost.2017.10.009.
79. Zhen, T.; Yan, L.; Yuan, P. Walking Gait Phase Detection Based on Acceleration Signals Using LSTM-DNN Algorithm. Algorithms **2019**, 12, 253, doi:10.3390/a12120253.
80. Robberechts, P.; Derie, R.; van den Berghe, P.; Gerlo, J.; Clercq, D.D.; Segers, V.; Davis, J. Predicting gait events from tibial acceleration in rearfoot running: a structured machine learning approach, 2019. Available online: http://arxiv.org/pdf/1910.13372v2.

81. Flood, M.W.; O'Callaghan, B.P.F.; Lowery, M.M. Gait Event Detection From Accelerometry Using the Teager-Kaiser Energy Operator. IEEE Trans. Biomed. Eng. **2020**, 67, 658–666, doi:10.1109/TBME.2019.2919394.
82. Wu, R.; Wu, J.; Xiao, W. Gait Detection using a Single Accelerometer. In 2019 IEEE 15th International Conference on Control and Automation (ICCA). 2019 IEEE 15th International Conference on Control and Automation (ICCA), Edinburgh, United Kingdom, 16/07/2019 - 19/07/2019; IEEE, 2019 - 2019; pp 178–183, ISBN 978-1-7281-1164-3.
83. Catalfamo, P.; Ghoussayni, S.; Ewins, D. Gait event detection on level ground and incline walking using a rate gyroscope. Sensors (Basel) **2010**, 10, 5683–5702, doi:10.3390/s100605683.
84. Mannini, A.; Sabatini, A.M. A hidden Markov model-based technique for gait segmentation using a foot-mounted gyroscope. Annu. Int. Conf. IEEE Eng. Med. Biol. Soc. **2011**, 2011, 4369–4373, doi:10.1109/IEMBS.2011.6091084.
85. Evans, R.L.; Arvind, D.K. Detection of Gait Phases Using Orient Specks for Mobile Clinical Gait Analysis. In 2014 11th International Conference on Wearable and Implantable Body Sensor Networks. 2014 11th International Conference on Wearable and Implantable Body Sensor Networks (BSN), Zuirch, Switzerland, 16/06/2014 - 19/06/2014; IEEE, 2014 - 2014; pp 149–154, ISBN 978-1-4799-4959-5.
86. Mannini, A.; Genovese, V.; Maria Sabatini, A. Online decoding of hidden Markov models for gait event detection using foot-mounted gyroscopes. IEEE J. Biomed. Health Inform. **2014**, 18, 1122–1130, doi:10.1109/JBHI.2013.2293887.
87. Taborri, J.; Scalona, E.; Palermo, E.; Rossi, S.; Cappa, P. Validation of Inter-Subject Training for Hidden Markov Models Applied to Gait Phase Detection in Children with Cerebral Palsy. Sensors (Basel) **2015**, 15, 24514–24529, doi:10.3390/s150924514.
88. Taborri, J.; Rossi, S.; Palermo, E.; Patanè, F.; Cappa, P. A novel HMM distributed classifier for the detection of gait phases by means of a wearable inertial sensor network. Sensors (Basel) **2014**, 14, 16212–16234, doi:10.3390/s140916212.
89. Gouwanda, D.; Gopalai, A.A. A robust real-time gait event detection using wireless gyroscope and its application on normal and altered gaits. Med. Eng. Phys. **2015**, 37, 219–225, doi:10.1016/j.medengphy.2014.12.004.
90. Figueiredo, J.; Felix, P.; Costa, L.; Moreno, J.C.; Santos, C.P. Gait Event Detection in Controlled and Real-Life Situations: Repeated Measures From Healthy Subjects. IEEE Trans. Neural Syst. Rehabil. Eng. **2018**, 26, 1945–1956, doi:10.1109/TNSRE.2018.2868094.
91. Formento, P.C.; Acevedo, R.; Ghoussayni, S.; Ewins, D. Gait event detection during stair walking using a rate gyroscope. Sensors (Basel) **2014**, 14, 5470–5485, doi:10.3390/s140305470.
92. Taborri, J.; Scalona, E.; Rossi, S.; Palermo, E.; Patane, F.; Cappa, P. Real-time gait detection based on Hidden Markov Model: Is it possible to avoid training procedure? In 2015 IEEE International Symposium on Medical Measurements and Applications (MeMeA) Proceedings. 2015 IEEE International Symposium on Medical

Measurements and Applications (MeMeA), Torino, Italy, 07/05/2015 - 09/05/2015; IEEE, 2015 - 2015; pp 141–145, ISBN 978-1-4799-6477-2.

93. Maqbool, H.F.; Husman, M.A.B.; Awad, M.I.; Abouhossein, A.; Iqbal, N.; Dehghani-Sanij, A.A. A Real-Time Gait Event Detection for Lower Limb Prosthesis Control and Evaluation. IEEE Trans. Neural Syst. Rehabil. Eng. **2017**, 25, 1500–1509, doi:10.1109/TNSRE.2016.2636367.
94. Kim, J.; Bae, M.-N.; Lee, K.B.; Hong, S.G. Gait event detection algorithm based on smart insoles. ETRI Journal **2020**, 42, 46–53, doi:10.4218/etrij.2018-0639.
95. Vu, H.T.T.; Gomez, F.; Cherelle, P.; Lefeber, D.; Nowé, A.; Vanderborght, B. ED-FNN: A New Deep Learning Algorithm to Detect Percentage of the Gait Cycle for Powered Prostheses. Sensors (Basel) **2018**, 18, doi:10.3390/s18072389.
96. Sahoo, S.; Saboo, M.; Pratihar, D.K.; Mukhopadhyay, S. Real-Time Detection of Actual and Early Gait Events During Level-Ground and Ramp Walking. IEEE Sensors J. **2020**, 20, 8128–8136, doi:10.1109/JSEN.2020.2980863.
97. Seel, T.; Landgraf, L.; Escobar, V.C. de; Schauer, T. Online Gait Phase Detection with Automatic Adaption to Gait Velocity Changes Using Accelerometers and Gyroscopes. Biomed. Tech. (Berl) **2014**, 59 Suppl 1, s758-909, doi:10.1515/bmt-2014-5011.
98. Nazmi, N.; Abdul Rahman, M.A.; Yamamoto, S.-I.; Ahmad, S.A. Walking gait event detection based on electromyography signals using artificial neural network. Biomedical Signal Processing and Control **2019**, 47, 334–343, doi:10.1016/j.bspc.2018.08.030.
99. Joshi, C.D.; Lahiri, U.; Thakor, N.V. Classification of gait phases from lower limb EMG: Application to exoskeleton orthosis. In 2013 IEEE Point-of-Care Healthcare Technologies (PHT). 2013 IEEE Point-of-Care Healthcare Technologies (PHT), Bangalore, India, 16/01/2013 - 18/01/2013; IEEE, 2013 - 2013; pp 228–231, ISBN 978-1-4673-2767-1.
100. Meng, M.; She, Q.; Gao, Y.; Luo, Z. EMG signals based gait phases recognition using hidden Markov models. In The 2010 IEEE International Conference on Information and Automation. 2010 International Conference on Information and Automation (ICIA), Harbin, China, 20/06/2010 - 23/06/2010; IEEE, 2010 - 2010; pp 852–856, ISBN 978-1-4244-5701-4.
101. Huang, H.; Kuiken, T.A.; Lipschutz, R.D. A strategy for identifying locomotion modes using surface electromyography. IEEE Trans. Biomed. Eng. **2009**, 56, 65–73, doi:10.1109/TBME.2008.2003293.
102. Zhang, F.; Liu, M.; Huang, H. Effects of locomotion mode recognition errors on volitional control of powered above-knee prostheses. IEEE Trans. Neural Syst. Rehabil. Eng. **2015**, 23, 64–72, doi:10.1109/TNSRE.2014.2327230.
103. Bae, J.; Tomizuka, M. Gait phase analysis based on a Hidden Markov Model. Mechatronics **2011**, 21, 961–970, doi:10.1016/j.mechatronics.2011.03.003.
104. Attal, F.; Amirat, Y.; Chibani, A.; Mohammed, S. Automatic Recognition of Gait phases Using a Multiple Regression Hidden Markov Model. IEEE/ASME Trans. Mechatron. **2018**, 1, doi:10.1109/TMECH.2018.2836934.

105. Agostini, V.; Balestra, G.; Knaflitz, M. Segmentation and classification of gait cycles. IEEE Trans. Neural Syst. Rehabil. Eng. **2014**, 22, 946–952, doi:10.1109/TNSRE.2013.2291907.
106. Crea, S.; Rossi, S.M.M. de; Donati, M.; Reberšek, P.; Novak, D.; Vitiello, N.; Lenzi, T.; Podobnik, J.; Munih, M.; Carrozza, M.C. Development of gait segmentation methods for wearable foot pressure sensors. Annu. Int. Conf. IEEE Eng. Med. Biol. Soc. **2012**, 2012, 5018–5021, doi:10.1109/EMBC.2012.6347120.
107. Rossi, S.M.M. de; Crea, S.; Donati, M.; Rebersek, P.; Novak, D.; Vitiello, N.; Lenzi, T.; Podobnik, J.; Munih, M.; Carrozza, M.C. Gait segmentation using bipedal foot pressure patterns. In 2012 4th IEEE RAS & EMBS International Conference on Biomedical Robotics and Biomechatronics (BioRob). 2012 4th IEEE RAS & EMBS International Conference on Biomedical Robotics and Biomechatronics (BioRob 2012), Rome, Italy, 24/06/2012 - 27/06/2012; IEEE, 2012 - 2012; pp 361–366, ISBN 978-1-4577-1200-5.
108. Feng, Y.; Wang, Q. Using One Strain Gauge Bridge to Detect Gait Events for a Robotic Prosthesis. Robotica **2019**, 37, 1987–1997, doi:10.1017/S0263574719000390.
109. Martini, E.; Fiumalbi, T.; Dell'Agnello, F.; Ivanić, Z.; Munih, M.; Vitiello, N.; Crea, S. Pressure-Sensitive Insoles for Real-Time Gait-Related Applications. Sensors (Basel) **2020**, 20, doi:10.3390/s20051448.
110. Kotiadis, D.; Hermens, H.J.; Veltink, P.H. Inertial Gait Phase Detection for control of a drop foot stimulator Inertial sensing for gait phase detection. Med. Eng. Phys. **2010**, 32, 287–297, doi:10.1016/j.medengphy.2009.10.014.
111. Lau, H.; Tong, K. The reliability of using accelerometer and gyroscope for gait event identification on persons with dropped foot. Gait Posture **2008**, 27, 248–257, doi:10.1016/j.gaitpost.2007.03.018.
112. Meng, X.; Yu, H.; Tham, M.P. Gait phase detection in able-bodied subjects and dementia patients. Annu. Int. Conf. IEEE Eng. Med. Biol. Soc. **2013**, 2013, 4907–4910, doi:10.1109/EMBC.2013.6610648.
113. Ding, S.; Ouyang, X.; Liu, T.; Li, Z.; Yang, H. Gait Event Detection of a Lower Extremity Exoskeleton Robot by an Intelligent IMU. IEEE Sensors J. **2018**, 18, 9728–9735, doi:10.1109/JSEN.2018.2871328.
114. Khandelwal, S.; Wickstrom, N. Gait Event Detection in Real-World Environment for Long-Term Applications: Incorporating Domain Knowledge Into Time-Frequency Analysis. IEEE Trans. Neural Syst. Rehabil. Eng. **2016**, 24, 1363–1372, doi:10.1109/TNSRE.2016.2536278.
115. Zhou, H.; Ji, N.; Samuel, O.W.; Cao, Y.; Zhao, Z.; Chen, S.; Li, G. Towards Real-Time Detection of Gait Events on Different Terrains Using Time-Frequency Analysis and Peak Heuristics Algorithm. Sensors (Basel) **2016**, 16, doi:10.3390/s16101634.
116. Ji, N.; Zhou, H.; Guo, K.; Samuel, O.W.; Huang, Z.; Xu, L.; Li, G. Appropriate Mother Wavelets for Continuous Gait Event Detection Based on Time-Frequency Analysis for Hemiplegic and Healthy Individuals. Sensors (Basel) **2019**, 19, doi:10.3390/s19163462.

117. Ledoux, E.D. Inertial Sensing for Gait Event Detection and Transfemoral Prosthesis Control Strategy. IEEE Trans. Biomed. Eng. **2018**, 65, 2704–2712, doi:10.1109/TBME.2018.2813999.
118. Sánchez Manchola, M.D.; Pinto Bernal, M.J.; Munera, M.; Cifuentes, C.A. Gait Phase Detection for Lower-Limb Exoskeletons using Foot Motion Data from a Single Inertial Measurement Unit in Hemiparetic Individuals. Sensors (Basel) **2019**, 19, doi:10.3390/s19132988.
119. Mannini, A.; Sabatini, A.M. Gait phase detection and discrimination between walking-jogging activities using hidden Markov models applied to foot motion data from a gyroscope. Gait Posture **2012**, 36, 657–661, doi:10.1016/j.gaitpost.2012.06.017.
120. Kidziński, Ł.; Delp, S.; Schwartz, M. Automatic real-time gait event detection in children using deep neural networks. PLoS ONE **2019**, 14, e0211466, doi:10.1371/journal.pone.0211466.
121. Jung, J.-Y.; Heo, W.; Yang, H.; Park, H. A Neural Network-Based Gait Phase Classification Method Using Sensors Equipped on Lower Limb Exoskeleton Robots. Sensors (Basel) **2015**, 15, 27738–27759, doi:10.3390/s151127738.
122. Müller, P.; Seel, T.; Schauer, T. Experimental Evaluation of a Novel Inertial Sensor Based Realtime Gait Phase Detection Algorithm. Proc. of the 6th European Conference on Technically Assisted Rehabilitation - TAR, Berlin, 2015.
123. Chia Bejarano, N.; Ambrosini, E.; Pedrocchi, A.; Ferrigno, G.; Monticone, M.; Ferrante, S. A novel adaptive, real-time algorithm to detect gait events from wearable sensors. IEEE Trans. Neural Syst. Rehabil. Eng. **2015**, 23, 413–422, doi:10.1109/TNSRE.2014.2337914.
124. Lee, J.K.; Park, E.J. Quasi real-time gait event detection using shank-attached gyroscopes. Med. Biol. Eng. Comput. **2011**, 49, 707–712, doi:10.1007/s11517-011-0736-0.
125. Liu, D.-X.; Wu, X.; Du, W.; Wang, C.; Xu, T. Gait Phase Recognition for Lower-Limb Exoskeleton with Only Joint Angular Sensors. Sensors (Basel) **2016**, 16, doi:10.3390/s16101579.
126. Zakria, M.; Maqbool, H.F.; Hussain, T.; Awad, M.I.; Mehryar, P.; Iqbal, N.; Dehghani-Sanij, A.A. Heuristic based gait event detection for human lower limb movement. In 2017 IEEE EMBS International Conference on Biomedical & Health Informatics (BHI). 2017 IEEE EMBS International Conference on Biomedical & Health Informatics (BHI), Orland, FL, USA, 16/02/2017 - 19/02/2017; IEEE, 2017 - 2017; pp 337–340, ISBN 978-1-5090-4179-4.
127. Zhao, H.; Wang, Z.; Qiu, S.; Wang, J.; Xu, F.; Wang, Z.; Shen, Y. Adaptive gait detection based on foot-mounted inertial sensors and multi-sensor fusion. Information Fusion **2019**, 52, 157–166, doi:10.1016/j.inffus.2019.03.002.
128. Yan, L.; Zhen, T.; Kong, J.-L.; Wang, L.-M.; Zhou, X.-L. Walking Gait Phase Detection Based on Acceleration Signals Using Voting-Weighted Integrated Neural Network. Complexity **2020**, 2020, 1–14, doi:10.1155/2020/4760297.

129. Winter, D.A. The biomechanics and motor control of human gait: Normal, elderly and pathological, 2nd edition; Waterloo Biomechanics: Waterloo, 1991, ISBN 0-88898-105-8.
130. Ng, M.F.W.; Tong, R.K.Y.; Li, L.S.W. A pilot study of randomized clinical controlled trial of gait training in subacute stroke patients with partial body-weight support electromechanical gait trainer and functional electrical stimulation: six-month follow-up. Stroke **2008**, 39, 154–160, doi:10.1161/STROKEAHA.107.495705.
131. Dundar, U.; Toktas, H.; Solak, O.; Ulasli, A.M.; Eroglu, S. A comparative study of conventional physiotherapy versus robotic training combined with physiotherapy in patients with stroke. Top. Stroke Rehabil. **2014**, 21, 453–461, doi:10.1310/tsr2106-453.
132. Anaya, F.; Thangavel, P.; Yu, H. Hybrid FES–robotic gait rehabilitation technologies: a review on mechanical design, actuation, and control strategies. Int J Intell Robot Appl **2018**, 2, 1–28, doi:10.1007/s41315-017-0042-6.
133. Sousa, A.C.C. de; Valtin, M.; Bó, A.P.; Schauer, T. Automatic Detection of Stimulation Artifacts to Isolate Volitional from Evoked EMG Activity. IFAC-PapersOnLine **2018**, 51, 282–287, doi:10.1016/j.ifacol.2018.11.628.
134. Schwartz, I.; Meiner, Z. Robotic-assisted gait training in neurological patients: who may benefit? Ann. Biomed. Eng. **2015**, 43, 1260–1269, doi:10.1007/s10439-015-1283-x.
135. Shultz, S.J.; Houglum, P.A.; Perrin, D.H. Examination of musculoskeletal injuries, Fourth edition; Human Kinetics: Champaign, Illinois, 2016, ISBN 1450472923.
136. Haslwanter, T. Hands-on Signal Analysis with Python: An Introduction, 1st ed. 2021; Springer International Publishing; Imprint: Springer: Cham, 2021, ISBN 978-3-030-57903-6.
137. Lüthi, H. Assessment: Functional Independence Measure – Alltagsfähigkeiten zuverlässig messen. ergopraxis **2009**, 2, 28–29, doi:10.1055/s-0030-1254445.
138. Mehrholz, J.; Wagner, K.; Rutte, K.; Meissner, D.; Pohl, M. Predictive validity and responsiveness of the functional ambulation category in hemiparetic patients after stroke. Arch. Phys. Med. Rehabil. **2007**, 88, 1314–1319, doi:10.1016/j.apmr.2007.06.764.
139. Cometti, C.; Babault, N.; Deley, G. Effects of Constant and Doublet Frequency Electrical Stimulation Patterns on Force Production of Knee Extensor Muscles. PLoS ONE **2016**, 11, e0155429, doi:10.1371/journal.pone.0155429.
140. Dudley-Javoroski, S.; Littmann, A.E.; Iguchi, M.; Shields, R.K. Doublet stimulation protocol to minimize musculoskeletal stress during paralyzed quadriceps muscle testing. J. Appl. Physiol. **2008**, 104, 1574–1582, doi:10.1152/japplphysiol.00892.2007.
141. Ibitoye, M.O.; Hamzaid, N.A.; Hasnan, N.; Abdul Wahab, A.K.; Davis, G.M. Strategies for Rapid Muscle Fatigue Reduction during FES Exercise in Individuals with Spinal Cord Injury: A Systematic Review. PLoS ONE **2016**, 11, e0149024, doi:10.1371/journal.pone.0149024.
142. Qiu, S.; Draghici, A.E.; Picard, G.; Taylor, J.A. Muscle Fatigue in Response to Electrical Stimulation Pattern and Frequency in Spinal Cord Injury. PM R **2020**, 12, 699–705, doi:10.1002/pmrj.12282.
143. Karu, Z.Z.; Durfee, W.K. Using pulse doublets to enhance muscle force for FES. In Proceedings of the Annual International Conference of the IEEE Engineering in

Medicine and Biology Society. 1992 14th Annual International Conference of the IEEE Engineering in Medicine and Biology Society, Paris, France, 29 Oct.–01 Nov. 1992; IEEE, 1992 - 1992; pp 1356–1357, ISBN 0-7803-0785-2.
144. Kroon, J.R. de; Ijzerman, M.J.; Chae, J.; Lankhorst, G.J.; Zilvold, G. Relation between stimulation characteristics and clinical outcome in studies using electrical stimulation to improve motor control of the upper extremity in stroke. J. Rehabil. Med. **2005**, 37, 65–74, doi:10.1080/16501970410024190.
145. Baker, L.L.; Bowman, B.R.; McNeal, D.R. Effects of waveform on comfort during neuromuscular electrical stimulation. Clin. Orthop. Relat. Res. **1988**, 75–85.
146. Bhadra, N.; Peckham, P.H. Peripheral nerve stimulation for restoration of motor function. J. Clin. Neurophysiol. **1997**, 14, 378–393, doi:10.1097/00004691-199709000-00004.
147. Kebaetse, M.B.; Turner, A.E.; Binder-Macleod, S.A. Effects of stimulation frequencies and patterns on performance of repetitive, nonisometric tasks. J. Appl. Physiol. **2002**, 92, 109–116, doi:10.1152/jappl.2002.92.1.109.
148. Sluka, K.A.; Walsh, D. Transcutaneous electrical nerve stimulation: basic science mechanisms and clinical effectiveness. J. Pain **2003**, 4, 109–121, doi:10.1054/jpai.2003.434.
149. McLoda, T.A.; Carmack, J.A. Optimal burst duration during a facilitated quadriceps femoris contraction. J. Athl. Train. **2000**, 35, 145–150.
150. Eser, P.C.; Donaldson, N.d.N.; Knecht, H.; Stüssi, E. Influence of different stimulation frequencies on power output and fatigue during FES-cycling in recently injured SCI people. IEEE Trans. Neural Syst. Rehabil. Eng. **2003**, 11, 236–240, doi:10.1109/TNSRE.2003.817677.
151. Janssen, T.W.J.; Bakker, M.; Wyngaert, A.; Gerrits, K.H.L.; Haan, A. de. Effects of stimulation pattern on electrical stimulation-induced leg cycling performance. J. Rehabil. Res. Dev. **2004**, 41, 787–796, doi:10.1682/JRRD.2004.03.0030.
152. Kebaetse, M.B.; Binder-Macleod, S.A. Strategies that improve human skeletal muscle performance during repetitive, non-isometric contractions. Pflugers Arch. **2004**, 448, 525–532, doi:10.1007/s00424-004-1279-0.
153. Grill, W.M.; Mortimer, J.T. The effect of stimulus pulse duration on selectivity of neural stimulation. IEEE Trans. Biomed. Eng. **1996**, 43, 161–166, doi:10.1109/10.481985.
154. Lagerquist, O.; Collins, D.F. Influence of stimulus pulse width on M-waves, H-reflexes, and torque during tetanic low-intensity neuromuscular stimulation. Muscle Nerve **2010**, 42, 886–893, doi:10.1002/mus.21762.
155. Bracciano, A.G. Physical agent modalities: Theory and application for the occupational therapist; Slack; Eurospan [distributor]: Thorofare, N.J., London, 2008, ISBN 978-1556426490.
156. Mesin, L.; Merlo, E.; Merletti, R.; Orizio, C. Investigation of motor unit recruitment during stimulated contractions of tibialis anterior muscle. J. Electromyogr. Kinesiol. **2010**, 20, 580–589, doi:10.1016/j.jelekin.2009.11.008.
157. Gondin, J.; Cozzone, P.J.; Bendahan, D. Is high-frequency neuromuscular electrical stimulation a suitable tool for muscle performance improvement in both healthy

humans and athletes? Eur. J. Appl. Physiol. **2011**, 111, 2473–2487, doi:10.1007/s00421-011-2101-2.
158. Maffiuletti, N.A.; Pensini, M.; Martin, A. Activation of human plantar flexor muscles increases after electromyostimulation training. J. Appl. Physiol. **2002**, 92, 1383–1392, doi:10.1152/japplphysiol.00884.2001.
159. Stevens-Lapsley, J.E.; Balter, J.E.; Wolfe, P.; Eckhoff, D.G.; Kohrt, W.M. Early neuromuscular electrical stimulation to improve quadriceps muscle strength after total knee arthroplasty: a randomized controlled trial. Phys. Ther. **2012**, 92, 210–226, doi:10.2522/ptj.20110124.
160. Piva, S.R.; Goodnite, E.A.; Azuma, K.; Woollard, J.D.; Goodpaster, B.H.; Wasko, M.C.; Fitzgerald, G.K. Neuromuscular electrical stimulation and volitional exercise for individuals with rheumatoid arthritis: a multiple-patient case report. Phys. Ther. **2007**, 87, 1064–1077, doi:10.2522/ptj.20060123.
161. Kinesiology of the musculoskeletal system: Foundations for physical rehabilitation /[edited by] Donald A. Neumann; Neumann, D.A., Ed., 2nd ed.; Mosby/Elsevier: St. Louis, Mo., 2010, ISBN 9780323039895.
162. Teufl, W.; Lorenz, M.; Miezal, M.; Taetz, B.; Fröhlich, M.; Bleser, G. Towards Inertial Sensor Based Mobile Gait Analysis: Event-Detection and Spatio-Temporal Parameters. Sensors **2019**, 19, 38, doi:10.3390/s19010038.
163. Backus, D.; Tefertiller, C. Incorporating Manual and Robotic Locomotor Training into Clinical Practice: Suggestions for Clinical Decision Making. Top. Spinal Cord Inj. Rehabil. **2008**, 14, 23–38, doi:10.1310/sci1401-23.
164. Agostini, V.; Ghislieri, M.; Rosati, S.; Balestra, G.; Knaflitz, M. Surface Electromyography Applied to Gait Analysis: How to Improve Its Impact in Clinics? Front. Neurol. **2020**, 11, 994, doi:10.3389/fneur.2020.00994.
165. Willerslev-Olsen, M.; Petersen, T.H.; Farmer, S.F.; Nielsen, J.B. Gait training facilitates central drive to ankle dorsiflexors in children with cerebral palsy. Brain **2015**, 138, 589–603, doi:10.1093/brain/awu399.
166. Sacco, I.; Amadio, A.C. Influence of the diabetic neuropathy on the behavior of electromyographic and sensorial responses in treadmill gait. Clinical Biomechanics **2003**, 18, 426–434, doi:10.1016/S0268-0033(03)00043-3.
167. Otter, A.R. den; Geurts, A.C.H.; Mulder, T.; Duysens, J. Gait recovery is not associated with changes in the temporal patterning of muscle activity during treadmill walking in patients with post-stroke hemiparesis. Clinical neurophysiology : official journal of the International Federation of Clinical Neurophysiology **2006**, 117, 4–15, doi:10.1016/j.clinph.2005.08.014.
168. Bovi, G.; Rabuffetti, M.; Mazzoleni, P.; Ferrarin, M. A multiple-task gait analysis approach: kinematic, kinetic and EMG reference data for healthy young and adult subjects. Gait Posture **2011**, 33, 6–13, doi:10.1016/j.gaitpost.2010.08.009.
169. Agostini, V.; Nascimbeni, A.; Gaffuri, A.; Imazio, P.; Benedetti, M.G.; Knaflitz, M. Normative EMG activation patterns of school-age children during gait. Gait Posture **2010**, 32, 285–289, doi:10.1016/j.gaitpost.2010.06.024.

170. McCamley, J.; Donati, M.; Grimpampi, E.; Mazzà, C. An enhanced estimate of initial contact and final contact instants of time using lower trunk inertial sensor data. Gait Posture **2012**, 36, 316–318, doi:10.1016/j.gaitpost.2012.02.019.
171. Rondón, R.; Gidlund, M.; Landernäs, K. Evaluating Bluetooth Low Energy Suitability for Time-Critical Industrial IoT Applications. Int J Wireless Inf Networks **2017**, 24, 278–290, doi:10.1007/s10776-017-0357-0.
172. Cavanagh, P.R.; Komi, P.V. Electromechanical delay in human skeletal muscle under concentric and eccentric contractions. European journal of applied physiology and occupational physiology **1979**, 42, 159–163, doi:10.1007/BF00431022.
173. Hopkins, J.T.; Feland, J.B.; Hunter, I. A comparison of voluntary and involuntary measures of electromechanical delay. The International journal of neuroscience **2007**, 117, 597–604, doi:10.1080/00207450600773764.
174. Nordez, A.; Gallot, T.; Catheline, S.; Guével, A.; Cornu, C.; Hug, F. Electromechanical delay revisited using very high frame rate ultrasound. J. Appl. Physiol. **2009**, 106, 1970–1975, doi:10.1152/japplphysiol.00221.2009.
175. Yavuz, S.U.; Sendemir-Urkmez, A.; Türker, K.S. Effect of gender, age, fatigue and contraction level on electromechanical delay. Clinical neurophysiology : official journal of the International Federation of Clinical Neurophysiology **2010**, 121, 1700–1706, doi:10.1016/j.clinph.2009.10.039.
176. Cè, E.; Rampichini, S.; Agnello, L.; Limonta, E.; Veicsteinas, A.; Esposito, F. Effects of temperature and fatigue on the electromechanical delay components. Muscle Nerve **2013**, 47, 566–576, doi:10.1002/mus.23627.
177. Sözen, H.; Cè, E.; Bisconti, A.V.; Rampichini, S.; Longo, S.; Coratella, G.; Shokohyar, S.; Doria, C.; Borrelli, M.; Limonta, E.; et al. Differences in electromechanical delay components induced by sex, age and physical activity level: new insights from a combined electromyographic, mechanomyographic and force approach. Sport Sci Health **2019**, 15, 623–633, doi:10.1007/s11332-019-00563-z.
178. Esposito, F.; Cè, E.; Rampichini, S.; Limonta, E.; Venturelli, M.; Monti, E.; Bet, L.; Fossati, B.; Meola, G. Electromechanical delay components during skeletal muscle contraction and relaxation in patients with myotonic dystrophy type 1. Neuromuscular disorders : NMD **2016**, 26, 60–72, doi:10.1016/j.nmd.2015.09.013.
179. Blackburn, J.T.; Bell, D.R.; Norcross, M.F.; Hudson, J.D.; Engstrom, L.A. Comparison of hamstring neuromechanical properties between healthy males and females and the influence of musculotendinous stiffness. J. Electromyogr. Kinesiol. **2009**, 19, e362-9, doi:10.1016/j.jelekin.2008.08.005.
180. Grosset, J.-F.; Piscione, J.; Lambertz, D.; Pérot, C. Paired changes in electromechanical delay and musculo-tendinous stiffness after endurance or plyometric training. Eur. J. Appl. Physiol. **2009**, 105, 131–139, doi:10.1007/s00421-008-0882-8.
181. Ateş, F.; Davies, B.L.; Chopra, S.; Coleman-Wood, K.; Litchy, W.; Kaufman, K.R. Intramuscular Pressure of Human Tibialis Anterior Muscle Reflects in vivo Muscular Activity. Frontiers in physiology **2019**, 10, 196, doi:10.3389/fphys.2019.00196.

182. Conchola, E.C.; Thompson, B.J.; Smith, D.B. Effects of neuromuscular fatigue on the electromechanical delay of the leg extensors and flexors in young and old men. Eur. J. Appl. Physiol. **2013**, 113, 2391–2399, doi:10.1007/s00421-013-2675-y.
183. Downey, R.J.; Merad, M.; Gonzalez, E.J.; Dixon, W.E. The Time-Varying Nature of Electromechanical Delay and Muscle Control Effectiveness in Response to Stimulation-Induced Fatigue. IEEE Trans. Neural Syst. Rehabil. Eng. **2017**, 25, 1397–1408, doi:10.1109/TNSRE.2016.2626471.
184. Kent-Braun, J.A.; Fitts, R.H.; Christie, A. Skeletal muscle fatigue. Compr. Physiol. **2012**, 2, 997–1044, doi:10.1002/cphy.c110029.
185. Wan, J.-J.; Qin, Z.; Wang, P.-Y.; Sun, Y.; Liu, X. Muscle fatigue: general understanding and treatment. Exp. Mol. Med. **2017**, 49, e384, doi:10.1038/emm.2017.194.
186. Seel, T.; Schauer, T.; Raisch, J. Iterativ Lernende Regelung mit variabler Zykluslänge für FES-basierte Kompensation einer Fußheberschwäche / Iterative Learning Control with Variable Pass Length applied to FES-based Drop Foot Treatment. at - Automatisierungstechnik **2013**, 61, doi:10.1524/auto.2013.0065.
187. Micera, S.; Keller, T.; Lawrence, M.; Morari, M.; Popović, D.B. Wearable neural prostheses. Restoration of sensory-motor function by transcutaneous electrical stimulation. IEEE Eng. Med. Biol. Mag. **2010**, 29, 64–69, doi:10.1109/MEMB.2010.936547.
188. Popović-Maneski, L.; Kostić, M.; Bijelić, G.; Keller, T.; Mitrović, S.; Konstantinović, L.; Popović, D.B. Multi-pad electrode for effective grasping: design. IEEE Trans. Neural Syst. Rehabil. Eng. **2013**, 21, 648–654, doi:10.1109/TNSRE.2013.2239662.
189. Heller, B.W.; Clarke, A.J.; Good, T.R.; Healey, T.J.; Nair, S.; Pratt, E.J.; Reeves, M.L.; van der Meulen, J.M.; Barker, A.T. Automated setup of functional electrical stimulation for drop foot using a novel 64 channel prototype stimulator and electrode array: results from a gait-lab based study. Med. Eng. Phys. **2013**, 35, 74–81, doi:10.1016/j.medengphy.2012.03.012.
190. Quandt, F.; Hummel, F.C. The influence of functional electrical stimulation on hand motor recovery in stroke patients: a review. Exp. Transl. Stroke Med. **2014**, 6, 9, doi:10.1186/2040-7378-6-9.
191. Di Nardo, F.; Morbidoni, C.; Mascia, G.; Verdini, F.; Fioretti, S. Intra-subject approach for gait-event prediction by neural network interpretation of EMG signals. Biomed. Eng. Online **2020**, 19, 58, doi:10.1186/s12938-020-00803-1.
192. Su, B.; Gutierrez-Farewik, E.M. Gait Trajectory and Gait Phase Prediction Based on an LSTM Network. Sensors (Basel) **2020**, 20, doi:10.3390/s20247127.